TIMING OF GEODYNAMIC PROCESSES IN ARUNACHAL HIMALAYA USING Rb-Sr AND FISSION TRACK AGES

A THESIS

Submitted in partial fulfilment of the requirements for the award of the degree of

DOCTOR OF PHILOSOPHY

in

EARTH SCIENCES

by

JAMES PEBAM

DEPARTMENT OF EARTH SCIENCES
INDIAN INSTITUTE OF TECHNOLOGY ROORKEE
ROORKEE - 247 667 (INDIA)

NOVEMBER, 2009

INDIAN INSTITUTE OF TECHNOLOGY ROORKEE
ROORKEE

CANDIDATE'S DECLARATION

I hereby certify that the work which is being presented in the thesis entitled **"TIMING OF GEODYNAMIC PROCESSES IN ARUNACHAL HIMALAYA USING Rb-Sr AND FISSION TRACK AGES"** in partial fulfilment of the requirements for the award of the Degree of Doctor of Philosophy and submitted in the Department of Earth Sciences, Indian Institute of Technology Roorkee, Roorkee is an authentic record of my own work carried out during the period from July, 2006 to November, 2009 under the supervision of Prof. Sandeep Singh and Prof. A. K. Jain, Department of Earth Sciences and Prof. A. K. Choudhary, Institute Instrumentation Centre, Indian Institute of Technology Roorkee, Roorkee-247 667.

The matter presented in this thesis has not been submitted by me for the award of any other degree of this or any other Institute.

James Pebam
11/11/2009
(JAMES PEBAM)

This is to certify that the above statement made by the candidate is correct to the best of our knowledge.

Date: 11/11/2009

(A. K. Choudhary) 11.11.9
Supervisor

(A. K. Jain)
Supervisor

Sandeep Singh
11th Nov. 2009
(Sandeep Singh)
Supervisor

The Ph.D. Viva Voce Examination of **Mr. JAMES PEBAM**, Research Scholar, has been held on 17th Aug 2010.

Sandeep Singh
17th Aug 2010
Signature of Supervisors 17.8.10

17.8.10

Signature of External Examiner

Acknowledgements

Firstly, I would like to express my sincere gratitude to my supervisors **Prof. Sandeep Singh**, **Prof. A.K. Jain** and **Prof. A.K. Choudhary** for their guidance, advice and motivation from the very early stage to the final level of this research work. I am especially thankful to **Prof. A.K. Jain** who has provided me unflinching encouragement and support in various ways. His truly scientific intuition has made him a constant oasis of ideas and passions in science, which has exceptionally inspired and enriched my growth as a student, a researcher and a scientist want to be. I am indebted to him more than he knows.

I am grateful to **Prof. R.P Gupta** and **Prof. V.N. Singh**, the present and former Heads of the Department, respectively for extending all the possible facilities during the course of this research work.

I take this opportunity to thank **Prof. Nand Lal** and **Dr. R.C. Patel**, Department of Geophysics, Kurukshetra University, Kurukshetra for patiently teaching me the basics of Earth Science during my M. Sc. days and also extend my deepest gratitude to them for introducing me to this research group and for patiently teaching me the Fission Track Dating method at their outstanding laboratory. I would like to thank **Dr. Rajeev Kumar** and **Dr. V. Ravikant**, who besides my supervisors, have given me guidance in operating the Thermal Ionization Mass Spectrometer at the Institute Instrumentation Centre, IIT Roorkee. I am thankful to them for their discussion and encouragement, also.

This work would not have been possible without the financial support from the Department of Science and Technology, New Delhi as the Junior Research Fellowship (JRF) and Senior Research Fellowship (SRF) from the projects (DST-230-ESD, DST-380-ESD).

I am thankful to my Lab seniors **Dr. Rajeev Kumar**, **Dr. Nikunja Bihari** and **Dr. Soumyajit Mukherjee** for their continuous encouragement, advice and willingness to share their bright thoughts with me. These were very fruitful for shaping up my ideas and research. My present Lab mates and friends **Ramesh Laishram, Rogibala Maibam, Vinay Kumar** and **Shalini Maurya** are especially thanked for presenting the very cordial and friendly atmosphere in the Lab. I have learnt a lot both scientifically and socially from the day to day talks, research material and sometimes heated debates. Hope we continue working together in future. Thank you all for the help in finalizing the write up.

I am extremely thankful to **Vikas Adlakha**, **Paramjeet Swami** and **Sarjesh Khuman** for making my work at Kurukshetra University very fruitful and enjoyable. My scientific interests have been immensely enriched by you all. I wish we can work together in future.

I am thankful to all the other research students (past and present) of the department with whom I share tons of fond memories. I am thankful to **Bhimji** and **Surenderji** and other non-teaching staffs of the department especially **Nairji** and **Rakeshji** for their generous help in many ways during my Ph. D. work.

Finally, this thesis would have been impossible without the confidence, endurance and support of my family. My family has always been a source of encouragement and inspiration. I wish to thank my parents, **Shri Pebam Ibomcha Singh** and **Smt. Geetabali Devi** whose love, teachings and support have brought me this far. I wish to thank my sisters, **Jesma**, **Jasooda** and **Sanjeeta** for their everlasting love, affection and inspiration. I wish to thank my late brother **David**, who gave me the meaning of brother. I wish you were with me today. I also thank my relatives and friends for their continuous support and encouragement.

JAMES PEBAM

Abstract

Recent thermochronological works in different sectors of the Himalayan orogenic belt highlighted the positive feedback between tectonics and exhumation, while high precipitation and climate-induced erosion control the exhumation, and still remain controversial. The present work focuses this aspect in parts of the Arunachal Himalaya in the east with the following objectives **(Chapter 1-Introduction).**

(i) Cooling and exhumation histories of different tectonic units of the Arunachal Himalaya in relation to major faults in the Subansiri and Siyom catchment areas, using Rb-Sr mica and Fission Track - zircon and apatite ages.

(ii) Source rock characterization from present-day river detrital sediments, using Apatite Fission Track ages.

(iii) To investigate the factors controlling the exhumation, i.e. the tectonics, the erosion or a combination of the both in Arunachal, which receives almost twice the rainfall during the Indian Monsoon in contrast to the NW Himalaya.

The Arunachal Himalaya is characterized by the Sub-Himalayan Siwalik Belt, the Lesser Himalayan Sedimentary Belt, the Himalayan Metamorphic Belt (HMB), the Tethyan Sedimentary Zone, the Indus Tsangpo Suture Zone (ITSZ) and the Trans-Himalayan Batholiths between 26° 30':29 ° 30' N and 91° 30':99° 30'E **(Chapter 2-Geological Framework).** The main core of the Eastern Himalayan Syntaxis lies just beyond this region in the northeast as a major antiform. All these tectonic units trend ENE-WSW in the west and swing to the NE-SW before bending to NW–SE along the Siang gorge. A newly-compiled geological map of the Arunachal Himalaya and the adjoining regions by Singh and Jain (2007) is the base for the mutual geological relationships and thermochronological works in the present study.

In the Subansiri Valley, the Siwalik Group of the Cenozoic Himalayan foreland basin rises abruptly over the Brahmaputra Alluvium along the Main Frontal Thrust (MFT). Further north, the Permian Gondwana Belt overrides this belt along the Main Boundary Thrust (MBT). The Lesser Himalayan metasediments are separated from the Himalayan Metamorphic Belt (HMB) along the folded Main Central Thrust (MCT). The southernmost exposure of the MCT is locally named as the Tamen Thrust. In the upper reaches of the Subansiri River, the folded HMB gets eroded of, leading to the exposure of the underlying Lesser Himalayan sequence in two windows. The MCT is again exposed near Taliha and Nacho, and separates the high grade metamorphics of the Higher Himalayan Crystalline (HHC) belt from the Lesser Himalayan (LH) sedimentary belt. Further north, the HHC unit is separated from the Tethyan Sedimentary Sequence by the South Tibetan Detachment Zone (STDZ).

Cooling and exhumation histories of different tectonic units of the Arunachal Himalaya have been investigated in the Subansiri and Siyom catchment areas, using Rb-Sr mica and Fission Track (FT) - zircon and apatite ages so as to cover the cooling temperature range between about 500 to 120^{O} C (**Chapters 3 and 4).** For the Rb-Sr dating of muscovite and biotite, 19 gneiss and gneissose granite samples were selected from the Himalayan Metamorphic Belt (HMB) and Lesser Himalaya (LS) of the Arunachal Himalaya; out of which 18 biotite and 4 muscovite mineral ages were obtained against the respective whole-rock isotopic ratios These samples were analyzed by the Thermal Ionization Mass Spectrometer (TIMS, TRITON T1) after standard sample preparation, isotopic dilution, ion chromatography etc. (**Chapter 3-Rb-Sr Dating**). The biotite ages spans from 6.85±0.07 to 18.73±0.02 Ma, whereas the muscovite ages vary from 10.32±0.17 Ma to as old 24.90±0.02 Ma. Out of these, the oldest mica ages were obtained from the Lesser Himalayan gneissose granite, which intruded the Khetabari

Formation. The Daporijo Gneiss of the Lesser Himalayan metamorphic belt yielded ages between 11.1±0.02 and 14.80±0.02 Ma (5 samples from western Kimin–Koluriang Section), while these are somewhat older as 15.18±0.30 and 15.77±0.16 Ma in the Subansiri River Section (3 samples). Muscovite could be dated only from one Daporijo Gneiss sample, yielding an age of 22.68±0.02 Ma in the extreme west. In contrast to the Lesser Himalayan Metamorphic Belt, the HHC metamorphics revealed a distinct drop in biotite and muscovite ages to 9.19±0.02 Ma and 20.36±0.08 Ma, respectively on the hanging wall of the MCT in the western section. In the middle section, biotite ages were between 7.24±0.09 and 8.24±0.09 (3 samples), while these range between 6.85±0.07 and 10.53±0.21 Ma (4 samples) with an exception 17.83±0.21 Ma at the base of the HHC in the eastern Siyom Valley.

Chapter 4-Fission Track Dating deals with the FT dating of bedrock across most of the tectonic units of the Arunachal Himalaya, where a total of 22 AFT (Apatite Fission Track) and 16 ZFT (Zircon Fission Track) ages were generated from 26 samples along three traverses, using the EDM method and the Zeta calibration approach. The AFT ages from the HHC belt range between 2.2±0.3 and 6.0±0.6 Ma with a northward younging. The ZFT ages fall between 3.3±0.3 and 7.9±0.4 Ma. Within the Lesser Himalayan windows, the AFT and ZFT ages are 2.0±0.3 and 5.6±0.5 Ma, respectively. These are in contrast to the AFT data between 5.1±0.6 and 12.1±1.2 Ma from the overthrust Lesser Himalayan Daporijo Gneiss, which reveals a string-shaped pattern. A ZFT age of 13.2±0.7 Ma from this belt is the oldest from the Arunachal Himalaya samples under consideration. The Lesser Himalayan intrusive granite gave an AFT age of 4.7±0.4 Ma and a quartzite sample an age of 11.0±0.6 Ma. A zircon FT age from the quartzite sample yielded an age of 12±0.8 Ma. A Permian gritty sandstone sample from within the Gondwana Belt yielded a reset AFT age of 8.5±1.1 Ma.

Apatite FT detrital thermochronology of the Subansiri and Siyom rivers sands as well as the Upper Siwalik Group (Pliocene-Pleistocene) on 436 apatite grains **(Chapter 5-Detrital AFT Thermochronology)** from the 10 samples have been undertaken with the objective to decipher the source rocks of these modern sands. Individual AFT grain ages range from 0.4 to 39.0 Ma and reveal the time elapsed since it attained its closure temperature of 135° C. These mixed population of different ages were reduced to individual peaks between 1.9 to 19.5 Ma, using the BINOMFIT software (Brandon, 2002), and have been assigned to different sources in the Higher and Lesser Himalayas.

Thermochronological mineral ages are the proxies for cooling and exhumation rates since these attained their respective closure temperatures (**Chapter 6-Discussions and Conclusions**). These rates have been calculated for the FT mineral ages, described in Chapter 4, using AGE2EDOT programme for 1D modelling. Cooling rates, calculated from the closure temperatures of AFT, ZFT, Rb-Sr biotite and muscovite thermochronometers, indicate spatio-temporal variations in cooling patterns across the Himalayan orogen in Arunachal. The cooling rates vary between 204.9° C/Ma and 6.8° C/Ma. The exhumation rates vary between 0.25 mm/yr to 1.2 mm/yr, using 1D numerical modelling and confirm their correlation with the structural layout. The fastest exhumation rate is observed in the LH windows and has been followed by the HHC. The LH sedimentary sequences and LH crystallines sequences experienced slower exhumation rates. Hence, cooling and exhumation of different lithotectonic units in the Arunachal Himalaya are mainly controlled by the folded MCT and simultaneous doming, thus providing evidences for tectonics forcing on exhumation.

Detrital AFT thermochronology of river sediments of the Subansiri and Siyom Rivers along with the Upper Siwalik Group highlighted the source characteristics of the

sediments carried by these rivers. Correlation of different AFT peak ages with bedrock AFT ages from this region showed the contribution from all the lithounits of this area.

Thermochronological FT age distribution in different parts of the NW Himalaya reveals that young ages are mainly concentrated in the HHC rocks, separated from the LH sedimentary belts by the MCT. Besides this, young ages are also observed within the HHC domes and the LH windows, which are exposed due to the folding of the MCT and simultaneous erosion. These regions consistently experienced high exhumation rates with a strong east-west similarity. A strong thermochronological evidence for tectonic control on the exhumation of Himalayan orogen is thus indicated in the present work.

Contents

List of Tables

List of Figures

Chapter 1: Introduction

1.1. Introduction

The Himalaya is one of the youngest and most spectacular mountain belt on the Earth, and offers a unique opportunity for understanding the processes of mountain building. It represents the southern margin of the largest zone of active crustal deformation on the Earth, resulting from the continental collision between the Indian and Asian Plates. The Himalayan kinematic evolution is largely controlled by major faults such as South Tibetan Detachment System (STDS), Main Central Thrust (MCT), Main Boundary Thrust (MBT) and Main Frontal Thrust (MFT), which bound the various tectonic units (Fig.1.1). Following the collision, the thrusting and folding in the Himalaya led to crustal thickening and metamorphism (Brunel, 1986; Mattauer, 1986; Jain and Anand, 1988; Jain and Manicksavagam, 1993). The estimated timing of this collision, based on stratigraphic, paleontological, structural, geochronological and paleomagnetic records varies between 65-50 Ma (Leech et al., 2005; Jain et al., 2009 and references therein). These units were subsequently exhumed in the Miocene by thrusting along the MCT (Hubbard and Harrison, 1989; Metcalfe, 1993) and coeval normal faulting along STDS (Hodges et al., 1993). The surface expression of thrusting subsequently transferred to the south along the MBT and presently-active MFT (DeCelles et al., 2001).

Mechanism of the crustal thickening and southward extrusion of the HHC are largely based on the structural, metamorphic and magmatism studies, and estimates of the timing, duration and displacements of the thrusting episodes (Hodges, 2000; Yin, 2006). These works are mainly restricted to the Western and Central Himalayas. Very little data related to structural, metamorphic and geochronological studies are available from the

eastern sector of this orogenic belt. It incapacitates the complete understanding of the tectonic evolution and exhumation of the NE Himalaya, and the Himalaya as whole. The available information in the NE Himalaya is insufficient to answer critical questions concerning the tectonic evolution and rate of exhumation of the whole Himalaya from northwest to the northeast.

During mountain building process, erosion plays a vital role in its tectonic and geomorphologic evolution (Beaumont et al., 1992; Masek et al., 1994; Avouac and Burov, 1996). Quantifying this process is one of the most challenging tasks in the mountains. The present-day erosion rate is estimated from the sediment load carried by the rivers (Burbank, 2002). The information on long-term rate can be reconstructed from the sediment accumulation rate in the basin (Curray, 1994; Clift et al., 2008). Thermochronological analysis of rocks constrains their cooling and exhumation (long-term erosion) histories (England and Molnar, 1990). In the Himalayan orogen, the understanding of its evolutionary history is never complete until the exhumation and the factors that govern these processes are fully understood. In the Arunachal Himalaya, such field of study is almost missing in spite of being crucial in research of the Himalayan orogen. The present work fills this gap in our existing knowledge by generating mineral cooling ages and then deciphering exhumation history in this region.

Recent thermochronological works in different sectors of the Himalayan orogenic belt highlighted the positive feedback between tectonics and exhumation (Jain et al., 2000; Dadson et al., 2003; Burbank et al., 2003; Malusa and Vezolli, 2006; Patel and Carter, 2009; Thiede et al., 2009). Another school of thought proposes climatic control on exhumation, based on the coincidence of areas of high exhumation rate with the areas of high precipitation rate (Thiede et al., 2004; Grujic et al., 2006). However, in the Marsyandi River valley of the Nepal Himalaya, Burbank et al. (2003) observed consistent

young AFT ages in spite of five-fold increase in precipitation along the same valley. It gives a clue about non-interference of climate in the Himalayan collision tectonics, but the interplay between tectonics and climate-induced erosion still remains a controversial topic.

1.2. Previous thermochronological work in the Eastern Himalaya

Thermochronological dating has been extensively carried out in the Namcha Barwa region of the Eastern Syntaxis of the Himalaya. It is dominated by a northeast-plunging antiform (Seward and Burg, 2008). In this area, the Apatite Fission Track (AFT) ages range between 0.4 to 8.2 Ma, while the ZFT ages range between 0.2-17.6 Ma (Burg et al., 1997, 1998; Seward and Burg, 2008). The age pattern in this region is because of the domal effect on the thermal signatures and tectonic control on the geometry of Eastern Himalayan river system (Seward and Burg, 2008). The Trans-Himalayan rocks have the K-Ar ages ranging between 18 and 39 Ma, while the HHC part has a range of 1.2–15 Ma (Group et al., 1979; Zheng and Chang, 1979; Zhang et al., 1981, 1987; Ratschbacher et al., 1992). Ding et al. (2001) reported $^{40}Ar/^{39}Ar$ hornblende ages of 7.9±0.2 Ma and 17.5±0.3 Ma in the core of the syntaxis, while in the Trans-Himalaya the ages range between 14 and 74 Ma (Geng et al., 2005). These ages show direct correlation with the structural position in the region. Similar pattern is also reported for the zircon U-Pb ages with a range of 2.9-14 Ma for fault-bounded HHC part (Booth et al., 2004) and 21-118 Ma for the Asian Plate (Ding et al., 2001) in the Namcha Barwa region. The timing of peak metamorphism is considered to be 16.0±2.5 Ma, as interpreted from the Sm-Nd whole rock/garnet age of the granulite facies rock (Burg et al., 1997, 1998). However, decompression starts at 3.9-3.3 Ma (Burg et al., 1997), as reported from the U-Th-Pb xenotime age of leucosome and dates the last anatectic event. This serves as an evidence

for the initiation of vertical and lateral domal growth at Namcha Barwa around 4 Ma (Seward and Burg, 2008).

In the Bhutan Himalaya, the AFT ages range from 1.4 to 8.6 Ma (Stuwe and Foster, 2001; Grujic et al., 2006). A closer look at the age distribution indicates younger age near the Paro Window. Gansser (1983) reported Rb-Sr muscovite ages of 9-26 Ma, while the $^{40}Ar/^{39}Ar$ biotite and muscovite ages range from 16.6 to 43.4 Ma and 11 to 14.7 Ma, respectively (Maluski et al., 1988; Stuwe and Foster, 2001). These biotite ages appears to be anomalous, as there could be variable concentration of excess argon (Stuwe and Foster, 2001). The ages confirm the north-south extension along the STDZ until around 10 Ma that was outlasted by thrust kinematics along the MCT.

Recent $^{40}Ar/^{39}Ar$ thermochronology work in westernmost region of the Arunachal Himalaya along the Bhalukpong-Zimithang section in Kameng region (Yin et al., 2009a) indicated distinct patterns in which the Lesser Himalayan Sedimentary Zone has the biotite age of 19.2 Ma and in the HHC part the biotite ages vary from 7.8 to 16.7 Ma. In the same region, the muscovite ages are less than the biotite ages in general, which have been explained due to the excess presence of argon in biotite (Yin et al., 2009a). However, the ages follow an interesting pattern in which the $^{40}Ar/^{39}Ar$ muscovite ages gradually increase with the increase of structural level. The ages vary from 7.7 to 12.3 Ma. There are no available published records of the fission track and Rb-Sr works on bedrocks of Arunachal Himalaya.

1.3. Tectonic zones of the Himalaya

Tectonostratigraphically, the Himalaya can be divided into different units, which are as follows from north to south (Fig. 1; Jain et al., 2002; Yin, 2006).

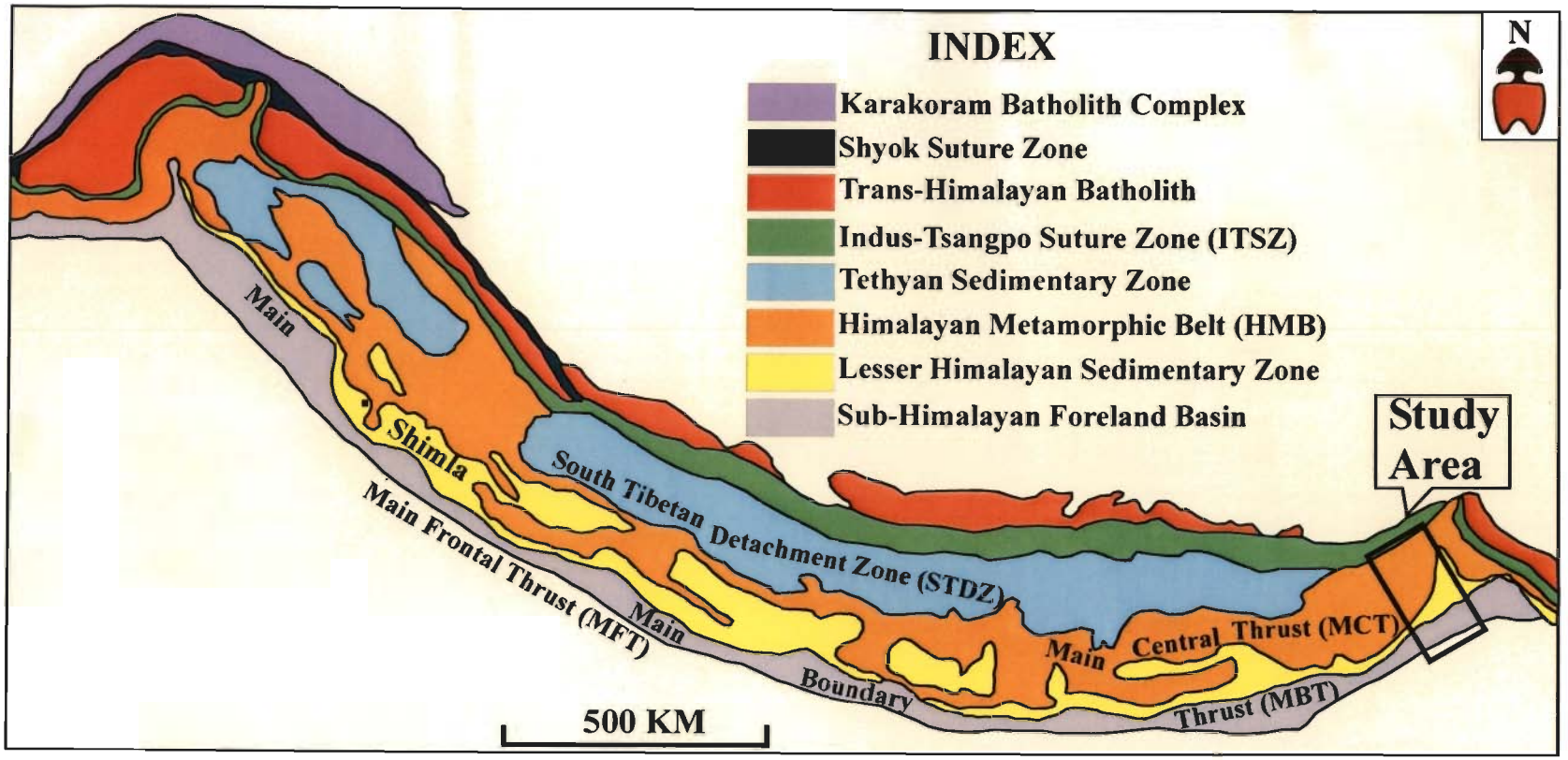

Figure 1:. Simplified geological map of the Himalaya in plate tectonic framework (Hodges, 2000; Jain et al., 2002; Yin, 2006). STDZ-South Tibetan Detachment Zone, MCT-Main Central Thrust, MBT-Main Boundary Thrust, MFT-Main Frontal Thrust.

1.3.1. India–Asia junction: Trans-Himalayan Tectonic Units

The junction between the Indian and Asian Plates is marked by two suture zones, viz. the Indus Tsangpo Suture Zone (ITSZ) and the Shyok Suture Zone (SSZ), where the former plate subducts beneath the Asian southern margin of the Paleo-Mesozoic platform.

(a) Indus Tsangpo Suture Zone (ITSZ): Being an almost continuous southern junction between the two plates, the Indus Tsangpo Suture Zone (ITSZ) encompasses an island arc of the Dras Volcanics containing basalt and dacite flows, pillow lavas; basalts, volcaniclastic sediments, radiolarian cherts and Orbitolina-bearing limestone of Callovian to Cenomanian age (Honegger et al., 1982; Garzanti and Van Haver, 1988; Rolland et al., 2000). Dismembered ophiolite occurrences at Nidar, Shergol and Zildat within the suture zone, and ophiolite nappe at Spongtang within immature greywacke-type flysch sequence represent a part of the Neo-Tethys oceanic crust (Gansser, 1964; Honegger et al., 1982; Searle et al., 1986; Thakur, 1993). These ophiolites are tectonically imbricated, but an undeformed succession at Nidar has harzburgite with chromite, followed upwards by cumulate gabbro, basalt and sheet dyke complex, pillow lavas, thin shale and chert (Maheo et al., 2005; Ahmed et al., 2008). This ophiolitic complex has radiolarian cherts of Hauterinian to Aptian (Early Cretaceous) age, which is consistent with Sm-Nd whole rock-mineral age (139.6±32.2 Ma) of gabbro having an intra-oceanic volcanic arc affinity, like the Dras volcanic arc in Ladakh further west and Kohistan arc in Pakistan (Satouru et al., 2001).

(b) Trans-Himalayan Batholiths: The Trans-Himalayan plutonic complex comprises the Lohit Batholith in the Mishmi Block in the east and corresponds to the Ladakh Batholith and Gangdese Plutons. These are Andean-type plutons, developed due to

partial melting of the mantle above the subducted Neo-Tethyan slab beneath the Asian Plate (Schlup et al., 2003). In the NW Himalaya, this activity is estimated to have been initiated at 102 Ma (Honegger et al., 1982) and ended by 50 Ma (Weinberg and Dunlop, 2000).

The Trans-Himalayan Batholiths are exposed immediately to the north of the Indus Tsangpo Suture Zone (ITSZ) for almost entire length of the Himalaya. These represent an Andean-type calc-alkaline magmatism due to northward subduction of the Neo-Tethyan oceanic crust below an island arc, located on the Asian Plate during the early Cretaceous-Lower Eocene (Honegger et al., 1982; Sharma and Choubey, 1983; Scharer et al., 1984; Rolland et al., 2001; Jain et al., 2002, 2003; Jain and Singh, 2009). This linear belt constitutes an important segment of the Trans-Himalaya that extends from Astor through Deosai–Skardu in Pakistan, known as the Kohistan Batholith (Auden, 1935; Desio, 1977; Wadia, 1937) to Leh–Upshi–Nyoma–Demchuk in India called as the Ladakh Batholith (Frank et al., 1977; Honegger et al., 1982; Sharma, 1982; Singh and Jain, 2003; Srikantia et al., 1982; Thakur, 1993). Further southeast in southern Tibet, it is well known as the Kailash Tonalite and the Gangdese pluton (Academica Sinica, 1980; Debon et al., 1981, 1986; Scharer et al., 1984). It has been called as the Lohit Batholith in Mishmi Hills of Arunachal Himalaya (Thakur and Jain, 1975; Sharma et al., 1991). The northern boundary of the Ladakh Batholith is demarcated by another suture zone-the Shyok Suture Zone (SSZ) or Main Karakoram Thrust (MKT in Pakistan), having dismembered tectonic mélanges of ultramafics, gabbro, basalt and sediments (Rolland et al., 2000).

1.3.2. Tethyan Sedimentary Sequence

The Tethyan Himalaya comprises a fossiliferous sedimentary sequence along the northern margin of the Indian Plate. It consists of low grade metamorphosed Proterozoic

to Eocene siliciclastic and carbonate sedimentary rocks, interbedded with Paleozoic and Mesozoic volcanic rocks (Yin, 2006). The Tethyan Sedimentary Sequence is juxtaposed against the Higher Himalayan Crystallines in the south along a series of normal faults, the South Tibetan Detachment Zone (STDZ).

1.3.3. Himalayan Metamorphic Belt (HMB)

The Himalayan Metamorphic Belt makes the northern margin of the Indian Plate, which is a remobilized Proterozoic basement and sedimentary cover after the closure of the Neo-Tethys, largely due to subduction of the Indian Plate during the Himalayan collision tectonics. It consists of the allocthonous Himalayan nappe within the Lesser Himalaya, and the Higher Himalayan Crystalline Belt, which occupies the root zone (Jain et al., 2002). A few examples of the former are the Salkhala nappe (Kashmir), the Chamba, Jutogh and Chail nappes (Himachal), the Garhwal and Almora nappes (Uttarakhand), Paro and Samchi in Bhutan, and the Bomdila in Arunachal Himalaya. These constitute the part of Lesser Himalayan Crystalline belt.

The Higher Himalayan Crystalline (HHC) Belt is composed of medium to high grade metamorphics, gneisses and migmatites, and is intruded by leucogranite crustal melts in the upper part (Hodges, 2000; Jain et al., 2002; Yin, 2006). It is the central core of the Himalaya, occupying the highest elevation of the orogen. This zone is characterized by ductile shear zones and inverted metamorphism. This package is overlain by the Tethyan Sedimentary Sequence along the South Tibetan Detachment Zone (STDZ).

1.3.4. Lesser Himalaya

The LH belt is made up of the Paleoproterozoic quartzite, slate, phyllite, dolomite, volcanics and granitoids (Valdiya, 1980; Srikantia and Bhargava, 1998), and

is overlain by the latest Proterozoic–Cambrian Krol–Tal sequence, the Permian Gondwana sequences (Gansser, 1977) along with the unconformably deposited Eocene Subathu Formation in the southern parts (Thakur, 1993). This belt is thrust southwards over the Sub–Himalayan foreland sequence along the Main Boundary Thrust (MBT). The LH belt extends farther towards northeast beneath the overriding metamorphic nappes, and is exposed in many windows e.g., the Kishtwar and Kulu-Rampur windows, where the Rampur volcanics, Bandal granite and Kishtwar granitoids have yielded U-Pb zircon ages of 1840 Ma, respectively (Miller et al., 2000).

1.3.5. Sub–Himalayan Cenozoic foreland basin

The outermost Cenozoic foreland basin has accumulated ~10 km of predominantly fluvial sediments, which were derived from the rising Himalaya. (Najman, 2006; Yin, 2006). This unit rises abruptly above the Indo-Gangetic alluvial plane along the Main Frontal Thrust (MFT) and is overridden by the Lesser Himalaya (Valdiya, 1980; Srikantia and Bhargava, 1998) along the Main Boundary Thrust (MBT). Four major stratigraphic units characterize this belt in the NW Himalaya.

(i) The Subathu Formation. The Paleocene-Middle Eocene marine transgression commenced with the unconformable deposition of the Subathu Formation on the Sub-Himalaya and Proterozoic–Early Paleozoic Lesser Himalayan domains. Carbonaceous/coaly shale is overlain by dull green-gray fossiliferous splintery shale/siltstone, thin fossiliferous limestone and sandstone intercalations. Felsic volcanics, chert, serpentine schist clasts and high-Al and Cr spinel reflect a mixed source from the proto-Himalayan ITSZ (Najman and Garzanti, 2000; Bhatia and Bhargava, 2006). The age of the Subathus has been estimated to range between 61.5

and 43.7 Ma, while its uppermost part may be even 41.5 Ma, magnetostratigraphically (Sangode et al., 2005).

(ii) Dagshai Formation. The overlying unfossiliferous Dagshai Formation in Shimla Hills or the Dharamsala Formation of Punjab (Raiverman et al., 1983) is red-colored siltstone and mudstone in lower parts, while sandstone and caliche appear in the upper parts. The precise contact relationship between the Subathu and Dagshai Formations remains controversial since the transition was postulated from marine to fluvial environment (Bhatia, 2000 and references therein; Bhatia and Bhargava, 2006). On the contrary, an unconformity was proposed between these two sequences with a hiatus ranging from ~10 Myr to <3 Myr (Najman et al., 1993, 2004; Bera et al., 2008; Jain et al., 2009).

(iii) Kasauli Formation. The overlying Kasauli Formation contains about 2000 m-thick gray–green sandstone and alternating siltstone-mudstone with litharenites having larger percentage of metamorphic fragments than the Subathu and Dagshai formations, and isotopic characters like the latter. The formation appears to have been deposited in migratory braided river system under humid climate (Singh, 1978; Najman et al., 1993). As an equivalent of the Dharamsala Group, magnetostratigraphic age of the uppermost Kasauli is either 13 Ma (White et al., 2002) or 11.5 Ma (Lakshami et al., 2000).

(iv) Siwalik Group. Bulk of the Sub-Himalayan basin is comprised of over ~6000 m-thick coarsening upwards Siwalik Group and is divisible into three subgroups in the northwest. The 1800 m-thick Lower Siwalik Subgroup of <13–11 Ma (White et al.,

2001, 2002) contains highly indurated fine to coarse purple-gray sandstone and interbedded brown shale. The Lower Siwalik sediments were deposited by south–flowing highly sinuous meandering rivers in broad muddy flood plains. Over 2300 m-thick Middle Siwalik Subgroup contains cross-bedded, medium to coarse sandstone, intercalated siltstone and shale, and was deposited between 11 and 4.5 Ma by major braided rivers with alluvial fan complexes. The Upper Siwalik Subgroup (~2300 m-thick) of conglomerate, sandstone and mudstone were deposited as coalescing alluvial fans during 4.5 and 1 Ma (Sangode et al., 1996).

1.4. Objectives

The broad objective of the present work is to study the timing of geodynamic processes in the Arunachal Himalaya and the factors controlling the processes. The detail objectives are:

(i) To study the cooling and exhumation histories of different tectonic units of the Arunachal Himalaya in the Subansiri and Siyom catchment areas, using Rb-Sr mica and Fission Track zircon and apatite ages.

(ii) Source rock characterization from present-day river detrital sediments, using Apatite Fission Track ages.

(ii) To investigate the factors controlling the exhumation: tectonics vs. erosion.

1.5. Scope of the work

Keeping in mind the above objectives, new geochronological data along three major traverses, viz. (i) the Kimin-Kolurinag road section, (ii) the Subansiri River Valley and (iii) the Siyom River Valley in Arunachal Himalaya are generated to work out a detailed reconstruction of the tectonic and exhumation history in the present research.

1.6. Methodology

The following methodologies have been adopted in this work to achieve the above objectives.

1.6.1. Field work

(i) Detailed systematic geological mapping of the area along the above traverses.

(ii) Rock sample collection from different traverses.

1.6.2. Rb-Sr dating of micas

(i) Standard crushing and powering of samples for whole rock analysis.

(ii) Dissolution, ion chromatography and analysis by Thermal Ionization Mass Spectrometer.

(iii) Standard crushing, sieving, heavy liquid and magnetic separation followed by hand-picking of micas. Ion chromatography and analysis in Thermal Ionization Mass Spectrometer.

1.6.3. Fission Track Dating

(i) Collected sample processed for FT Dating of apatite and zircon.

(ii) Standard crushing, sieving, heavy liquid and magnetic separation, followed by hand-picking, mounting, and etching of rock samples, while river sands are thoroughly washed and then processed.

(iii) Irradiation and track counting for determination of fission track ages of apatite and zircon.

1.6.4. Integration and compilation

All the generated data are compiled and modeled for estimating the cooling and exhumation history of the Arunachal Himalaya and are finally compared with those of the NW Himalaya.

Chapter 2: Geological Framework

2.1. Introduction

The Northeast India consists of six distinct domains that are spatially and tectonically related with each other (Fig. 2.1; Verma, 1999; Nandy, 2002; Yin et al., 2009b). These units include the following:

1. Eastern Himalaya
2. Mishmi Hills
3. Indo-Myanmar Range
4. Shillong Plateau
5. Brahmaputra Valley, and
6. Bengal Basin

The Eastern Himalaya marks the most important unit and extends from Bhutan in the west to Dibang and Lohit Valleys in Arunachal Pradesh, where all the tectonic units undergo gradual bending into the NW-SE trending Mishmi Hills. These mountains in the extreme east are considered to be the continuation of the Trans-Himalayan Batholith, lying to the north of the Indus Tsangpo Suture Zone (Kumar, 1997). The Eastern Himalaya has been divided into the Bhutan Himalaya and the Arunachal Himalaya (Yin et al. 2009a).

The Arunachal Himalaya occupies the sector between Long. 91° 31′ E and 99° 30′ E and includes the Eastern Himalayan Syntaxis as a major antiform (Thakur and Jain, 1974; Burg et al., 1997, 1998; Ding et al., 2001; Stewart et al., 2008). From south to north this mountain belt is characterized by the Siwaliks, the Lesser Himalayan sedimentary belt, the Himalayan Metamorphic Belt (HMB), the Tethyan Sedimentary Zone, the Indus Tsangpo Suture Zone and the Trans-Himalayan Batholith. These tectonic units trend ENE-WSW in the western parts and swings to NE–SW before their bending to NNW–

SSE along the Siang gorge. A newly-compiled geological map of Arunachal Himalaya and the adjoining regions by Singh and Jain (2007), published in DST New Letters, is the base for mutual geological relationships and thermochronological work in the subsequent chapters (Fig. 2.3).

2.2. Drainage

The rivers, draining the Arunachal Himalaya, form a part of the Brahmaputra River system, which originates from Mount Kailash in Tibet. This river is known as the Tsangpo in this region and Siang in the Arunachal Himalaya (Fig. 2.2). The Tsangpo follows the Indus Tsangpo Suture Zone for nearly 1135 km before taking a U-turn at Namcha Barwa to enter Arunachal Pradesh. The Siyom and Yamne Rivers are the two main tributaries of the Siang River draining the Himalayan region. The Siyom River originates at Tonokar Ogo as a subsequent stream and joins the Siang River at Pangin, while the Yamne River flows almost due S in the eastern part of the Siang District. The Siang River finally enters Brahmaputra Plain at Pasighat at an elevation of 170 m. Further east, the Brahmaputra is joined by two major river systems: the Dibang and Lohit Rivers after draining the Mishmi Hills (Fig. 2.2). The Dibang River flows transversely towards south, while the Lohit River originates in southeastern Tibet and flows almost towards SE before turning southwest in the Mishmi Hills. The Kameng and Subansiri Rivers are the main tributaries of the Brahmaputra draining the Arunachal Himalayan domain from the north. In the study area, the Subansiri River originates from southern Tibet and cuts through the Great Himalayan domain after crossing the Tethyan Sedimentary Zone. It approximately drains 30,000 km^2 in the Lesser Himalaya and Sub-Himalayan region as well (Kumar, 1997). It joins the Brahmaputra at Dulangmukh at a height of 152 m. The Kamla, Dikrang and Ranga Rivers are the important tributaries of the Subansiri River.

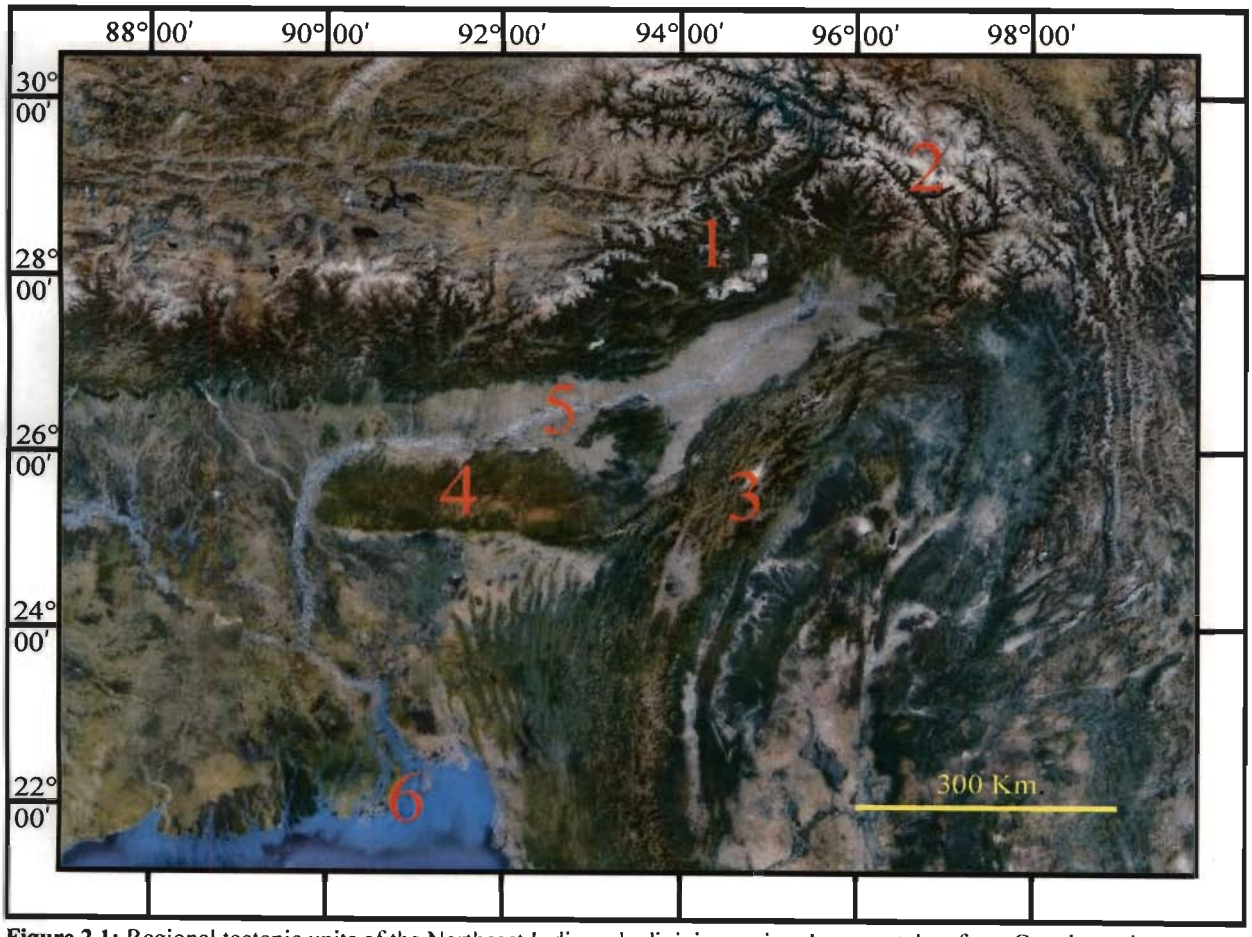

Figure 2.1: Regional tectonic units of the Northeast India and adjoining region, Imagery taken from Google earth. Notes: 1. Eastern Himalaya 2. Mishmi Hills 3. Indo-Myanmar Range 4. Shillong Plateau 5. Brahmaputra Valley and 6. Bengal Basin

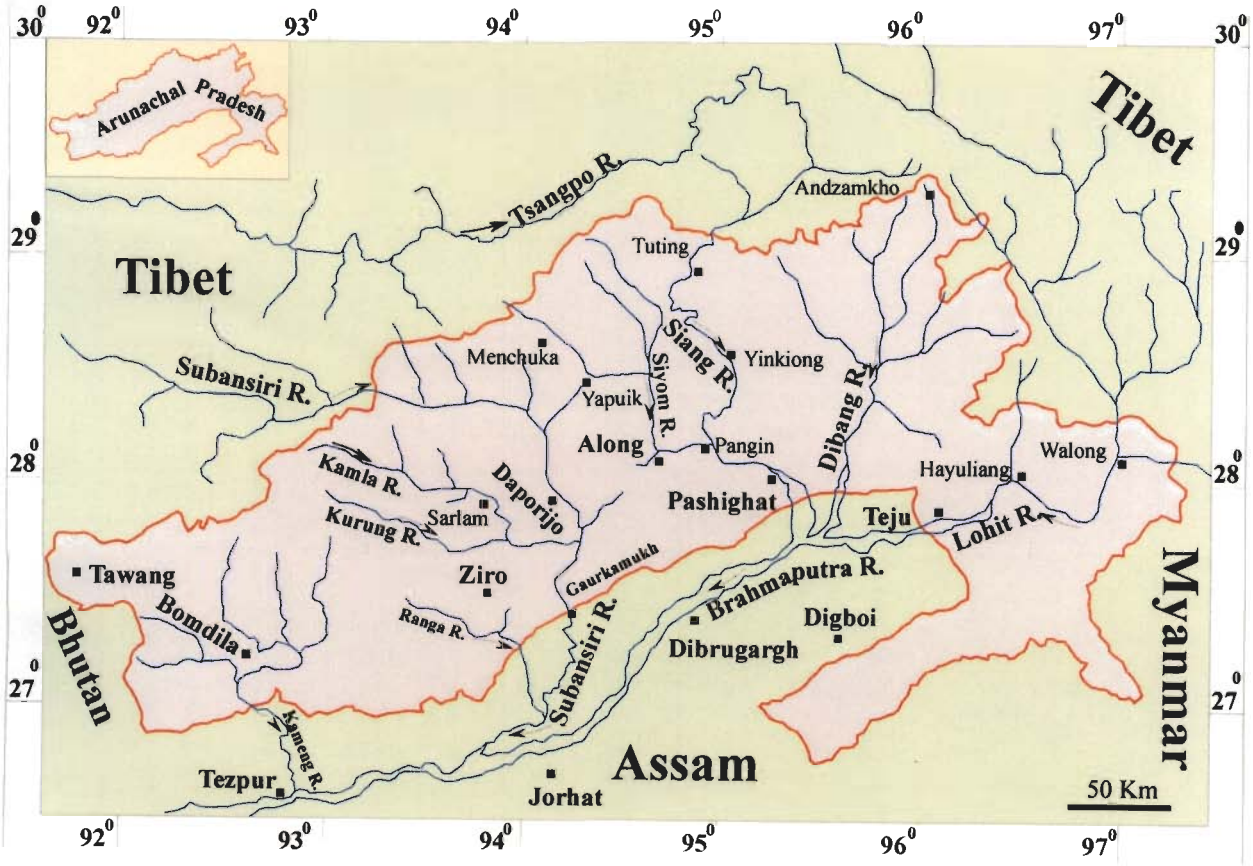

Figure 2.2: Drainage map of Arunachal Himalaya.

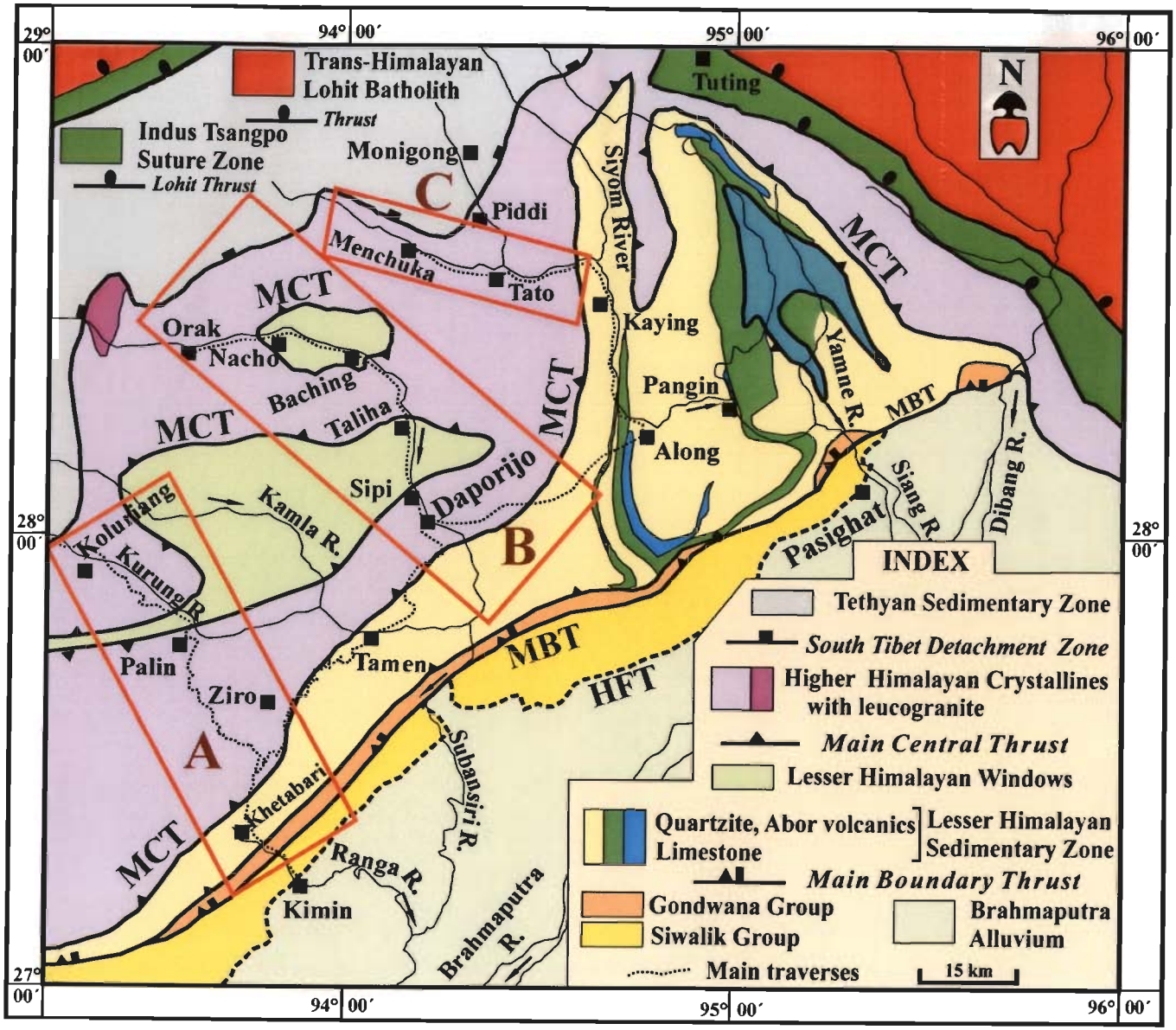

Figure 2.3: Geological map of Arunachal Himalaya (Compiled by A.K.Jain). Rectangular boxes A, B and C indicate the corridors taken for the present study.

2.3. Geology of the Subansiri and Siyom Valleys, Arunachal Pradesh

Detailed geology of the Subansiri and Siyom River Basins has been explained by previous workers (Singh and De, 1989; Singh, 1993; Singh and Jain, 2007; Choudhari et al., 2009; Yin et al. 2009b). The different units extend from Kameng District in the west to the Siang District in the east as the ENE-WSW trending units. From south to north, the following lithotectonic units are observed in this region (Fig. 2.3).

2.3.1. Siwalik Group

The Siwalik Group comprises the outermost lithotectonic unit of the Himalaya and belongs to the Cenozoic Foreland basin. In the Eastern Himalaya, it extends from Bhutan in the west to the Dibang Valley in the east. The belt rises abruptly over the Holocene Brahmaputra Alluvial Plain in the south along the Main Frontal Thrust (MFT). In the north, this belt abuts against the Lesser Himalayan sedimentary sequence, which overrides the Siwaliks along the Tipi Thrust/Main Boundary Thrust (MBT). In Arunachal Himalaya, the Siwaliks have been divided into three formations (Biswas et al., 1979; Karunakaran and Ranga Rao; 1983; Agarwal et al., 1991).

(i) The Lower Siwalik Formation or Formation I (Biswas et al., 1979) is also known by other names like the Dafla Formation and the Kimi Formation (Tripathi et al., 1983) of the Miocene age. The estimated thickness of the Lower Siwalik/Dafla Formation is around 3500 m. The lithologies in this sequence consist of discontinuous and isolated outcrops of calcareous sandstone, siltstone, claystone, silty claystone and mudstone. The sandstone also resembles the Gondwana sandstone but differs from it due to hardness, less micaceous and quartzose character.

(ii) The Middle Siwalik Formation or Formation II (Biswas et al., 1979) or Subansiri Formation comprises massive sandstone with calcareous concretions. It has an estimated

thickness of 2000 m. The characteristic sandstone sequence in this formation has a salt and pepper texture, coarse to medium-grained, grey coloured, micaceous and soft. A few claystone, shale and conglomeratic intercalations occur towards the top of the sequence. Various leaf impressions are preserved within the clays. Cross-bedding structures up to a thickness of 3 m are observed in this sequence. The sandstone of this sequence is best exposed along the Kimin-Ziro Road.

(iii) The Upper Siwalik Formation or Kimin Formation has an estimated thickness of 1450 m and is exposed all along the foothills. The sequence is comprised of alternating bands of conglomerate, soft sandstone and clays. The pebbles within conglomerate are of gneiss, quartzite and schist, which were derived by erosion of the rising Himalaya and deposited in the foreland basin by southward draining river system during the Pliocene-Pleistocene.

2.3.2 Lesser Himalayan Sequence

The Lesser Himalaya in the Arunachal Himalaya can be divided into two sequences (Singh and Jain, 2007), namely (i) Outer Lesser Himalaya and (ii) Inner Lesser Himalaya (Fig. 2.3).

(i) Outer Lesser Himalayan Sedimentary Belt: This sequence consists of the Gondwana Belt and Khetabari Formation.

(a) Gondwana Belt: The Gondwana Belt comprises a long narrow belt of sedimentary sequence, which extends from Bhutan in the west to Basar and to the north of Pasighat (Siang District) in the east. It overrides the Siwalik along the Main Boundary Thrust (MBT). The sequence has undergone mild metamorphism, intense crushing and tectonization (Agarwal et al., 1991). It contains rocks of both marine and fluvial origin.

The fluvial rocks comprise sandstone, shale and mudstone with coal beds and are termed as the Bhareli and the Khelong Formations (Acharyya et al., 1975). The marine Gondwana is named as the Garu Formation (Kumar and Singh, 1974) and comprises of carbonaceous shale, siltstone alternating with fine grained sandstone, thin basic volcanics and diamictite.

(b) Khetabari Group: This belt comprises of low grade metasedimentary sequence, which is sandwich between the Gondwana and the Himalayan Metamorphic Belt. It has been named as the Yazali Formation (Das, 1979), Khetabari Formation (Balasundram, 1972; Kumar, 1997), Migi Formation along the Kamla River, exposed to the east of Tamen (Das and Ray, 1982), or the Nikte Formation and Ragidoke Formation in the Siyom Valley (Singh, 1989). It comprises intercalated sequence of quartzite, phyllite and schist having intrusive granite gneiss between the underlying Gondwana belt and the overthrust granite gneiss. This sequence is best exposed in Tago-Potin road section and Tamen-Daporijo road section. Major rock types consist of quartzite, mica schist, carboniferous schist, phyllite and limestone. This sequence is intruded by granite bodies, which are gneissose in character and are strongly foliated.

In the Siyom Valley, the western limb of the Siyom Synform exposes the N-S trending linear belt of the Nikte Formation and Ragidoke Formation. In the Nikte Formation, quartzite sequence swings further north and extends towards Kaying. The Nikte quartzite is considered to be of Lower to Middle Paleozoic in age. These consist of purple to white quartzite and feldspathic sandstone, showing profuse development of burrow structures. Beside these, it also has polymictic and oligomictic conglomerate and purple shale (Singh and De, 1989). It preserves sedimentary structures and contains a 50 m thick polymictic conglomerate horizon. The Formation was correlated with the Miri Quartzite (Jain et al., 1974). This formation is named after Nikte village and has

maximum development along the Bine-Nikte section. This formation is unconformably succeeded by the Ragidoke Formation (Singh and De, 1989), which consists of highly weathered metavolcanics, white-light grey ash beds, brownish sandstone and siltstone, black shale and slate exposed around Ragidoke, Sododoke and Tabasara. Maximum development of this formation is in the Bame-Daporijo section. These packages are overridden by the Kaying Formation rocks of the Siyom Group (Singh and De, 1989). This is a N-S trending belt of about 1-1.5 km width. This can be best studied along the Along-Kaying, Along-Bame and Along-Kambang road section, as reported by Singh and De (1989). It consists of hard, massive to schistose and profusely jointed quartzite of white, cream and light brown colours. This is succeeded by the Pari Mountain Formation of the Siyom Group.

(ii) Inner Lesser Himalayan Sedimentary Belt: This belt comprises of series of windows, exposed beneath the overthrust Himalayan Metamorphic Belt (Fig. 2.3). In the Subansiri valley, it is exposed in two elliptical-shaped outcrops in the Menga Window in the south and the Nacho Window in the north (Singh and Jain, 2007). Earlier, this has been classified as the Menga Formation by Tripathi et al. (1982), while Singh and Jain, (2007) renamed it as the Menga-Nacho Group. This group extends to the west as the Pungrung Formation (Reddy et al., 1981) and the Chilliepam Formation (Kumar, 1997) in the Kurung valley and the Tenga Formation (Kumar, 1997) in the eastern Kameng. The Menga-Nacho Group contains the following units:

(a) Menga Dolomite: It derives its name from the Menga River (Tripathi et al., 1982) and contains light to buff colored massive and hard siliceous dolomite, dolomitic limestone, having irregular masses of pink limestone and white marble. Tewari (2001, 2003) have suggested a Terminal Proterozoic age for the dolomite and

associated limestone with this sequence on the basis of microfossils, sedimentary facies, carbon isotopic excursions and stromatolites. The dolomite is best exposed in one of the adits of the Upper Subansiri Dam Site at Menga.

(b) Nacho Slate: It is an oval-shape sedimentary outcrop exposed in the upper reaches of the Subansiri valley around Nacho. It is characterized by an association of low grade metamorphosed to un-metamorphosed sequence of dark grey to blackish, brownish black shale, grey siltstone, grey slate-phyllite and thin grayish white quartzite intercalations. The Nacho Slate is best exposed on either limbs of the Menga Antiform as very low grade metamorphosed sequence. The grade of metamorphism is distinctly more in the core of the antiform around Nacho than around Sipi.

(c) Sipi Quartzite: The Sipi Quartzite comprises a brownish yellow, grey and white, fine to medium grained flaggy quartzite with biotite-muscovite bearing schistose phyllite intercalations. Sedimentary characters are well preserved in the quartzite exposure near the Sipi Village along the Daporijo–Taliha road section. The preservations include detrital grains, faint bedding and cross-bedding. This sequence is more metamorphosed between Mara and Taliha on the northern limb of the Menga Antiform, while wide exposure of the Sipi Quartzite in the upper Subansiri region is in the muscovite grade of metamorphism. A few deformed thin bands of tourmaline-bearing granite gneiss occur within the Sipi Quartzite to the north of Kobaso Nala (Tripathi et al., 1982).

The Sipi Quartite possibly extends along the strike towards west and is exposed to the north of Palin at Pungrung. Detrital zircon grains from this formation near this locality are between 1600 to 2000 Ma in age (Yin et al., 2009a) and led these authors to postulate that this formation was unconformably deposited over the ca. 1750 Ma gneissic basement.

2.3.3. Himalayan Metamorphic Belt

The Himalayan Metamorphic belt (HMB) in Arunachal Himalaya comprises of medium-high grade metamorphic rocks, which are thrust over the Lesser Himalayan sedimentary sequence along the folded Main Central Thrust (MCT) and its splays (Singh and Jain, 2007). The rocks are essentially gneissic in character and contain garnetiferous mica schist, kyanite-sillimanite-bearing schist and gneiss, migmatite and leucogranite. This belt mainly constitutes the Proterozoic and a few Paleozoic granitoids, and is intruded by late Cenozoic leucogranite in extreme northern parts. The erosion of this folded sequence has exposed the Lesser Himalayan windows in the north and metamorphic klippe, both in the north and south. The various units of the HMB are as follows.

(i) Lesser Himalayan Daporijo Gneiss: This sequence comprises gneissose granite of batholitic dimension and occupies the southernmost part of the HMB. It extends from the west in Kameng as a part of Bomdila Group to Ziro-Hapoli region and further towards ENE in the Siang Valley. It has been variously named as the Ziro Gneiss, the Palin Gneiss, Chakoo or the Bomdila Gneiss (Kumar, 1997). This is equivalent to part of the Lesser Himalayan Crystalline series of Chaudhari et al. (2009). The Daporijo Gneiss overrides the Lesser Himalayan sedimentary sequence along the southernmost exposure of the MCT/Tamen Thrust. Recent observations pertaining to this unit along the Hapoli-Geevan road section by Yin et al. (2009a) have revealed presence of many low grade metamorphic bands, within gneiss, and have been considered to be the part of the Lesser Himalayan Sedimentary Belt on the footwall of the MCT (Fig. 2.4). The type locality of the Daporijo Gneiss at Daporijo is comprised of highly contorted and mylonitized

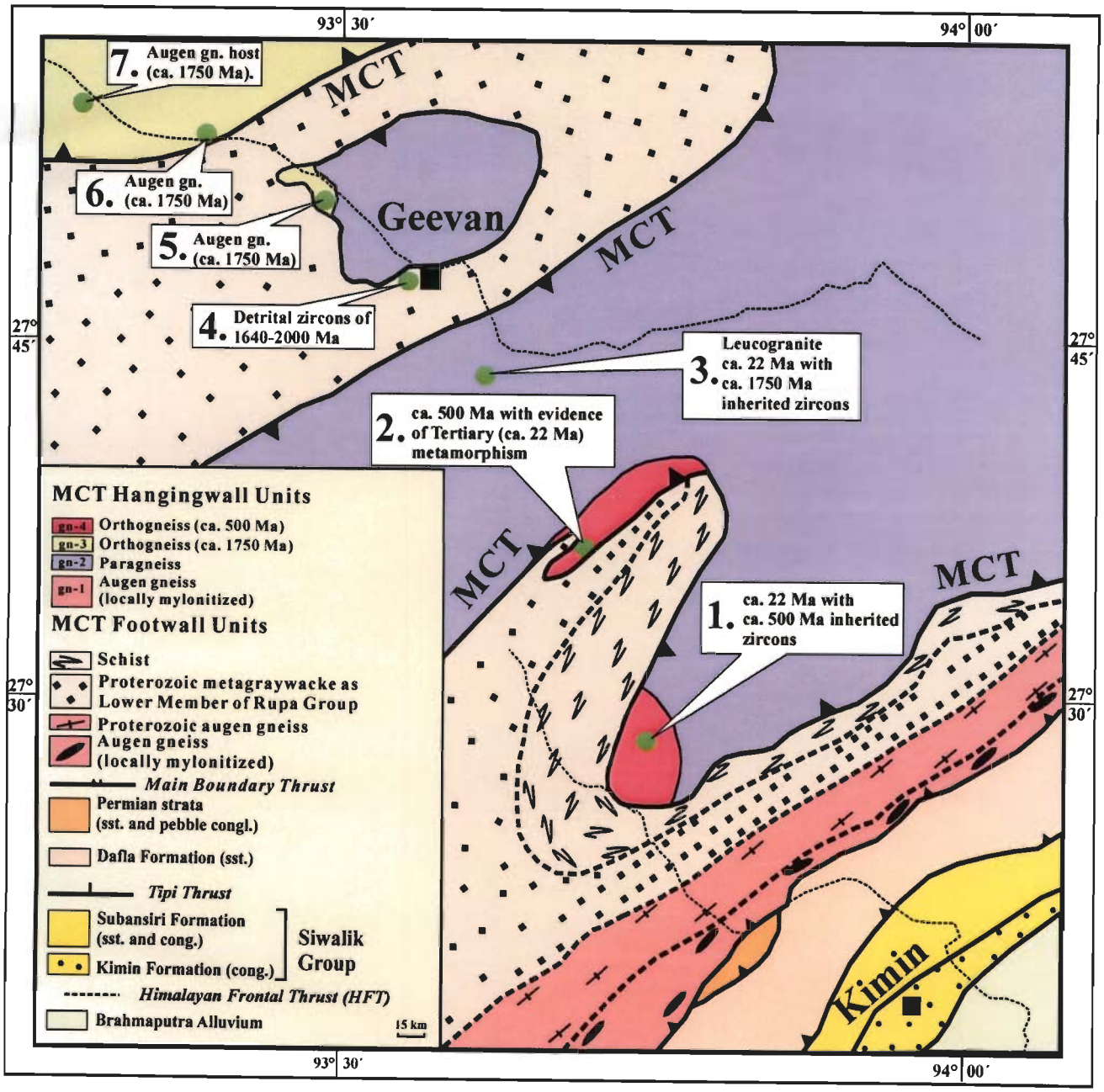

Figure 2.4: Simplified geological map of the Kimin-Geevan road section of western Subansiri showing folded Main Central Thrust and U-Pb zircon ages (After Yin et al., 2009a).

streaky, banded and augen gneiss, having very strong development of mylonitic foliation and an associated mineral/stretching lineation (Singh and Jain, 2007). The quartz and feldspar crystals in the rock dominantly reveal top-to-SW sense of ductile shearing in these mylonitic gneisses. In western Kameng district, biotite gneiss have been dated as 1644±40 Ma and 1676±122 Ma, using the Rb-Sr isochron method (Bhalla and Bishui, 1989), while the Bomdila Gneiss has been dated as 1914±23 Ma with a younger phase of 1536±60 Ma (Dikshitulu et al., 1995). This gives a clue that the Daporijo Gneiss should be of Mesoproterozoic in age between 1500 Ma-1900 Ma. Along the Kimin-Geevan section, Yin et al. (2009a) obtained U-Pb ages of ca. 1750 and 500 Ma inherited zircon within leucogranite of ca. 22 Ma and evidences of the Cenozoic metamorphism of this age within the Daporijo Gneiss by laser-ablation-ICPMS (Fig. 2.4).

(ii) Higher Himalayan Crystallines (HHC): The highest grade metamorphic rocks in the upper reaches of the Himalaya are called as Higher Himalayan Crystallines (HHC) (Le Fort, 1975 and Pêcher , 1977, 1989). In the Arunachal Himalaya, this sequence has been named as the Sela Group in western Kameng after the Se La Pass. This group has been mapped in higher reaches of Kurung, Kamla, Subansiri and Siyom Rivers (Kumar, 1997; Singh and De, 1989; Singh, 1993; Singh and Jain, 2007; Chaudhari et al., 2009; Yin et al. 2009a). It is divided into the Taliha and Galensiniak Formations (Kumar, 1997; Singh and Jain, 2007) in the Subansiri Valley and Pari Mountain Formation and Piddi Formation in the Siyom Valley (Singh and De, 1989). The HHC is intruded by young hornblende granite of 481±23 Ma (Dikshitulu et al., 1995) and tourmaline granite of 29±7 Ma (Bhalla et al., 1990) in Kameng and by the Maza Granite in the Upper Subansiri Valley.

(a) Taliha Formation: This sequence is exposed between Taliha and Baching in the Subansiri River valley. The rock types of this sequence comprise graphitic schist, well-

foliated garnetiferous schist/gneiss, kyanite-sillimanite bearing schist/gneiss, calc silicates and migmatite (Kumar, 1997; Singh and Jain, 2007). These schist and gneiss have well-developed porphyroblastic growth of garnet, kyanite and sillimanite and provide a clue of high-grade metamorphism at least up to sillimanite-muscovite grade in the Taliha Formation rocks. In the Kurung River valley, the Taliha Formation is known as the Palin Group (Reddy et al., 1981).

(b) Galensiniak Formation: This sequence is exposed in the upper reaches of the Kurung and Subansiri Rivers and is predominantly comprise gneissic bodies. They were first mapped by Dutta (1982) and Dutta et al. (1983) around Galensiniak. This formation includes biotite gneiss, garnetiferous biotite gneiss containing kyanite and sillimanite, calc-silicates and amphibolite, migmatite and intercalated schist of different types. This Formation shows inverted metamorphism (Singh and Jain, 2007). Recent U-Pb zircon dating of 2 samples by LA-ICPMS has yielded ca. 1750 Ma ages from the MCT hangingwall of the MCT along the Kurung River near Koluriang (Yin et a., 2009a).

(c) Pari Mountain and Piddi Formation: In the upper reaches of the Siyom valley to the northwest of Kaying, the metamorphic belt consists of gneiss and migmatite, which are named as the Pari Mountain Formation (Singh and De, 1989) after the Pari Mountain (4660 m). The lower part mainly comprises kyanite-sillimanite bearing gneissic sequence, while an upper sequence consists of garnet-staurolite-kyanite and sillimanite-bearing graphitic and pelitic schist, micaceous quartzite, calc-silicates, amphibolite boudins and gneiss. Various types of gneisses are exposed in this sequence, which include quartzo-feldspathic gneiss, biotite gneiss, augen gneiss, banded gneiss and migmatite. The migmatite has been observed near Tato and exhibits augen, boudin, stromatic, agmatic and schiller structures. This formation is also invaded by tourmaline-bearing pegmatite

and granite (Singh and De, 1989).

The Piddi Formation is exposed in the upper reaches of the Siyom Valley and well described by Singh and De (1989). It comprises massive to schistose quartzite intercalated with biotite schist. Its trend deflects from NE-SW to E-W. Thin quartz veins are ubiquitous along the foliation.

(d) Maza Granite: Tongues and apophyses of tourmaline-bearing granite, pegmatite and aplite intrude the metamorphics in the upper reaches of Subansiri River and Tsari Chu (Singh and Jain, 2007). This is extensively cut across by tourmaline-bearing leucogranite-the Maza Granite further north (Singh et al., 1986). Biotite gneiss and hornblende gneiss are also observed in this sequence. Hypidiomorphic granular texture of quartz, orthoclase and sodic plagioclase characterize this granite with myrmekitic intergrowth. Bhalla and Bishui (1989) dated such intrusions into the Lum La Formation in the west as 29±7 Ma. A few leucogranite bodies within the Lesser Himalayan Daporijo Gneiss yielded U-Pb zircon ages of ca. 22 Ma along the Kimin-Geevan section (Yin et al., 2009a).

2.3.4. Tethyan Sedimentary Zone

The Tethyan sequence in the Arunachal Himalaya includes the Lum La Formation in the Kameng region, the Sarli Formation in the Kurung River Valley (Reddy et al., 1981), the Takshing Formation in the upper Subansiri Valley (Kumar, 1997; Singh et al., 1997) and the Monigong Formation or part of the Singing Formation in the Siang region (Singh and De, 1989; Singh, 1993). This sequence lies over the HMB and comprises of metasedimentary rocks. It includes schistose quartzite and interbedded with staurolite-biotite schist, garnet-biotite schist, calc silicates with minor amount of amphibolite.

(i) Takshing Formation: It is exposed in the upper part of the Subansiri Valley near the Indo-Tibetan border (Singh et al., 1997). This formation is mainly characterized by white

to light grey, fine grained schistose quartzite having strongly oriented quartz, muscovite and biotite. These alternate with biotite-muscovite schist and thin bands of staurolite-garnet schist (Singh et al., 1986). In the Kurung River valley, it is named as the Sarli Formation and has pelite-psammite alterations (Reddy et al., 1981).

(ii) Monigong Formation: The Monigong Formation has been divided into the Lower Monigong and the Upper Monigong Formations. The former comprises marble with intercalation of black slate and graphite schist. The Upper Monigong differs from the lower part in having more abundance of quartz-muscovite schist and quartz-biotite schist bands. This formation covers part of the Singing Formation as described by Singh (1993).

2.4. Tectonics

A geological profile along the along the Subansiri Valley (Singh and Jain, 2007) describes the relationship of various tectonic units in the Arunachal Himalaya (Fig. 2.5). The Siwalik Group rises abruptly over the Brahmaputra Alluvium along the Main Frontal Thrust (MFT). Further north, the Permian Gondwana Belt overrides the Siwalik Group along the Main Boundary Thrust (MBT). The Lesser Himalayan metasediments are separated from the Himalayan Metamorphic Belt (HMB) along the folded Main Central Thrust (MCT). The southernmost exposure of the MCT is locally named as the Tamen Thrust. In the upper reaches of the Subansiri River, the folded HMB gets eroded of, leading to the exposure of the underlying Lesser Himalayan sequence in two windows. The MCT is again exposed near Taliha and Nacho and separates the high grade metamorphics of the Higher Himalayan Crystalline from the Lesser Himalayan sedimentary belt. Further north, the HHC unit is separated from the Tethyan Sedimentary Sequence by the South Tibetan Detachment Zone (STDZ).

2.4.1. Main Frontal Thrust (MFT)

The Main Frontal Thrust (MFT) marks the boundary between Holocene

Brahmaputra Alluvium in the south and the Siwalik Group of the Cenozoic Foreland Basin. This tectonic boundary has been identified as a high angle reverse fault, which is not continuously exposed along its ENE-WSW strike (Agarwal et al., 1991). Within this belt, east-plunging folds are common, while the Tipi Thrust separates the older Miocene Dafla Formation from the underlying Pliocene Kimin Formation.

2.4.2. Main Boundary Thrust (MBT)

The term Main Boundary Thrust (MBT) was coined by Medlicott (1864) for the western Himalaya and is defined as the thrust placing the Lesser Himalayan sequence over the Cenozoic sedimentary strata (Heim and Gansser, 1939). This boundary thrust parallels the ENE-WSW trending Main Frontal Thrust (MFT), and demarcates the NNW-dipping and narrow Gondwana Belt from the Siwalik Belt along the southern boundary. It is a north-dipping steep thrust. Ranga Rao (1983) joined this boundary with the Mishmi Thrust in the northeast. It has also been known by local name like Dafla thrust, which demarcates the southern boundary of the Gondwana Belt with the Siwalik Belt (Agarwal et al., 1991).

2.4.3. Tamen Thrust

In the Subansiri Valley, high grade metamorphics override the Lesser Himalayan Sedimentary Zone along a well-demarcated folded thrust. The southernmost exposure of this thrust surface has been called as the Tamen Thrust, named after the locality Tamen (Singh and Jain, 2007). Best exposure of this thrust can be observed near village Tago on the Kimin-Ziro road section and all along the Tamen-Daporijo road section.

2.4.4. Sipi Thrust

In the Subansiri Valley, the Daporijo Gneiss overrides the Sipi Quartzite of the Menga Window along a thrust contact. This tectonic contact has been called as the Sipi

Thrust (Singh and Jain, 2007). It runs all along the Sipi River and extend towards the Kamla and Kurung Valley.

2.4.5. Siyom Thrust

This thrust tectonically juxtaposes the Ragidoke and Nikte Formations with that of Kaying Formation and are considered to be equivalent to the thrust which separate Lesser Himalayan metasediments with that of Gondwana (Singh and De, 1989).

2.4.6. Main Central Thrust (MCT)

The Main Central Thrust (MCT) is the most important tectonic boundary in the Himalaya and has various criteria for demarcating this thrust (Yin, 2006). For example, the thrust may be identified along the lithological contact separating the LHS below from the HHC above (Heim and Gansser, 1939). At places, it may be identified by an abrupt change in metamorphic grade (Le Fort, 1975; Pêcher , 1977, 1989). Alternatively, it may also be defined as the surface or the basal surface of a broad ductile shear zone several kilometers thick across the uppermost part of the LHS and the lowermost part of the GHC (Arita, 1983; Jain and Anand, 1988; Pêcher, 1989; Searle et al., 2003).

Along the Subansiri Valley, the main exposure of the MCT has been observed around Taliha, where low-grade metamorphosed quartzite-phyllite alterations of the Sipi Quartzite are overridden by the garnetiferous and kyanite-sillimanite schist/gneiss. The thrust is folded into a synform between Taliha and Baching and is again exposed around Nacho into an antiform; erosion of this nappe has produced the Menga and Nacho Windows. Yin et al. (2009a) have shown this thrust as a folded unit and joined it with the southern boundary of the MCT around Menga Window.

The placing of the MCT at different locations in this region is based on (i) distinct lithological changes at the boundary, (ii) abrupt change in the metamorphic grade, i.e.

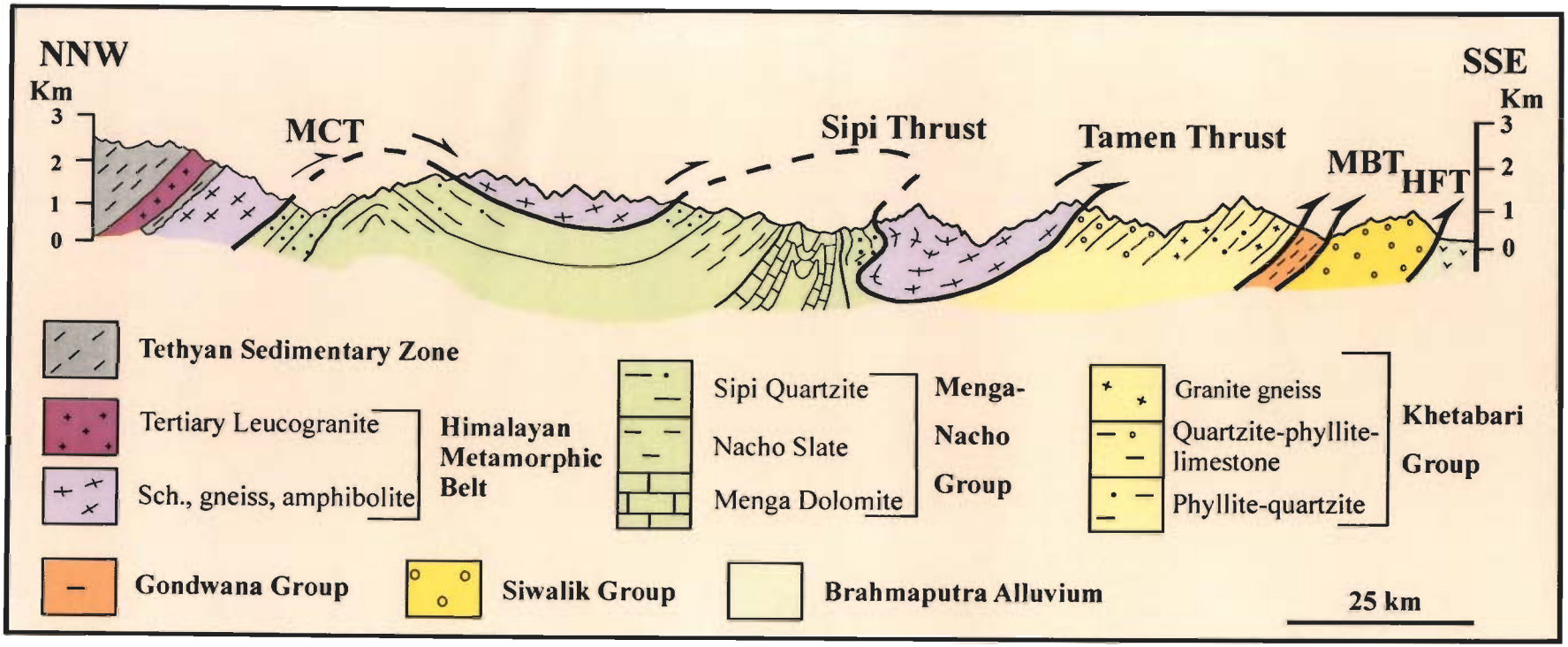

Figure 2.5: Geological cross section across Subansiri Valley, Arunachal Himalaya

garnet-bearing schist or quartzo-feldspathic gneiss over the low grade metasediments with distinct lithology, (iii) appearance of leucogranite as a proxy for the presence of high grade rock in the hanging wall of the MCT, and (iv) shear zone deformation and variation of strain (also Yin et al., 2009a).

2.5.7. South Tibetan Detachment Zone (STDZ)

The South Tibetan Detachment Zone was first observed by Caby et al. (1983), Burg and Chen (1984) and Burchfiel and Royden (1985) in Nepal, where a series of north-dipping normal faults separate the overlying Tethyan Sedimentary Zone from the HHC rocks. In the present study, the exposure of this thrust system could not be reached, but various works are available in this detachment system in the other part of the orogen.

Chapter 3: Rb-Sr Dating

3.1. Introduction

The rate of various geodynamic processes is very important in constraining various events with respect to time. Thermochronology is the tool which provides the opportunity to constrain various processes over geological past. For better understanding and quantification of exhumation of different terrains, radiometric thermal ages are significant and provide the cooling history of the terrain. It is based on the fact that different radiometric systems for different minerals have different closure temperatures (Table 3.1), which is the temperature below which isotopes in a system (mineral) behave as a close system and the radiometric dating clock starts. Different thermochronometer that are commonly used today are Rb/Sr (muscovite, biotite), Ar^{40}/Ar^{39} (amphibole, mica, k-feldspar), fission track (zircon, apatite), U-Th/He (zircon, apatite) etc. in order of decreasing closure temperatures. These technique have closure temperature ranging from as low as 60-70^{O} C to as high as >500^{O} C (Table 3.1). Different systematics are taken up based on the rock types and objective of the experiment. Application of multi-geochronometer can give a precise and highly resolved thermal history of a terrain (Dodson, 1973, 1981; Dickin, 1995; Faure, and Mensing, 2005)

Rb-Sr dating has developed as one of the most important technique adopted by the geological community (Jager et al., 1971; Mehta, 1977; Inger, 1988; Miyazaki et al., 2000; Masaudi et. al., 2002). This system is mainly used for dating acid plutonic rocks and other k-bearing minerals. The whole rock isochron gives the crystallization ages of the rock, whereas mineral ages give the cooling and exhumation of a geologic unit because these record the last geothermal event.

Table 3.1: Closure temperatures of different minerals and radiometric systems.

Sr. No.	Radiometric System	Minerals	Closure Temperature (^{O} C)	References
1.	Rb-Sr	Muscovite	500-550	Dodson (1981), Inger and Cliff (1994), Freeman et al. (1997)
		Biotite	310-320	Dodson (1973), Dodson (1981), Dodson and McClellad-Brown (1985)
2.	$^{40}Ar/^{39}Ar$	Hornblende	400-600	Harrison (1981), Dahl (1996).
		Biotite	350-400	Harrison et al. (1985), Grove and Harrison (1996)
		Muscovite	300-350	Robbins (1972), Hames and Bowring (1994)
		K-feldspar	150-350	Foland (1994), Lovera et al. (1991, 1997)
3.	Fission track	Titanite	380-420	Naeser and Faul (1969), Watt and Durani (1985)
		Zircon (natural)	232	Brandon and Vance (1992), Brandon et al. (1998)
		Zircon (zero-damage)	330-342	Tagami et al. (1998), Rahn et al. (2004)
		Apatite	90-135	Laslett et al. (1987), Ketcham et al. (1999), Patel and Carter (2009), Thiede et al. (2009)
4.	U-Th/He	Titanite	160-220	Reiners and Farley (1999)
		Zircon	160-200	Reiners et al. (2004)
		Apatite	55-80	Farley (2000)

A few Rb-Sr whole rock ages of the Lesser Himalayan Crystalline unit in Arunachal Himalaya reveal a crystallization range of 1536-1914 Ma (Bhalla and Bishui, 1989; Dikshitulu et al., 1995) suggesting an involvement of the Mesoproterozoic basement of 1900-1500 Ma (Singh and Jain, 2007). Recent geochronological work in western Kameng District of the Arunachal Himalaya has revealed episodic igneous and metamorphic events. Along

the Bhalukpong-Zimithang section, the $^{207}Pb/^{206}Pb$ ages of 1743±4 Ma in the Lesser Himalayan Crystalline Belt and 878±12.6 Ma for the HHC are reported (Yin et al., 2009a). The latter is signified by a metamorphic event at 627.6 Ma (Yin et al., 2009a) These ages agree with the earlier published detrital zircon U-Pb ages, which clustered around 1400 Ma and 1700 Ma (Yin et al., 2006) although it had an age range of 950 to 2960 Ma for metasedimentary samples collected around Lumla and Dirang (Yin et al., 2006). Further eastwards along the Kimin-Geevan section, the $^{207}Pb/^{206}Pb$ age of about 1750 Ma were recorded for mylonitic augen gneiss in both the hangingwall and footwall section of the MCT around Geevan, while orthogneiss in the MCT hangingwall around Hapoli indicated $^{207}Pb/^{206}Pb$ age of about 500 Ma. These bodies were intruded by leucogranite at later stages at around 373 Ma and 22 Ma (Yin et al., 2009a).

In the present study, Rb-Sr dating of biotite and muscovite pairing with whole rock has been adopted to work out the exhumation history of the rocks from the Arunachal Himalaya (Fig. 3.1). For this study, the closure temperatures of 300±50^{O} C for Rb-Sr (biotite) (Dodson, 1973; Dodson and McClellad-Brown, 1985) and 550^{O} C for Rb-Sr (muscovite) (Inger and Cliff, 1994; Freeman et al., 1997) have been used.

3.2. Geochemistry of Rb and Sr

In the earth, both Rb and Sr are present in trace amounts in a wide variety of rocks, and most abundantly in acidic rocks. The detail geochemical properties of these two elements are given in Table 3.2. Rb is an alkali metal (1A) with ionic radii 1.48 A^{0} and atomic weight of 85.8346 a.m.u. It has two naturally occurring isotopes $_{37}Rb^{85}$ (72.1654%) and $_{37}Rb^{87}$ (27.8346%), of which $_{37}Rb^{87}$ is radioactive having a half life of 48.8 x 10^{9} years. This decays

to $_{38}Sr^{87}$ with decay constant (λ) of $1.42x10^{-9}$ yr^{-1}. The ionic radius of Rb^{+} is similar to that of K^{+} (1.33 A) to allow it to substitute for K^{+} in all K-bearing minerals like mica, k feldspar, evaporates such as sylvite and carnalite etc (Faure and Mensing, 2005).

On the other hand, Sr is an alkali earth element (IIA) with atomic radii of 1.13 A^0 and atomic weight 87.62 a.m.u. with valency of +2. It has four stable and naturally occurring isotopes $_{38}Sr^{84}$, $_{38}Sr^{86}$, $_{38}Sr^{87}$and $_{38}Sr^{88}$ with isotopic abundance of 0.56%, 9.87%, 7.04% and 82.53%, respectively out of which $_{38}Sr^{87}$ is radiogenic daughter isotope, produced by decay of $_{37}Rb^{87}$. Apart from this, $_{38}Sr^{87}$ in the rock can also be incorporated during the formation of rock, which is known as initial strontium along with other isotopes. The ionic radius of Sr is similar with that of Ca (0.99 A^0), therefore Sr can replace Ca in Ca-bearing minerals. The ability of Sr^{2+} to replace Ca^{2+} is somewhat restricted by the fact that Sr ions favor eight-fold coordinated sites, whereas Ca ions can be accommodated in both six- and eight-fold coordinated lattice sites because of their smaller size. Sr^{2+} ions can be captured in place of K^{+} ions by k-feldspar, but the replacement of K^{+} by Si^{+} must be coupled by the replacement of Si^{4+} by Al^{3+} to preserve electrical neutrality. They occur in mineral like plagioclase, aragonite, apatite etc (Faure and Mensing, 2005).

3.3. Rb-Sr decay scheme

The Rb and Sr are joined in a parent-daughter relationship by beta emission, in which ^{87} Rb decays to stable ^{87}Sr, as shown in the following equation:

$$_{37}Rb^{87} \rightarrow {}_{38}Sr^{87} + \beta^{-} + \nu + Q \qquad (3.1)$$

where 'ν' is the antineutrino, and 'Q' is the decay energy (=0.275 MeV).

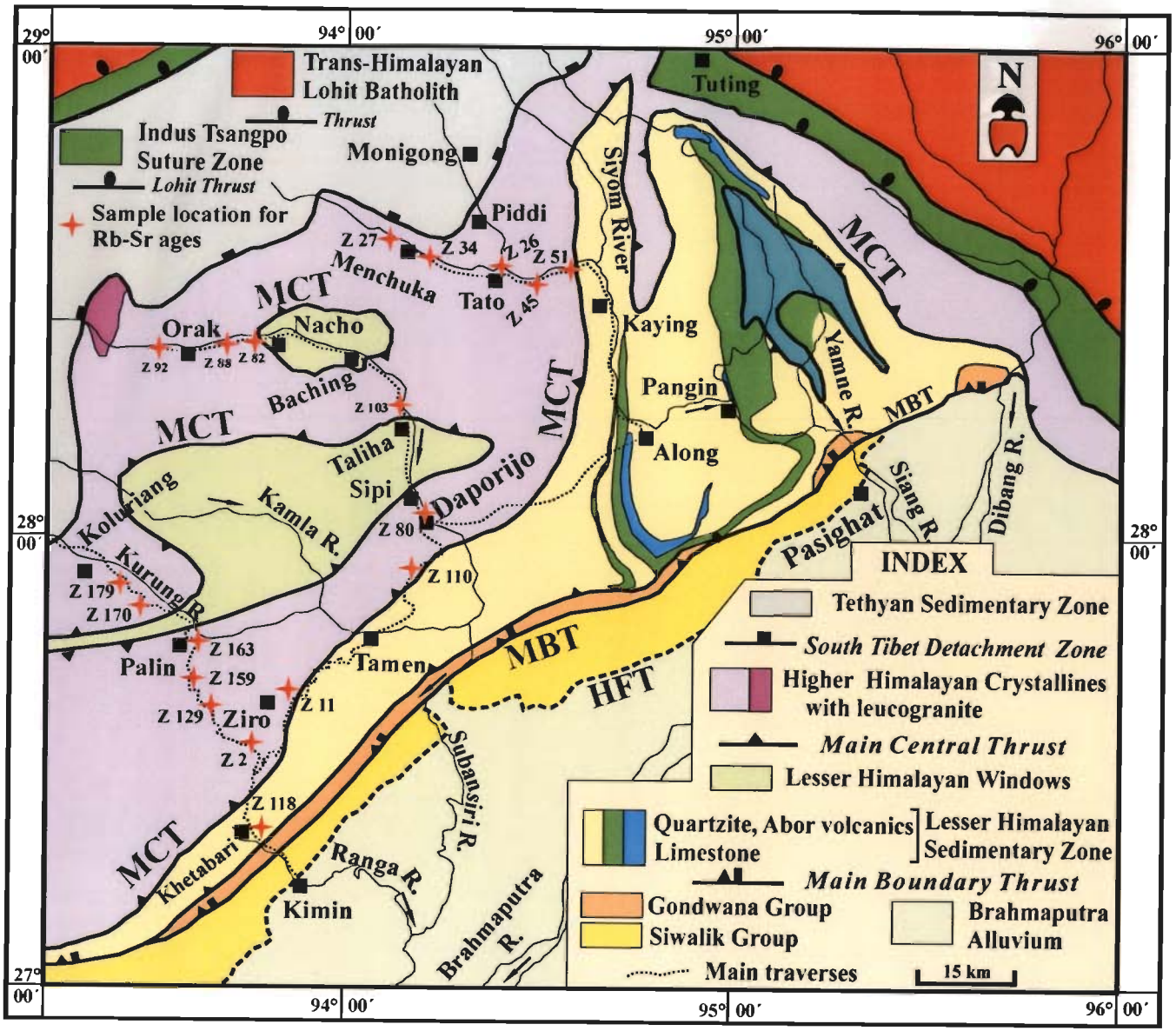

Figure 3.1: Geological map of the Subansiri and Siyom Valley showing location of samples fo the Rb-Sr biotite and muscovite ages.

Table 3.2 Geochemical properties of Rb and Sr (Faure, 1989).

Chemical properties	Rubidium (Rb)	Strontium (Sr)
Position in periodic table	Alkali metal (1A)	Alkali earth (IIA)
Atomic weight (a.m.u.)	85.8346	87.62
Ionic radius (A^0)	1.48	1.13
Relative density	1.53	2.583
Melting point(^{0}C)	38.9	770
Boiling point (^{0}C)	705	1390
Isotopes (abundance in %)	$_{37}Rb^{85}$(72.1654) $_{37}Rb87^{87}$ (27.8346)	$_{38}Sr^{84}$ (0.56) $_{38}Sr^{86}$ (9.87) $_{38}Sr^{87}$ (7.04) $_{38}Sr^{88}$ (82.53)
Occurrences	Micas, clays, feldspars and evaporates such as sylvite and carnalite	Plagioclase, aragonite, apatite etc.

The decay energy is very low, which has always caused problems in the accurate determination of the Rb decay constant (Dickin, 1995). There are number of workers, who came out with different values of decay constant of ^{87}Rb, but currently worldwide accepted value is the one submitted by Steiger and Jager (1977) in International Union of Geological Sciences (IUGS). The values are

Decay constant of $^{87}Rb = 1.42x10^{-11}\ y^{-1}$

Half life period of $^{87}Rb = 48.8x10^{9}$ years.

The mathematical equation, which relates radioactivity to geologic time, is

$$D = D_0 + N\,[e^{\lambda t}-1] \qquad (3.2)$$

where, t=age of the sample,

D=number of atoms of the daughter isotope in the sample,

D_0=number of atoms of the daughter isotope in the original composition,

N=number of atoms of the parent isotope in the sample,

λ=decay constant of the parent isotope,

The above equation makes use of information on the composition of parent and daughter isotopes at the time of formation. For Rb and Sr systematic, the equation can be shown in a rock which has remained closed for time t years can be expressed as

$$^{87}Sr = {}^{87}Sr_i + {}^{87}Rb\,[e^{-\lambda t}-1] \qquad (3.3)$$

In the equation (3.3) it is extremely difficult to measure absolute concentrations of atom by mass spectrometry, whereas, determinations of isotopic abundance ratios are much easier. Therefore, the equation is normalized with respect to a non-radiogenic isotope of Sr (Sr^{86}), the concentration of which is, therefore, assumed to remain unchanged throughout geological time. In this case, we can re-write the equation 3.3 as;

$$[^{87}Sr/^{86}Sr] = [^{87}Sr/^{86}Sr]_i + [^{87}Rb/^{86}Sr]\,[e^{-\lambda t}-1] \qquad (3.4)$$

The equation 3.4 represents an equation of a straight line, and forms the general age equation for the decay of ^{87}Rb to ^{87}Sr. This straight line has co-ordinates $[^{87}Rb/^{86}Sr]$ on the X- axis and $[^{87}Sr/^{86}Sr]$ on the Y-axis. The slope of this line gives the age and the intercepts on the Y-axis gives the initial $[^{87}Sr/^{86}Sr]$ ratio. In order to obtain data to construct this line, it is necessary to analyze a suite of samples by mass spectrometry to determine their $[^{87}Sr/^{86}Sr]$ ratios. The stable isotope ratio $[^{87}Rb/^{86}Sr]$ is normally determined by analyzing the bulk elemental concentration of Rb and Sr and then calculating the $[^{87}Rb/^{86}Sr]$ ratio from the known natural isotopic abundance of these elements. If the suite of rocks all crystallized at the same time and possesses a sufficient range of Rb and Sr concentrations or different minerals of a sample along with whole rocks are taken, then a plot of $[^{87}Sr/^{86}Sr]$ vs.

[$^{87}Rb/^{86}Sr$] will from a straight line called an isochron. The age of the sample may then be calculated from the slope of this line and the initial strontium ratio [$^{87}Sr/^{86}Sr]_i$ measured from the intercept (Faure, 1989). Since numerous points are taken for the construction of an isochron, may not necessarily fall in a perfect line, numerous regression method of line fitting are used (Mclyntyre et al., 1966; York, 1966, 1969; Brooks et al., 1972). However, if the scatter is beyond the tolerance limit, the line is called an errorchron and, thus, raised the presence of geological error. The concept of mean square weighted deviates (MSWD) was introduced by Yorks (1969) and Brooks et al. (1968, 1972) to identify relation between geological and analytical errors. When the scatter of data points precisely agrees with the predicted analytical errors, the MSWD=1. But if there is an excess scattering from the experimental errors, the MSWD>1 and less scattering gives MSWD<1. To separate out an errorchron from the isochron, a thumb rule has been introduced in which MSWD<2.5 is considered as isochron, otherwise it is errorchron (Brook et al., 1972). However, it is expected to get the MSWD close to unity in most of the cases to have a high degree confidence isochron (Dickin, 1995).

3.4. Methodology

3.4.1. Sample preparation

The selection and preparation of samples forms a very important stage of the any geochronological studies. Similarly, the preparation of samples for the Rb-Sr dating, one has to be very careful, starting from selection of the sample till the completion of the analysis. During whole procedure of sample treatment and chemical separation, precautions were taken to eliminate cross-contamination. Different stages of analysis are given below.

(i) Stage 1-Crushing: First, all the weathered parts of the sample were removed in the field as well as in the lab by hammer. One piece of each sample was kept for future reference. Remaining parts were crushed by using hammer in order to make them ready to use in the jaw crusher (Fritsch Pulverisette, Fig. 3.2 A). Before crushing, each surface of the jaw crusher was thoroughly cleaned with vacuum cleaner and metallic brush in order to avoid the contamination. The samples are crushed in different stages by reducing the spacing from 5 to 1 in the jaw crusher. After crushing, the samples were sieved with 60 mesh sized pan.

(ii) Stage 2-Coning and Quartering: The sieved fraction (<60 mesh) was collected in a clean white paper followed by homogenization of the sample by mixing it thoroughly. Coning and quartering of the sample was done using two mica sheets. One of the parts was taken and again coning and quartering was performed in order to obtain sufficient amount. After this, the final portion was divided in to two parts: one for the whole rock analysis and the rest for mineral separation.

(iii) Stage 3-Grinding: A small portion of the sample was taken in a ball mill (Retchs-100, Fig. 3.2 B) for getting it finer for the whole rock analysis. This portion was taken in such a way that it should represent the whole rock composition. The whole rock part of each sample was kept in two tungsten jars. Ten small balls also were put in to the jar. The sample amount should be up to the level in which the balls were seen. The ball mill was run at 500 rpm speed for 45 minutes. The sample has been again taken to agate mortar for hard grinding, when the sample was powdered very fine, then it was kept for digestion.

For the mineral separation, the samples were run in the same ball mill, but the speed was 250 rpm for 15 to 20 minutes. In mineral separation, two large tungsten balls were used

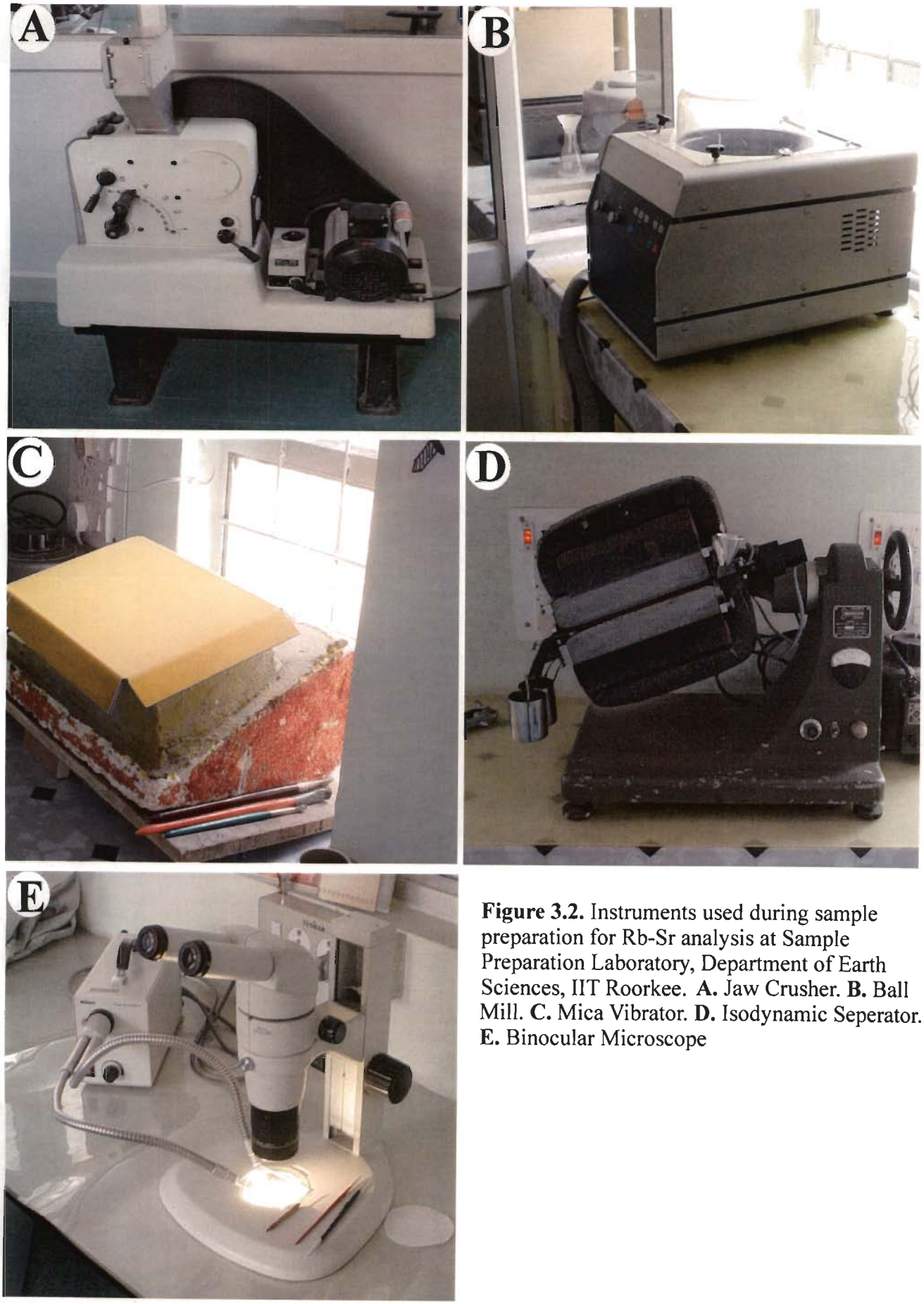

Figure 3.2. Instruments used during sample preparation for Rb-Sr analysis at Sample Preparation Laboratory, Department of Earth Sciences, IIT Roorkee. **A.** Jaw Crusher. **B.** Ball Mill. **C.** Mica Vibrator. **D.** Isodynamic Seperator. **E.** Binocular Microscope

instead of ten small balls. Each time samples were sieved and the fraction between 60 mesh and 170 mesh was kept for mineral separation.

(iv) Stage 4-Mineral separation: The 60 to 170 mesh samples were cleaned in distilled water to remove the dust. The cleaned fractions were carried to a mica vibrator (Fig. 3.2 C) where minerals were separated on the basis of roundness of minerals. Most of the quartz and feldspars (rounded) and mica (flat) minerals were separated in mica vibrator. The mica-rich portion was further cleaned in isopropyl alcohol along with mild crushing in the agate mortar to make a portion free from composite grains in the sample. Fractions were collected and dried down and were taken to Frantz Magnet Isodynamic Separator (Fig. 3.2 D), where the mineral grains were allowed to pass through a magnetic field, which removed minerals on the basis of their susceptibilities. The magnetic field was set up at 0.5 ampere with a constant tilt of 18°, followed by 0.7 ampere and 22° slope. By this process, biotite-rich portion was separated from quartz, feldspar and muscovite fractions. Further, quartz, muscovite and feldspar-rich portions were run at 14° slope and 1.3 ampere by which muscovite-rich portions were separated from quartz and feldspar. During the magnetic separation, precaution was taken to clean the interior of the isodynamic separator. Finally, pure biotite and muscovite were separated by hand picking with the help of a binocular microscope (Fig. 3.2 E). Now, the sample was ready for digestion.

3.4.2. Sample dissolution for the Rb-Sr analysis

The dissolution process for the Rb-Sr analysis consists of HF-HNO_3-HCl treatment. This is adequate for Rb-Sr-bearing phases and sample-spike equilibrium. High pressure is not necessary in this case, as refractory phases do not contain significant amount of Rb or Sr,

however it was taken into account to make clear solution. A set-up for sample dissolution unit is given in Figure 3.3 A. The dissolution steps are as follows:

(i) Batch of four samples was taken at one time in the Teflon vials (Savillex®) with proper identification. Teflon vials were equilibrated with the balance room temperature for at least one hour. Vial and sample numbers were systematically noted down in the logbook.

(ii) Sample powder of about 50 to 100 mg was weighed on the butter paper and then transferred into the vial. The weight was then cross-checked.

(iii) For mica, the ~50 mg samples were weighed and leached to remove any surficial contamination. For this a few drops of 2N HCl were put into the sample and mixed properly by mildly shaking the vial. Then, it is left to stand for 15-20 minutes. The supernatant was pipetted out. Each sample was washed three times by putting MQ water, which was pipetted out repeatedly. For every sample we used different pipette to avoid cross contamination. The sample is dried in the hot plate. Finally, the sample weight is measured and noted down in the log book.

(iv) A few drops of MQ water (Milli-Q water 20 times purified water in which 8 essential minerals are absent) were used for wetting the sample to avoid loss of sample due to charging.

(v) Spikes were also added at this stage for homogenization.

(vi) Approximately 3 ml of 48% HF and 1 ml 1:1 HNO_3 mixture was added to the sample. Caps were sealed and the samples were put up overnight at ~80-90°C.

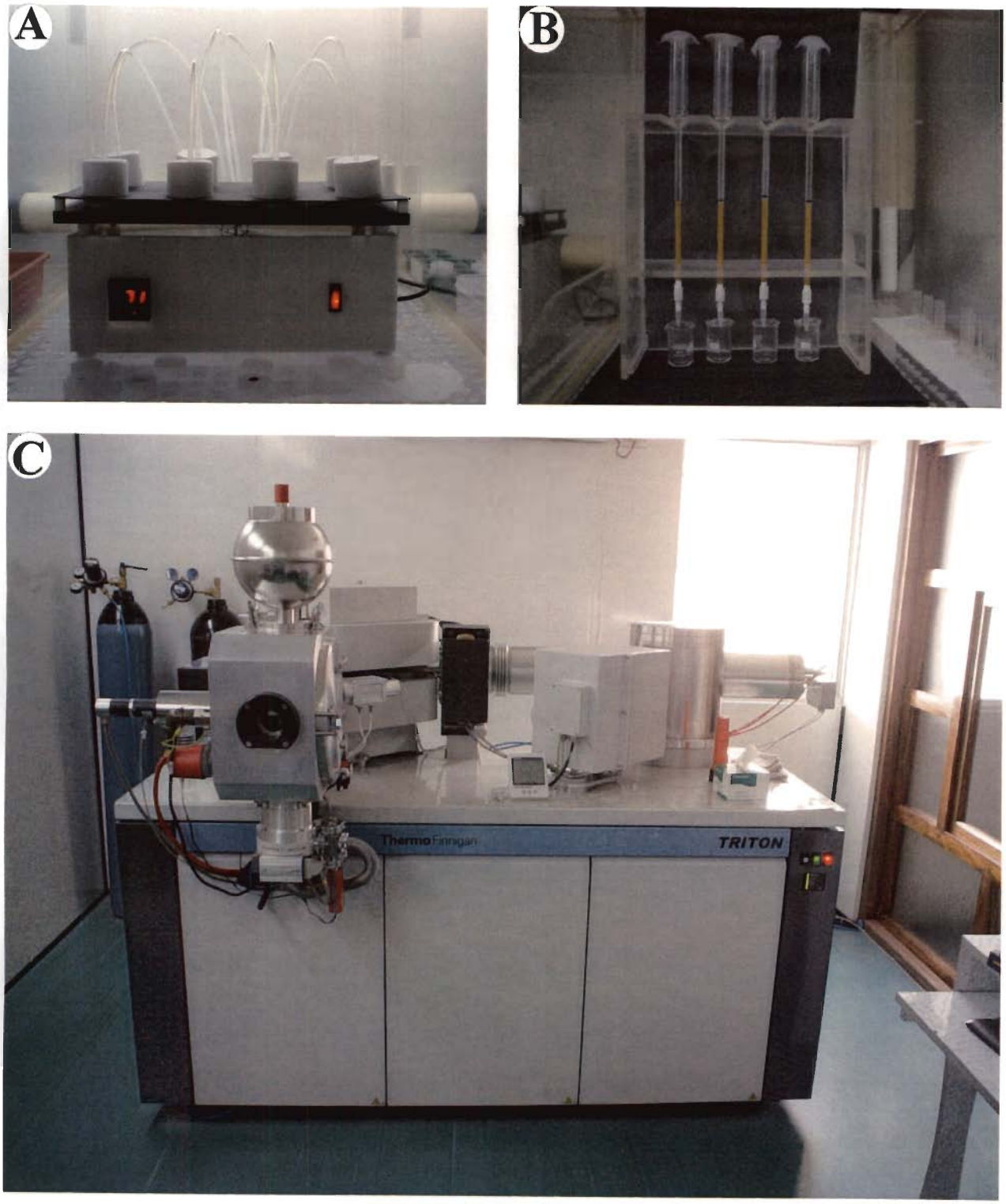

Figure 3.3. Instruments used at National Facility of Geochronolgy/ Isotoe geology Laboratory at the Institute Instrumentation Centre, IIT Roorkee. **A.** Ion Exchange Column. **B.** Sample Evaporation Unit. C. Themal Ionization Mass Spectrometer (TIMS)-Triton T1 Model.

(vii) Next day, vials were cooled and caps were washed down with MQ water and dried till they become jelly. 1 ml of 1:1 HNO_3 was added and, shaken carefully to see that samples have been dissolved.

(viii) Vials were dried slowly at low heat. When they were almost dry, 2 ml of Conc. HC1 was added in each vial, which were shaken slightly and place at ~80-90°C for complete dissolution. If there was clear solution, then one should follow Step 9. If not, evaporation was again done completely with 0.5 ml of Conc. HNO_3 also with 1.5 ml of Conc. HCl. Vials were caped and kept overnight. Cooled off and evaporated completely and again added 2 ml of Conc. HCl to check if there was clear solution.

(ix) If there was a residue and solution was not clear, sample was evaporated off completely. It was allowed to cool, 2 ml of 2N HCl added and made it stand for approximately 1 hr. Pippeted out the supernatant clear solution to another vial and evaporated the residue to dryness. Step 5, 6 and 7 were repeated. Both the solutions were added and evaporated off completely and move to Step 9.

(x) From the clear solution stage, sample was evaporated off completely, and 1 ml of 2N HCl was added before starting column chemistry for separation.

3.4.3. Isotopic dilution

(i) Principle: Isotope dilution is an analytical technique by means of which the concentration of an element in a sample can be determined by the Mass Spectrometer. Isotope Dilution Mass Spectrometry, abbreviated as the IDMS, is based on the estimation of the quantity of an element from the change, induced in its isotopic composition by the addition of a known quantity of spike of that element. The isotope dilution technique can be applied to any

element that exists as two or more naturally occurring isotopes, provided a spike, enriched in one of the isotopes of that element, is available (Blichert, 1993; Faure, 1989).

(ii) Spike: A spike is a solution (liquid or gaseous), which contains a known concentration of a particular element whose natural isotopic composition has been altered by the enrichment of one of its naturally-occurring isotopes (Faure, 1989). The exact concentration and isotopic composition of the spike element are verified separately by calibration using standard solutions of well-known concentrations. The spikes, which we have used in this analysis, are ^{84}Sr and ^{87}Rb.

(iii) Process of isotopic dilution: After the sample transferred and weighed in the vials a few drop of MQ water is added, isotopic dilution (spiking) is done. Vial along with the sample, was weighted, readings are noted and then ^{84}Sr spike (~30mg) was added to it. Weight of the vial+sample+spike was also noted down. After spike is added from first bottle the bottle was also weighted and reading noted down. ^{84}Sr (G) was used for whole rock and ^{84}Sr (Mica) for the minerals. After this ^{87}Rb (Low) spike (~40mg) was added to it and readings for both vial and spike bottle were taken. This is done to cross-check the amount of spike that was added.

(iv) Amount of spike added to sample: In case of whole rock samples, the ^{84}Sr spike amount that has been added is ~30 mg and ^{87}Rb spike is ~45 mg. In case of muscovite and biotite samples, the ^{84}Sr spike amount that has been added is ~30 mg and ^{87}Rb spike is ~35 mg. The amount of spike that has been added in case of whole rock is higher because the Rb content in the rock is already high, whereas in case of muscovite and biotite samples the Rb content is less as it has higher mobility and must have escaped from the mineral to the rock. In ideal case, spike should exactly equal to that of the concentration of the naturally-occurring

element in the sample. But this is very difficult to maintain, therefore, under spiking is always preferable.

3.4.4. Ion exchange chromatography

Ion exchange chromatography refers to any exchange method involving the distribution of components between a fixed (stationary) and a moving (mobile) phase. The latter is also called the eluent. The stationary phase is either a porous solid or coated with a stationary phase. Separation of individual components is possible because of differing affinities of the various components towards the stationary and mobile phases, causing different components to move at different rates along a column. This process, by which an eluent makes a compound move along a column, is called elution (Blichert, 1993).

Ion exchange chromatography involves the reversible exchange of ions between a solid phase (the resin itself) and a mobile phase (an aqueous ionic solution). The resin is normally packed in a suitable glass tube, the column held vertically, and the sample solution is poured (loaded) on the top of the column. An ion chromatography column is shown in Figure 3.3B. The sample is then eluted by washing its ionic components through the columns using a suitable solvent in a controlled manner. Ions are separated from one another due to differences in their affinity towards the ion exchange resin. The more strongly an ion is attracted to the resin, the larger the volume of the eluent required to wash that ion out of the ion exchange column (Blichert, 1993).

3.4.5. Elution Process

Sample is loaded into the column on the resin bed. As the sample moves through the column, all the ions in the samples are adsorbed on the surface of the resin. Elution is done with 2N HCI. Many experiments have been conducted and it is shown in these experiments

that 2N mode is the best for the elution of Rb and Sr. The range for collecting Rb and Sr fraction have been calibrated. Rb and Sr are both cation and they attach themselves to the sulphonate group of the resin. As we add more and more HCl to the column, the H+ ions keep on attaching themselves to the resin. Soon the resin becomes loaded with H+ ions and due to this, the Rb starts detaching from the resin. Later on, Sr follows the same process. The reason for elution of Rb before Sr is that Rb has positive charge of one and Sr has positive charge of two, so the Sr is more strongly bonded to the resin than the Rb. After elution of Rb and Sr, regeneration is done. This is done with help of 6N HCl. 6N HCl is used so that all other ions which are left in the column are removed from the column. We can use acids of higher strength also; but due to presence of more water in 6N, this is used. Water acts as a catalyst, thereby increasing the rate of the reaction and this reduces the time of regeneration. Acids of higher strength i.e., more concentrated ones will reduce the rate of the reaction and hence increasing the time of elution and may also harm the resin. Acids of lower strengths than 6N may not be able to elute all the left over ions from the column. A simplified scheme of the elution process followed in my present work is given in Table 3.3.

3.4.6. Sample loading in TIMS

(i) External heating instrument for filaments: For loading of Rb and Sr, a single filament assembly is used on which tungsten filaments are welded. The filaments are degassed before loading to remove all the gases present so that these do not interfere with ionization process at the time of analysis. The degassing is done in the Degassing Unit. This is a normal procedure followed every time before sample loading. These degassed filaments are then put in the socket of heating instrument. All these filaments are to be handled carefully with the help of forceps with no hand touch to prevent any contamination. One microlitre of TaF_5 is

put on filament in the centre with the help of one microlitre pipette. TaF_5 is used for the base and provides adhesive surface for the sample, and also removes the organic impurities from the sample (Birck, 1986).

The current was increased gradually up to 0.8 ampere to heat the filament and then maintained so that the TaF_5 base becomes viscous and forms a uniform layer over the filament. However, this layer sometimes does not spread over the whole of the filament uniformly as in the case of tantalum filament, and gets bent during the process of its making. As the TaF_5 becomes viscous, we slowly reduce the current to zero. With the help of the same microlitre tip, we put TaF_5 on all the filaments, which are to be used for the sample loading.

After this process, 2 μ litre of MQ water was put into the vial containing sample, which is in the nitrate form [for Sr, it is Sr $(NO_3)_2$]. In this form, it is easily dissolved in water. Then, one μ litre is taken in the pipette from this amount of sample and the sample is loaded on the filament again at the centre of the filament. We slowly increase the current up to 0.8 ampere and maintain this for some time till it becomes dry. Now, we start increasing the current till the fumes start coming. We maintain this current for some more duration till the fumes stop emerging. The temperature is again increased very slowly till the red glow appears on the filament. This current is maintained for 15 to 20 seconds and then we start reducing the current up to zero. Now the sample is ready to go into turret. This process has to be followed for all the samples but the tip of the pipette has to be changed for each sample. Care should be taken while loading the sample.

The following precautions are taken during sample loading:

(a) Tips should be changed for each and every sample after loading and care should be taken so that the same tip is not repeated for the other sample.

Table 3.3: Elution Process for Rb-Sr Separation Procedure

Sample Type: **Date:**

Sample Number: **Sample Location:**

The following steps have been followed for the elution.

Steps	Column Number			
	A	B	C	D
Load 8 ml 2N HC1, collect and discard.				
Load 1 ml sample in 2N HC1, collect and discard.				
Load 1 ml 2N HC1, collect and discard.				
Load 9 ml 2N HC1, collect and discard.				
Load 5 ml 2N HC1 (collect Rb in vial)				
Load 8 ml 2N HC1, collect and discard.				
Load 8 ml 2N HC1 (collect in Savillex vial for Sr.)				
Load and collect 12 ml 6N HCl (REE collection), if needed.				
Load 20 ml 6N HC1 for regeneration.				
Load 20 ml 6N HC1 for regeneration.				
Load 20 ml 6N HC1 for regeneration.				
Conditioning the column for next separation of Rb-Sr.				
Load 20 ml 2N HC1, collect and discard.				
Load 20 ml 2N HC1, collect and discard.				
Wash with 10 ml MQ.				

(b) Current should be increased very slowly otherwise it could lead to loss of sample or burning of filament.

(c) After loading the sample, the current should be maintained for some time till the fumes stop coming. This is done so that the fumes of phosphoric acid do not enter the source chamber during ionization process because it is very difficult to remove the fumes from the chamber.

(ii) Placing of loaded filament on turret: In TRITON T1 turret is a circular wheel with 21 notches, which are all numbered around the wheel, in which filaments can be fixed. In this turret, both single and double filaments can be loaded.

(iii) Sample analysis in TIMS: All the samples including the whole rock and the mineral separates were analyzed in the TRITON T1 Mass Spectrometer (Fig. 3.3C), installed at the Institute Instrumentation Centre, IIT Roorkee, Roorkee (Fig. 3.3C). The spiked Rb and Sr ratios (the isotope dilution fraction) were measured in static multi-collector mode. ^{88}Sr ion beam currents were ~1V and that of ^{85}Rb were ~0.3-0.5V. For Sr, isotopic ratios $^{88}Sr/^{86}Sr$, $^{87}Sr/^{86}Sr$ and $^{84}Sr/^{86}Sr$ of the mixture were measured and the mixture $^{85}Rb/^{87}Rb$ ratio for Rb was measured. Isobaric interference on ^{87}Sr from ^{87}Rb was corrected online.

(iv) Data acquisition procedure: When the source vacuum attained a pressure of $5x10^{-8}$ mbr in the turret, data acquisition procedure was started. Firstly, Triton software on the desktop was opened and 'Tune' window was selected. In the Cup Configuration Tab, appropriate cup configuration file was selected and 'Set Collector' button was clicked till all the cups were configured in position. A green signals came that indicated the cup configuration was ready for further procedure. Care was taken at this stage since the cup configuration is the most vulnerable part of the instrument. Appropriate sample position was then selected in the 'Sample Wheel' Tab. When the position is ready, a green signal came. 'Filament Control' Tab was then selected to control the current passing through the filament with the following settings:

For Strontium:

Up to 2000 mA at a speed of 1000 mA/minute.
The next 2000-3000 mA at a speed of 500 mA/minute, and.

for the rest 3000-3900 mA at a speed of 100 mA/ minute.

The signal for ^{88}Sr started coming out at around 3800 mA. As the current reached 3500 mA, ^{88}Sr and H3 in the 'Scan Control' Tab was selected and the 'set" button was clicked. Then, the analyzer gate was opened. Sometimes, signal came faster. In such case, heating was stopped as soon as the optimal signal came (~1.5–2.5V). If the signal came late, the filament was heated up a little more until a stable beam achieved. Care was taken so that the maximum possible ^{85}Rb was burned out and the intensity for it came to six decimal number or as low as possible.

For Rubidium:

Up to 1500 mA at a speed of 500 mA/minute.
The next 1500-2500 mA at a speed of 100 mA/minute.

Normally, the ^{87}Rb signal started coming out at around 2300 mA. As the current reached 2200 mA, in the 'Set Scan' Tab, the ^{87}Rb was selected in the center cup and the 'Set' button was clicked. Then the analyzer gate was opened. The optimum signal intensity for Rb is ~0.5–1V. Once a stable signal/beam was shown in the intensity window, wheel tuning was done in the 'Source Lens' Tab by clicking the 'Auto' button. Tuning of the wheel was done so that the instrument searched the maximum intensity and focused in the right position. After the wheel tuning was over, the tab became active. Further fine tuning of the lenses was done by clicking the 'Auto' button. This adjusted both the electrical and magnetic lenses so that the instrument finds the place for maximum intensity on the filament. Finally, in the 'Method Editor' window, the appropriate method file was opened and all the parameters were checked. Then, the data acquisition was initiated by clicking the 'Start' button.

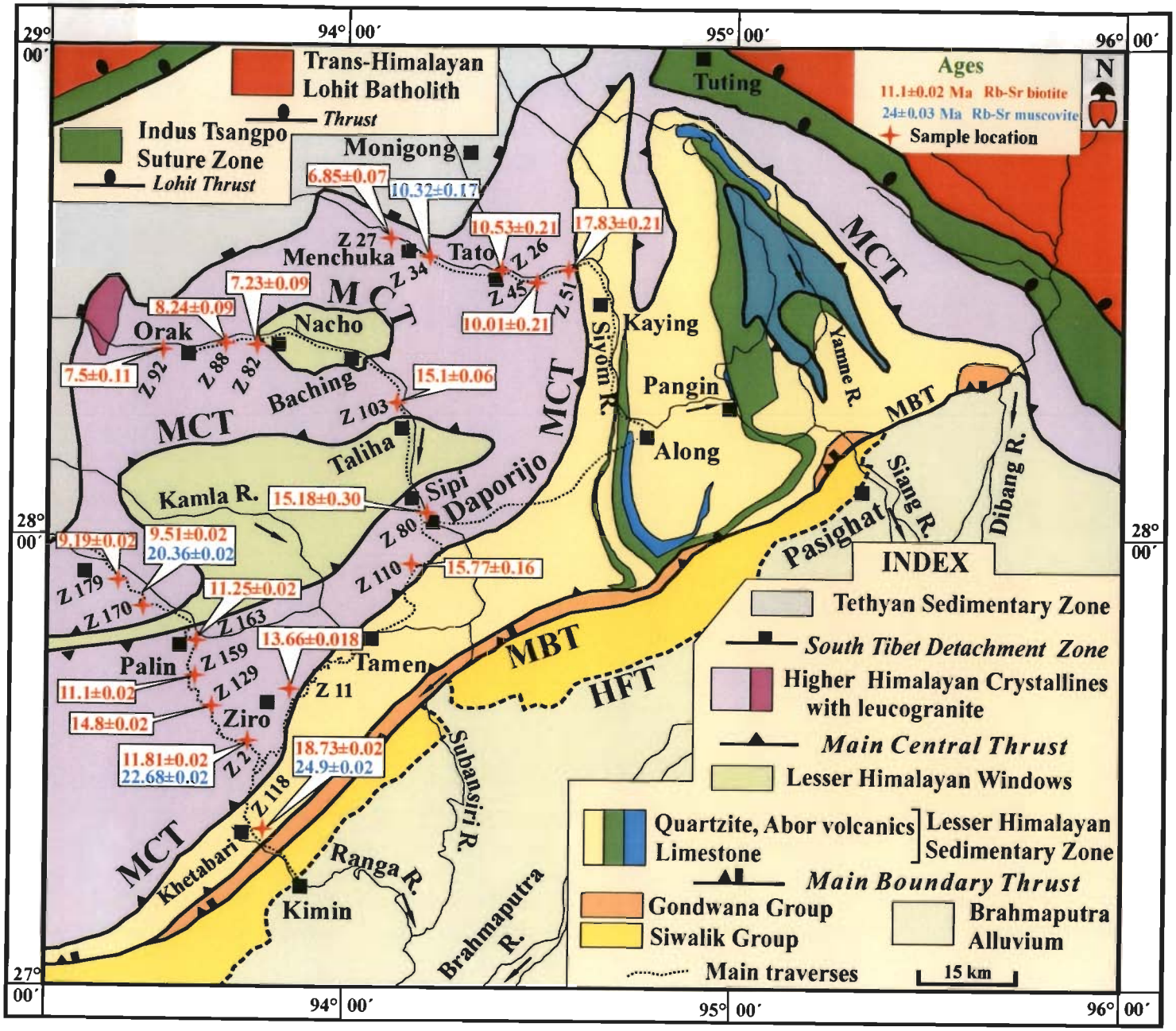

Figure 3.4: Rb-Sr biotite and muscovite ages from the Arunachal Himalaya along Subansiri and Siyom Valleys.

3.4.7 Age reduction: The isotopic ratios, given by the TIMS, were unmixed to correct for fractionation to preset-day $^{87}Sr/^{86}Sr$, Sr and Rb concentration and the $^{87}Rb/^{86}Sr$ atomic ratios, using a double isotope program on an Excel spreadsheet. The precision of $^{87}Sr/^{86}Sr$ (0.03%) ratios is the external precisions based on replicate determinations of standards; precision on the $^{87}Rb/^{86}Sr$ ratio is 1% by IDTIMS. To check efficiency and validation of the instrument, standards are run periodically, $^{87}Sr/^{86}Sr$ are crossed checked against the referred value of 0.710245 (Chaudhary et al. 2004). During the period of this study, the mean $^{87}Sr/^{86}Sr$ ratio was 0.71026±0.00008 (2σ, n=21) for the NIST NBS 987 Sr standard. As the estimated total procedural blanks were <2ng for Sr and <0.2ng for Rb, no correction of the measured isotopic ratios were done.

Mica ages were determined by plotting the corrected isotopic ratios of the whole rock and the isotopic ratios of the mica, i.e. whole-rock vs. biotite for the Rb-Sr biotite ages and whole-rock vs. muscovite for the Rb-Sr muscovite ages using Isoplot Programme (Ludwig, 2003).

3.5. Rb-Sr Results

For the Rb-Sr dating of biotite and muscovite of the crystalline rocks of the Himalayan Metamorphic Belt (HMB) and Lesser Himalaya (LS) of the Arunachal Himalaya, 19 samples have been selected, out of which, 19 whole rock, 18 biotite and 4 muscovite analyses were carried out to obtain the Rb-Sr mineral ages. Sample locations along with the mineral ages have been plotted on the geological map of the area (Fig. 3.4). The biotite ages span from 6.85±0.07 to 18.73±0.02 Ma, whereas the muscovite ages vary from 10.32±0.17 to 24.90±0.02 Ma. These ages will be used for determining the cooling and exhumation history

Table 3.4: Rb-Sr analytical data of the whole rock and micas from Subansiri region, Arunachal Himalaya.

Sr. No.	Sample no.	Rb ppm	Sr ppm	$^{87}Rb/^{86}Sr$	$^{87}Sr/^{86}Sr$	Age (Ma)	Tectonic unit
A. Kimin– Koluriang Section							
1.	Z 179 WR	263.98	79.23	16.31975	0.746999		
	Z 179 Bio	1964.21	21.56	452.9652	0.803959	**9.19±0.020**	**HHC**
2.	Z 170 WR	233.54	64.59	11.35986	0.750064		
	Z 170 Bio	2011.22	19.86	63.25634	0.761125	**9.51±0.091**	**HHC**
	Z 170 Mus	533.57	14.23	115.3341	0.780125	**20.36±0.075**	
3.	Z 163 WR	461.24	41.92	39.56798	0.923659		**DG**
	Z 163 Bio	1711.37	5.21	1130.154	1.097886	**11.25±0.015**	**(LHCS)**
4.	Z 159 WR	251.39	99.13	7.176939	0.742789		**DG**
	Z 159 Bio	932.11	5.13	497.1249	0.81999	**11.10±0.019**	**(LHCS)**
5.	Z 129 WR	242.4	96.77	7.279396	0.751189		**DG**
	Z 129 Bio	980.11	6.779	428.0579	0.839597	**14.80±0.024**	**(LHCS)**
6.	Z 2 WR	428.57	36.81	34.28771	0.896622		
	Z 2 Bio	1691.73	4.44	930	1.046878	**11.81±0.016**	**DG**
	Z 2 Mus	1965.24	2.43	1378.769	1.32977	**22.68±0.024**	**(LHCS)**
7.	Z 11 WR	243.57	96.09	7.361322	0.748676		**DG**
	Z 11 Bio	1459.31	8.27	705.8907	0.884201	**13.66±0.018**	**(LHCS)**
8.	Z 118 WR	508.18	436.01	3.392575	0.769872		
	Z 118 Bio	2458.28	1.075	7373.5	2.730139	**18.73±0.019**	**LH**
	Z 118 Mus	2855.21	0.89	8003.57	3.598763	**24.90±0.024**	
B. Subansiri River Section							
9.	Z 92 WR	253.3154	80.089	9.2707182	0.8335463		
	Z 92Bio	697.7414	2.004	1032.4067	0.9425219	**7.50 ± 0.11**	**HHC**
10.	Z 88 WR	99.4555	29.317	9.878	0.7727826		
	Z 88 Bio	807.9687	0.804	3318.64	1.1597134	**8.24±0.09**	**HHC**
11.	Z 82 WR	216.8987	122.879	9.1978947	0.8901158		
	Z 82 Bio	545.5299	0.893	1805.8286	1.0694272	**7.23 ± 0.09**	**HHC**

12.	Z 103 WR	488.886	46.11	31.322222	0.9079703	**15.10±0.16**	**HHC**
	Z 103Bio	1683.902	3.142	1599.2792	1.2442947		
13.	Z 80 WR	131.3195	137.934	2.7619388	0.7305091	**15.18±0.30**	**DG (LHCS)**
	Z 80 Bio	644.6823	7.147	262.24134	0.7864378		
14.	Z 110 WR	365.098	55.675	19.183077	0.8239979	**15.77±0.16**	**DG (LHCS)**
	Z 110Bio	1999.6372	1.049	6047.475	2.1743752		
C. Siyom River Section							
15.	Z 27 WR	369.5989	11.588	98.764935	1.3981623	**6.85±0.07**	**HHC**
	Z 27 Bio	2313.4781	0.831	8988.52	2.26245		
16.	Z 34 WR	59.7981	0.199	1212.7	0.9439039	**10.32±0.17**	**HHC**
	Z 34 Mus	728.84	30.299	71.827	1.0407522		
17.	Z 26 WR	205.9614	63.99	9.3726457	0.7794899	**10.53±0.21**	**HHC**
	Z 26 Bio	1091.9403	7.785	413.18125	0.8398704		
18.	Z 45 WR	168.6966	79.895	6.143	0.7668689	**10.01±0.21**	**HHC**
	Z 45 Bio	1204.3112	1.028	3429.25	1.2526429		
19.	Z 51 WR	164.6279	7.637	62.919608	0.7288067	**17.83±0.21**	**HHC**
	Z 51 Bio	857.6465	3.138	790.76667	0.9130959		

NOTES: WR–Whole rock, Bio–Biotite and Mus–Muscovite. **HHC**–Higher Himalayan Crystalline Belt (Gneiss, granite gneiss), DG–Daporijo Gneiss (Mylonitized granite gneiss of the Lesser Himalayan Crystalline(LHCS) Belt, LH–Lesser Himalaya (Gneissose granite).

of this region in Chapter 6.

3.5.1. Kimin–Koluriang Section

Eight samples were analyzed from this section, out of which the southernmost sample Z118 is gneissose granite, which has intruded the Khetabari Formation of the outer Lesser Himalayan Belt, and yielded biotite and muscovite ages of 18.73±0.02 and 24.90±0.02 Ma, respectively. These are the oldest mineral ages in the whole package. Samples Z2, Z11, Z129, Z159 and Z163 belong to the Daporijo Gneisses of the Lesser Himalayan Crystalline

Belt and yielded slightly younger biotite ages of 11.81±0.02, 13.66±0.02, 14.80±0.024, 11.1±0.02 and 11.25±0.02 Ma, respectively. Muscovite could be dated only from one sample Z2 from this belt and yielded an age of 22.68±0.02 Ma. Within the HHC, the biotite ages dropped further north, as we crossed the northernmost exposure of the MCT and the farthest sample Z179 yielded biotite age of 9.19±0.02 Ma. The HHC sample Z170, closest to the MCT, gave the biotite and muscovite ages of 9.51±0.09 and 20.36±0.08 Ma, respectively (Fig. 3.5A)

3.5.2. Subansiri River Section

This traverse runs right along the Subansiri River from where six samples were selected for the Rb-Sr analysis. Two porphyritic granite gneiss samples Z80 and Z110 from the Daporijo Gneiss yielded more or less similar biotite ages of 15.18±0.30 and 15.77±0.16 Ma, respectively as the Kimin-Koluriang section. Sample Z103 from the HHC belt, located between the Menga and Nacho Windows, has a biotite age of 15.10±0.16 Ma. However, biotite ages dropped abruptly again within the HHC rocks in this section. Three samples from this unit of the valley, Z82, Z88 and Z92 gave biotite ages of 7.24 ± 0.09, 8.24±0.09 and 7.50±0.11 Ma, respectively (Fig. 3.5B).

3.5.3. Siyom River Section

From this section, five samples were analyzed, out of which sample Z51 lies within the HHC just north of the MCT, yielded a biotite age of 17.83±0.21 Ma. Biotite age drops to10.01±0.10 Ma for the sample Z45. A sample Z26 from the migmatite zone yielded biotite age of 10.53±0.21 Ma. Going further north, Sample Z34 gave the muscovite age of

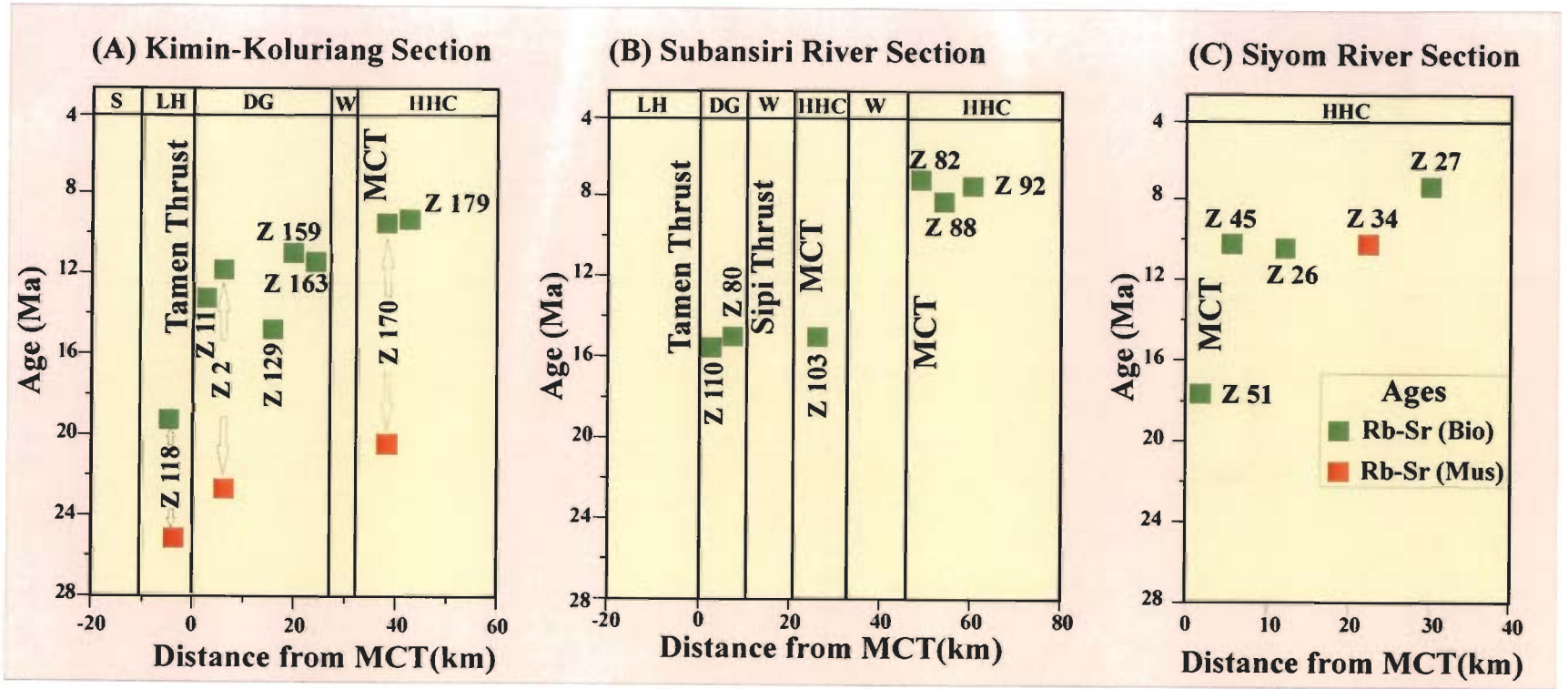

Figure 3.5: Rb-Sr mica ages vs. Distance from the MCT in the Subansiri and Siyom Valleys. **(A)** Kimin-Koluriang Section. **(B)** Subansiri River Section. **(C)** Siyom River Section. **Abbreviations:** S-Siwalik. LH-Lesser Himalaya. DG-Daporijo Gneiss (Lesser Himalayan Crystalline Series). W-Lesser Himalayan Window. HHC- Higher Himalayan Crystalline. MBT-Main Boundary Thrust. MCT-Main Central Thrust.

10.32±0.17 Ma. The northernmost sample from this section gave the biotite age of 6.85 ±0.07 Ma, which is youngest in the whole region (Fig. 3.5C).

3.6. Spatial variation of Rb-Sr ages

Rb-Sr biotite and muscovite age results in this region show significant spatial variation in their values. A plot of the ages vs. distance from the southernmost exposure of the MCT in different traverses indicate interesting pattern (Fig. 3.5). In the Kimin-Koluriang section, both the biotite and muscovite ages decreases gradually from the Lesser Himalaya to the Higher Himalayan Crystalline rocks, i.e. the biotite age from the granite body within the Lesser Himalayan Belt has an age of 18.7 Ma, which drops down to maximum of 14.8 Ma within the Daporijo Gneiss of the Lesser Himalayan Crystallines and finally to 9.2 Ma within the HHC (Fig. 3.5A). Similar is the case with the muscovite ages, which become younger from 24.9 Ma in the Lesser Himalaya to 22.69 Ma in the Daporijo Gneiss and then to 20.36 Ma within the HHC. However, pattern is entirely different in the Subansiri Valley (Fig. 3.5B) from the previous one; here we can observe two distinct groups of ages. The Daporijo Gneiss has Rb-Sr (biotite) ages which are approximately around 15 Ma and then abruptly drop down to another range of around 7 Ma in the HHC rocks. In the Siyom River section also, there is decrease of Rb-Sr (biotite) from 17.83 Ma in basal parts of the HHC nearest to MCT to around 10 Ma, which further reduces to 6.85 Ma in the northernmost sample (Fig. 3.5C).

Chapter 4: Fission Track Dating

4.1. Introduction

Fission track dating has developed into one of the most important technique throughout the geologic community for reconstructing the low-temperature thermal history of rocks over a geological time scale. It is one facet of technique, which is popularly known as Solid State Nuclear Track Detector (SSNTD) technique. The pioneers of the SSNTD are physicists like R.L. Fleischer, P.B. Price and R.M. Walker, who worked in the General Electric Company's Research Laboratory in Schenectady, New York. The geological applications of this technique were summarized by Fleischer et al. (1975) and subsequent a comprehensive overview of the FT dating and thermochronology was provided by Wagner and Van den haute (1992). Numerous recent reviews are available by Dumitru (2000), Gleadow et al. (2002), Tagami and Sullivan (2005), and others.

Fission track dating is based on the accumulation of narrow damage trails, i.e. fission tracks in uranium-rich mineral grains such as apatite, zircon, titanite etc. and natural glasses (Fig. 4.1). The tracks are formed as a result of spontaneous nuclear fission decay of ^{238}U in nature (Price and Walker, 1963). Time elapsed since fission track began to accumulate is estimated by determining the density of accumulated tracks in a particular material in relation to the uranium content of that material. Various applications of fission track dating along with other dating methods are exploited by geologists and archaeologists. More recently, this method has been extensively used in

interpreting the interplay between tectonics and climate-induced erosion (Jain et al., 2000; Burbank et al., 2003; Malusa and Vezolli, 2006; Thiede et al., 2009).

Many alternative strategies exist for obtaining spontaneous track to induced track density ratio from which the age is calculated. In practice two methods namely, Population Method and External Detector Method (EDM) are followed. The details of various other approaches are listed in Gleadow (1981) and Hurford and Green (1982). In the present work, EDM method is followed, which is the general procedure at the Low Temperature Thermochronology Laboratory, Department of Geophysics, Kurukshetra University, Kurukshetra, where this work was carried out. Numerous publications have come out from this laboratory (Paul, 1995; Kumar et al., 1995; Lal et al., 1999; Jain et al., 2000; Kumar et al., 2007; Patel et al., 2007; Jain et al., 2009). In the EDM method, spontaneous tracks are counted in etched minerals, while induced tracks are counted on an external detector of muscovite having low uranium content. It is held against the mineral during irradiation and subsequently etched. Spontaneous and induced tracks are measured in exactly matching areas from the same planar surface of an individual crystal and, thus, uranium inhomogeneity, both within and between the crystals, is of negligible consequence. The method also permits careful selection of crystals, which are badly etched, wrongly oriented or contained dislocations. Principle and detailed analytical procedure for this method of fission track dating is given below.

4.2. Basic principles

Fission tracks are formed during decay of heavy nuclides that belong to the actinide series of the elements. Of this, ^{232}Th and three U isotopes (^{234}U, ^{235}U and ^{238}U) are typical candidates that produce significant numbers of fission tracks. However, in

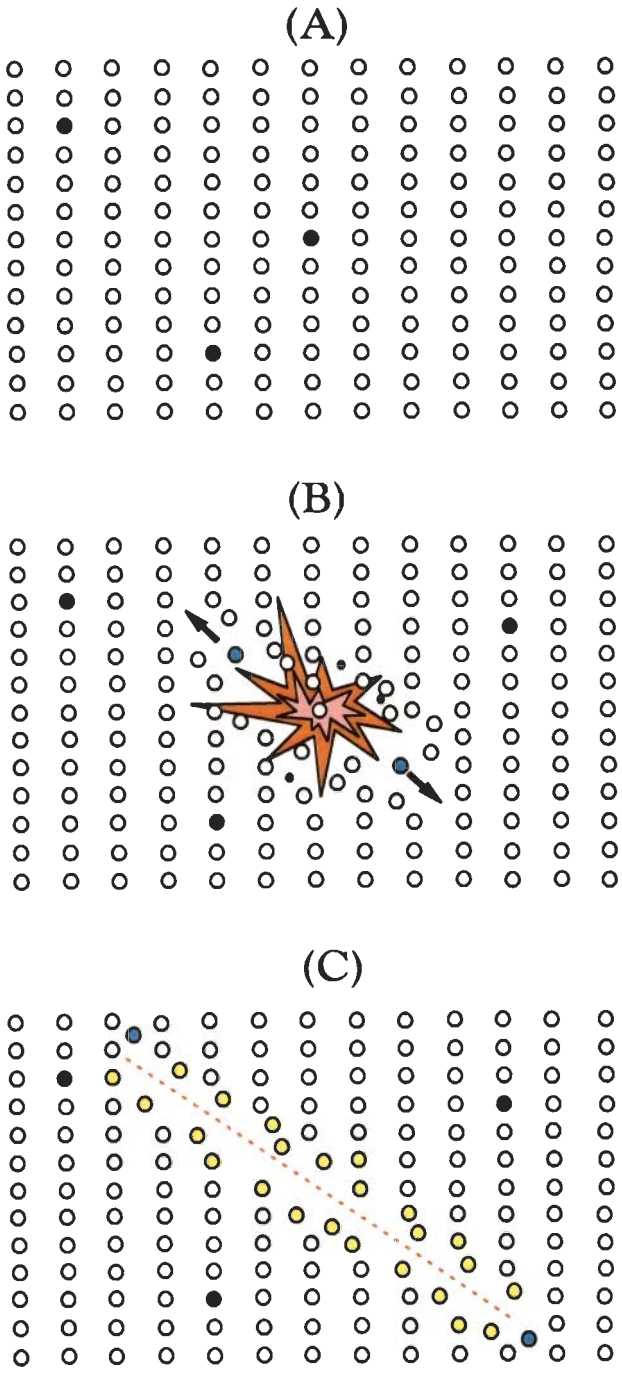

Figure 4.1: Cartoon representation of the ion spike explosion model and the formation of fission track in a mineral. **(A)** Trace amount of radioactive ^{238}U are present in the crustal lattice (dark dots). **(B)** Spontaneous fission of ^{238}U produces two highly charged heavy particles. **(C)** Damage trail or fission track left by the highly charged heavy particles.

terms of relative abundances and half-lives, ^{238}U is the only source of spontaneous tracks in terrestrial material including natural apatite and zircon. This decay can also be induced artificially, in which a heavy, unstable nuclei split into two pairs of fragments of similar size during bombardment by neutrons or other high energy particles or γ rays. This reaction is accompanied by the release of few neutrons and ~210 MeV of energy, of which majority is the kinetic energy of fission fragments. The propulsion of two massive positive charged fragments in opposite direction creates a damage trial, and is called fission track. The track formation during the fission reaction is best explained by "ion explosion spike" model (Fleischer et al., 1965, 1975). It treats electrostatic displacements as the primary process. In this model, track formation occurs in three stages (Fig. 4.1), which are summarized by Tagami and Sullivan (2005).

(i) The rapidly moving positively charged particles strip lattice electron along its trajectory, leaving an array of positively-ionized lattice atoms.

(ii) The resulting clusters of positive ions are displaced from their original sites as a result of Coulomb's repulsion, creating interstitials and vacancies.

(iii) The stressed region relaxes elastically, straining the surrounding undamaged lattice. The creation of long ranged strains in the third stage enables the direct observation of unetched (latent) tracks by transmission electron microscope (TEM) possible.

4.3. Fission track age equation

The number of fission tracks depends, not only on the time during which they have been accumulating, but also on the uranium content of the material, i.e. the greater uranium content, the greater will be the number of tracks. The total number of decay of

^{238}U in a given volume of mineral containing uranium atoms and distributed evenly throughout its volume during time T is

$$D_S = N_{238}(e^{\lambda dT} - 1) \qquad (4.1)$$

where, D_s and N_{238} are the number of decay events/cc and the number of ^{238}U/cc at present in the mineral sample respectively, λ_d is the total decay constant of ^{238}U.

Most of these decay events correspond to α emission. The fraction of ^{238}U decay that is due to spontaneous fission is λ_F/λ_d, so the number of fission events F_s per unit volume is given by

$$F_s = \lambda_F/\lambda_d N_{238}(e^{\lambda dT} - 1) \qquad (4.2)$$

The number density of spontaneous fission tracks ρ_s crossing a unit internal surface of the sample after etching is related to the volume density, F_s by

$$\rho_s = \eta R F_s \qquad (4.3)$$

where, R is the range of a single fission fragment and η is the etching efficiency of the material.

Combining equations 4.2 and 4.3, we obtain

$$\rho_s = \lambda_F/\lambda_d N_{238} \eta R (e^{\lambda dT} - 1) \qquad (4.4)$$

The determination age T, thus requires the measurement of ^{238}U concentration in the sample. Rather than measuring the ^{238}U content directly, it is more convenient to measure the ^{235}U content of the sample and to assume (as is always the case) that this stand in a constant ratio to ^{238}U. The determination of ^{235}U content by fast neutron fission is avoided as these neutrons would produce fission, also in the Th content of the sample.

If the sample irradiated with a known fluence, φ of thermal neutron, than the number of induced fissions per unit volume is

$$F_i = N_{235}\,\sigma\varphi \qquad (4.5)$$

where, σ is the thermal fission cross-section of ^{235}U, and N^{235} is the number of ^{235}U atoms per unit volume. If we assume that the range and etching efficiency for spontaneous and induced fission tracks are the same, then the number of induced fission tracks per unit area is

$$\rho_i = R\,F_i\,\eta = \eta\,RN_{235}\,\sigma\varphi \qquad (4.6)$$

Dividing equation 4.4 by 4.6 and rearranging the terms we get,

$$T = 1/\lambda_d \ln\left[1 + (\lambda_d\,\sigma I\,\varphi\,\rho_s)/\lambda_F\,\rho_i\right] \qquad (4.7)$$

This is the fundamental age equation of the fission track method.

The measurement of FT age is now reduced to determination of the ratio of a spontaneous to an induced track density (ρ_s/ρ_i), thermal neutron fluence φ and fission decay constant λ_F. In principle, since the values of the constants λ_d, σ and I are well established, it remains only to determine the track density ratio to measure the neutron fluence and insert a value for the fission decay constant λ_F in order to determine a FT age. Unfortunately, there is 20% value difference in the published values of λ_F by two groups (Thiel and Herr, 1976; Bigazzi, 1981). The values, obtained by the groups experimentally, lie around either $8.46\times10^{-17}a^{-1}$ or $7.00\times10^{-17}a^{-1}$. The lower value is supported by track accumulation experiments and the dating of minerals and natural glasses of independently known age, and the higher value by measurements made using rotating bubble chambers, ionization chambers, radiochemical measurements and by the

dating of man-made glasses of known date of manufacture. These are the two values of λ_F that are commonly used. In addition, the determination of absolute value for the neutron fluence, used to induce fission ^{235}U in the sample can be very complex. Also, the identification criteria of tracks in the mineral grains as well as the external detector may not only vary from one individual to another but also with the microscope conditions (dry or oil immersion objective and magnification). All the factors can lead to great variation in the calculated ages, obtained from the ρ_s/ρ_i track density ratio counted for a sample, thus, making the inter-laboratory comparison of FT data very difficult.

In order to make inter-laboratory comparison and thus establishing the reliability and reproducibility of the FT ages, the IUGS Subcommission on Geochronology recommended that a calibration factor, zeta (ζ), may be substituted into the age equation for λ_F, I, σ and B, (where $\varphi=B\rho_d$; ρ_d being the track density in the external detector, placed in contact with the uranium dosimeter glass, B is constant for given glass and very difficult to evaluate). Thus, the modified age equation is

$$T=1/\lambda_d \ln [1+ G \zeta \lambda_d (\rho_s \rho_d/ \rho_i)] \qquad (4.8)$$

Zeta represents a calibration base-line for the specific dosimeter in which ρ_d is counted and can be evaluated from a series of internationally-accepted age standards. ρ_s and ρ_i are assumed to be counted on surfaces of similar registration geometry, or else, modified by a suitable geometry factor. Such a system calibration should be based on a series of age standard, and not on a single measurement, which is far from precise. The etching and track identification criteria play a vital role in the determination of FT ages. In the present FT work, the etching and the track identification criteria as well as the microscope conditions were the same as adopted by Prof. Nand Lal in this laboratory and time to time reported by Thakur and Lal (1993) and Kumar (1999). Zeta factor was

calculated for the CN 5 glass by multiple analyses of age standards following the recommendation of Hurford (1990). The zeta factor for CN 5 for apatite was found to be 295.83±9.27 (Table 4.1). However zeta value of 110±1.3 for the CN1 glass was used for zircon age calculation (Jain et al., 2000).

Table 4.1: Fission track count data for Zeta Calibration and weighted mean zeta values for CN5 glass dosimeter using thermal irradiation facility of CIRUS reactor.

Sr. No.	Age Standard	Mineral (Number of Crystals)	Track Densities (Number of Tracks)			P (χ^2) % age	Zeta±1σ
			Spontaneous ρ_s (N_s)	Induced ρ_i (N_i)	CN5 ρ_d(N_d)		
1	Durango	Apatite (15)	0.21 (78)	1.30 (486)	1.33 (3316)	98.9	292.43±20.0
2	Durango	Apatite (13)	0.19 (62)	1.22 (395)	1.33 (3316)	98.5	302.82±16.9
3	Durango	Apatite (8)	0.19 (37)	0.65 (130)	0.59 (1463)	95.9	366.02±24.8
4	FCT	Apatite (14)	0.50 (105)	1.31 (277)	0.59 (1463)	97.5	254.38±18.8
5	Durango	Apatite (15)	0.22 (82)	0.63 (238)	0.58 (1438)	92.5	304.56±29.4
6	Durango	Apatite (15)	0.22 (83)	0.69 (260)	0.63 (1566)	77.4	305.72±34.0
7	Durango	Apatite (15)	0.25 (92)	0.66 (249)	0.63 (1566)	67.3	255.39±29.9

Weighted Mean Zeta Value=295.58±9.2

NOTES: FCT=Fish Canyon Tuff. ρ_s=Spontaneous fission track density. N_s=Total number of spontaneous tracks counted. ρ_i=Induced track density. N_i=Total number of induced tracks counted. ρ_d=Induced tracks in dosimeter glass CN5. N_d=Total number of induced tracks measured in dosimeter glass. P(χ^2)=Probability of obtaining the observed χ^2 value for v degrees of freedom.

4.4. Methodology

In this work, the following procedures have been adopted for the FT studies.

4.4.1. Mineral separation

The thin section of each sample is studied to examine the presence and abundance of suitable size grains (~100 μm) of either apatite and/or zircon. This step also helps in

assessing the quantity of the crop of apatite and/or zircon so as to get an idea of the amount of the rock specimen to be taken for processing. The flow chart, showing all the steps involved in mineral separation, is given in Figure 4.2.

4.4.2. Hand picking and mounting

After the apatite and/or zircon are separated from the rock sample by routine crushing by jaw crusher, heavy liquid and isodynamic separations, final selection of suitable grains is done by hand picking under a binocular microscope (see Fig. 4.2 for detailed steps). The hand-picked grains were arranged in an array to identify the mineral grains and corresponding replica. The array is mounted to facilitate the steps of pre-grinding and description procedure. The array size was adjusted according to the size of the capsule used for irradiation. The mounting of apatite and zircon was made in different material because of their track etching and fading conditions. The hand picking and mounting procedure are described below.

(i) Zircon: Small fraction of the zircon grains was spread on a silicon glass of size 5x5 cm. Using a sharp-tipped needle, the grains were picked one by one and arranged in a small place on the glass slide in such a manner that the c-axis of all the grains were in one direction. In selecting the zircon grains, care was taken so as to pick large transparent euhedral crystals having well-defined c-axis, and crystal of approximately the same size for a particular mount. One of the corner grains was slightly displaced from the regular array. The usefulness of arranging the grains along their c-axis and slight displacement of one of the grain helps during grinding/polishing, etching of zircon and track counting in the mica detector, respectively. The remaining unarranged grains were removed from the

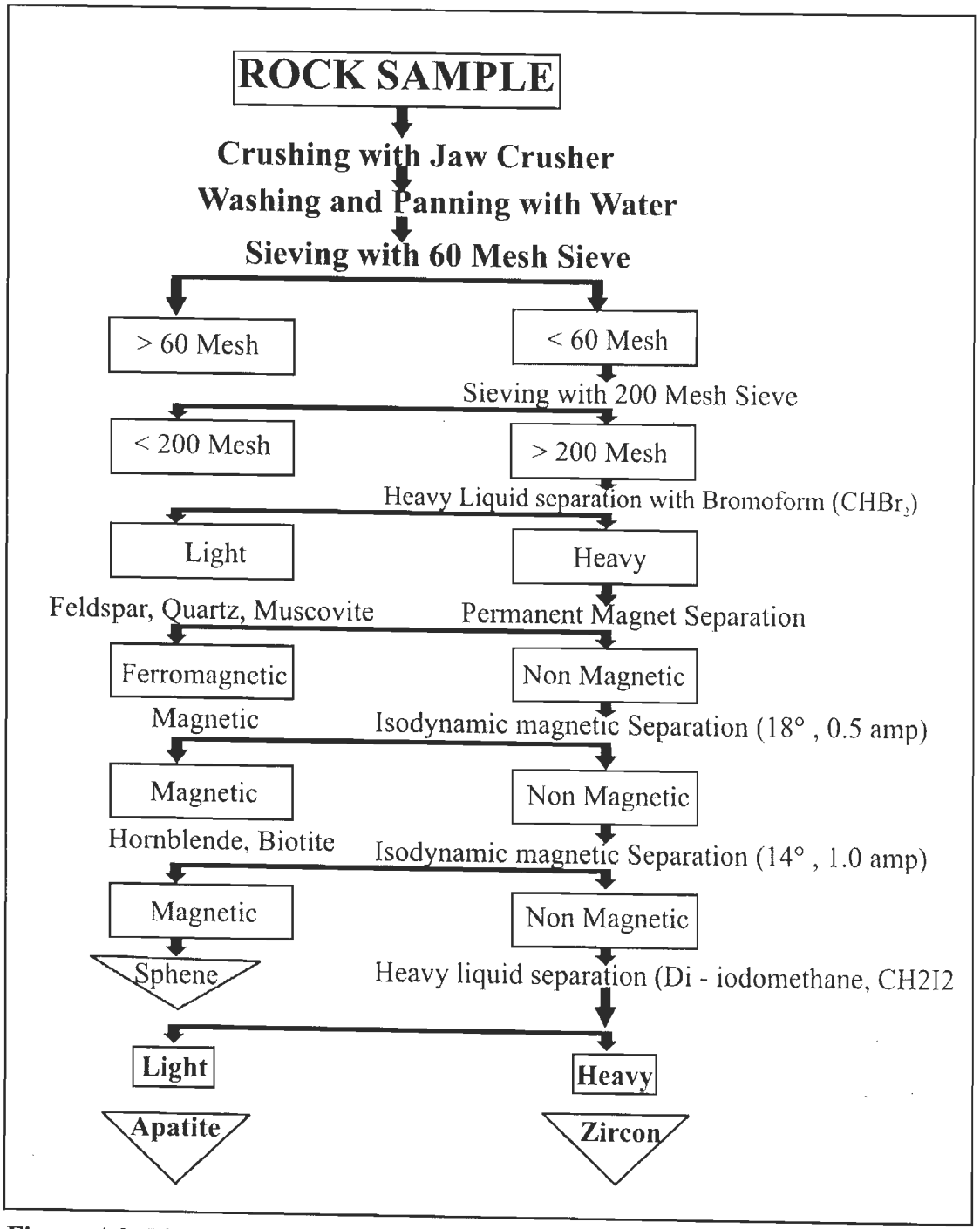

Figure 4.2: Flow chart for fission track mineral separation

glass slide and stored in a vial. The silica glass was then shifted to a hot plate having good temperature control. The zircon grains are mounted in a PFA (co-polymer of tetraflouroethylene perflouroalkoxy ethylene) Teflon piece (each with size of 1.5x1.5 cmx0.5 mm), because of its stability during the etching conditions. The temperature of the hot plate was maintained at 320° C. The Teflon mount was then slightly cut asymmetrically at its right top corner. This cutting makes it convenient to recognize the grain side of the Teflon sheet by naked eyes. The sample code was written with a needle pen on the back side of the Teflon mount.

(ii) Apatite: Since fission tracks in apatite are very sensitive to thermal effects, its mounting in Teflon is not possible. An alternative procedure, which does not involve high temperature treatment, was adopted. Epoxy is the best material for this purpose, as it gets solidified at room temperature. Resins and hardener were mixed in the ratio of 10:1 by volume, respectively. The epoxy resin mount cannot be detached from the glass slide after drying but can be easily removed from the Teflon slide, which is, therefore, very useful for apatite mounting. The Teflon slide was attached on the glass slide of the same size by means of a bifacial tape (henceforth this combination of Teflon and glass sheet will be called the TG slide). The TG slide is cleaned with alcohol and petroleum jelly was applied on the Teflon side of the TG slide so that apatite grains would stick to it. In the absence of the jelly, the electrostatic effect would disturb the grain arrangement during the hand picking. The handpicking of apatite grains was done similar to the zircon, but without any directional alignment of the grains.

All the TG slides containing apatite grains were arranged on a horizontal surface. On each slide, two small glass sheets of 15 mm thickness were placed as spacers. The epoxy resin of fixed amount was then poured on the grains carefully so that the grain

arrangement does not get disturbed during pouring of the epoxy resin. The amount of epoxy resin was adjusted in such a manner that when another TG slide was put on the glass spacers, the poured resin was made a flattened cylindrical form whose diameter was about 15 mm. This arrangement was kept for about 24 hrs at room temperature to allow the epoxy resin to solidify. After removing the mount from TG slide, sample code was written with a needle parallel to one of the four sides of the grain arrangement on the backside of the mount.

4.4.3. Grinding and polishing

In order to expose the internal surface of the crystals for measuring spontaneous track density, mineral grains were exposed by grinding and polishing. For using internal surfaces of the minerals, it is essential to remove a certain thickness to expose the 4π geometry. This thickness correspond to the half of an etchable track length, which varies from one mineral to another, i.e. 6μm for zircon (Krishnaswamy et al., 1974), 8 μm for apatite (Gleadow et al., 1986) and 7 μm for sphene (Gleadow and Lovering, 1975). If all the mineral grains are mounted so that the exposed crystal surface is equally flat, the grains were grounded almost uniformly and the removal of the thickness, which satisfies the 4π geometry, will be quite easy. However, in case mineral grains are inclined , eroded or have irregular shape or caves, all the surface area of each grain will not be grounded equally, and hence measurement of the removed thickness for the 4π geometry condition will not be possible from the first grinding. In such a case, grinding should be continued till maximum possible area is exposed for measuring the thickness. This step is called the "pre-grinding" stage.

After the pre-grinding, a brief description about the suitability of each grain is necessary. As discussed above, some part of the crystal might not have been exposed during pre-grinding and will not satisfy the condition of the 4π geometry. As it is possible to judge such non-exposed area after finishing the grinding, all these areas were recorded at this stage in a notebook by labelling individual grain.

The next step was to grind the mount and remove a certain thickness peculiar to each mineral for exposing the 4π geometry. After description, the mount was grounded perpendicular to the direction of pre-grinding (using 25 μm diamond paste) till all the preceding grinding scratches disappeared. Next step of grinding was carried out using 14 μm diamond paste, again perpendicular to the direction of previous grinding scratches and the new scratches on all the surfaces were checked. This alternate grinding of 25 μm and 14 μm diamond paste resulted in the removal of 1.75 μm thickness. While shifting from one grade of diamond paste to another, the mount was washed using ultrasonic cleaner for about 8-10 minutes. This process was repeated until the removed thickness reached half of etchable track length for each mineral. To be on the safe side, however, the thickness of the removed surface was kept more than 3/2 of the minimum depth for exposing $4\ \pi$ geometry. Thus, the above step of grinding was repeated 5 times for zircon and 7 times for apatite.

In case of zircon, grinding process was slightly different from those of apatite. It is not advisable to grind zircon crystal along their crystallographic c-axis, because it often produces deep crack or damage on the surface. The cracks or damages are enlarged during chemical etching and sometime disturbs the track counting. Hence, pre-grinding and grinding of zircon mounts should be carried out perpendicular to c-axis only, for which arrangement of zircons along the c-axis is desired. After each step of grinding, all

scratches were erased by 8 μm diamond paste polishing parallel to c-axis so that next grinding scratches could be easily observed.

After grinding, the mount was polished successfully using 8 μm, 3 μm, 1 μm and 0.25 μm diamond pastes. At every step of polishing, direction of polishing is changed by 90° from that of preceding polishing. The alternate change of polishing direction made it easy to distinguish the disappearance of the preceding polished scratches, thereby, ensuring the completion of each polishing step. Before switching from one diamond paste to another the samples were washed under running water and ultrasonic cleaner to make them clean of the preceding grade diamond paste.

4.4.4. Etching of tracks

(i) Zircon: The determination of the conditions for optimum etching in zircon requires a special care. It is quite necessary because zircon shows anisotropic etching behaviour of fission tracks and all the tracks in various crystallographic directions do not have same etching rate (Gleadow, 1981). Therefore, it is necessary to continue the etching until the tracks in all directions become visible. In case of zircon, isotropic arrangement of etched tracks is characterized by the complete revelation of thin tracks parallel to c-axis.

For etching large numbers of zircon mounts together, a specially-designed etching bath with temperature controller is used. After obtaining the desired temperature (230°C) in the etching bath, Teflon beaker/beakers containing the eutectic mixture of NaOH: KOH etchant (Gleadow et al., 1976) was kept in it for 12 hours. Then sample mount was put in the beaker. In doing so no air bubble were left in the etchant. The mount after etching for a desired time was put in 5% HCl in an ultrasonic cleaner for 15-20 minutes and subsequently in water for 5-10 minutes using ultrasonic cleaner to remove the traces

of the etchant to the mount. The etching time for zircon varies with the track density. Most zircons get etched within a period of 3-12 hrs.

(ii) Apatite: The tracks in apatite were etched in 0.6% HNO_3 (by volume) at 30°C for 55-70 seconds.

4.4.5. Packing

Before irradiating the samples in the reactor with thermal neutrons, uranium-free fission track detectors were fixed firmly in contact with the mineral mounts. The Brazillain muscovite, which is almost free from uranium impurities, was used in the present study. It was cut into the square pieces of size slightly larger than the area of the mounted grains and of suitable thickness (~0.1mm).

The sample code was written with a sharp needle on the back of the muscovite. To distinguish the surface fixed against the mineral grain, one corner of it was cut asymmetrically such that when fixed against the grain arrangement in the Teflon sheet, the cuts of both were in the same direction. For epoxy resin mounts, the corner cut of the muscovite detector was made in the same manner before putting detectors. All the mineral mounts were thoroughly washed with alcohol using ultrasonic cleaner. After keeping the mica detector on the grains, the entire arrangement was then wrapped up firmly with aluminium foil. The sample code is written on the top. The sample was, thus, ready for irradiation.

4.4.6. Thermal neutron irradiation

Thermal neutron irradiations for the present work were carried out at IC2 thermal column of the CIRUS reactor at Bhabha Atomic Research Centre, Trombay, Mumbai. The dimensions of the aluminium capsule for sample irradiation in this reactor are 3.5 cm

in length and 1.5 cm diameter. After fixing the muscovite detectors on mounts, the samples were stacked vertically and packed in the capsule. In order to measure thermal neutron fluence and to take into account dose gradient along the capsule, two uranium standard glasses (one at the top and other at the bottom of the capsule) were also packed with the samples. Each dosimeter mount was made using standard glass, namely Corning 5 (CN 5) for apatite and Corning 1 (CN 1) for zircon, prepared by Dr J.W.H Schreurs at Corning Glass Works, Corning, New York, USA. The mounting, polishing and packaging of these standard glasses was done in similar way with that of apatite. The muscovite detectors attached to these standard glass mounts were used for counting of the induced tracks. The track density ρ_d was calculated by taking mean of the counts of two dosimeter glasses. The Corning glass CN 5 contains ~12 ppm undepleted uranium of natural isotopic abundance ($^{235}U/^{238}U$=0.726%) and ~0.4 ppm thorium without any interfering trace element. After irradiation, external detectors (muscovite) were etched with 48% HF for 5-6 minutes.

The counting of spontaneous tracks (in apatite and zircon) as well as induced tracks on mica detector was carried out on the samples from Arunachal Himalaya after irradiation, using the NIKON Optiphot Microscope under 100X dry objective.

4.5. Results

Three most accessible road sections are currently available in the Subansiri region, which are largely drained by the Subansiri and its tributaries. The westernmost section from Kimin to Koluriang runs through the Kimin-Ziro-Palin road and the Kurung River. This traverse contains a total of 13 samples across most of the tectonic units in the Lesser and Higher Himalayas. The central traverse along the main Subansiri River and

part of Ziro-Tamen-Daporijo road section covers part of the Outer Lesser Himalayan Sedimentary Belt on the sub-thrust side of the Tamen Thrust/MCT along the strike and has only 3 samples yielding the FT ages. The overlying Daporijo Gneiss of the Lesser Himalayan Metamorphic Belt contains three samples from this area, while the HHC is covered by 4 samples only; one additional sample Z81 covers the inner window of the Lesser Himalayan quartzite beneath the HHC. Three samples came from the northern HHC belt in the north. A total of 8 samples provided the age spectrum of this section. The northernmost traverse along the Siyom River and its western tributary, draining the Bille-Tato-Menchuka region, is covered by the metamorphic belt of the Higher Himalaya and is represented by 5 samples for the FT analysis.

In this work, 22 AFT and 16 ZFT ages were generated from all the three traverses from a total of 26 samples. Fission track ages were determined by the EDM method, and the ages were calculated by the Zeta calibration approach. Zeta value of 295.83±9.27 for the CN 5 glass has been calculated by the author in the present work, while its value of 110±2.6 for the CN 1 glass was used for the age calculation (Jain et al., 2000). Zero track density grains in the young-aged rocks were also taken into account. Track length measurement was not done due to low track density. All the ages are reported as central age with 1σ error (Galbraith and Laslett, 1993). Location of the samples and their lithologies are listed in Table 4.2, while, the FT results of the present study are given in Table 4.3. Locations of samples and their ages are also plotted in Figures 4.3 and 4.4. A χ^2 test allows detection of supplementary variation in (ρ_s/ρ_i) ratio. If the track count passes the χ^2 test, i.e. P (χ^2)≥5%, the error calculation are through conventional method. If it fails, i.e. P (χ^2)≤5%, real differences in the FT ages are considered to exist between the individual grains. The detailed result of each traverses are described below.

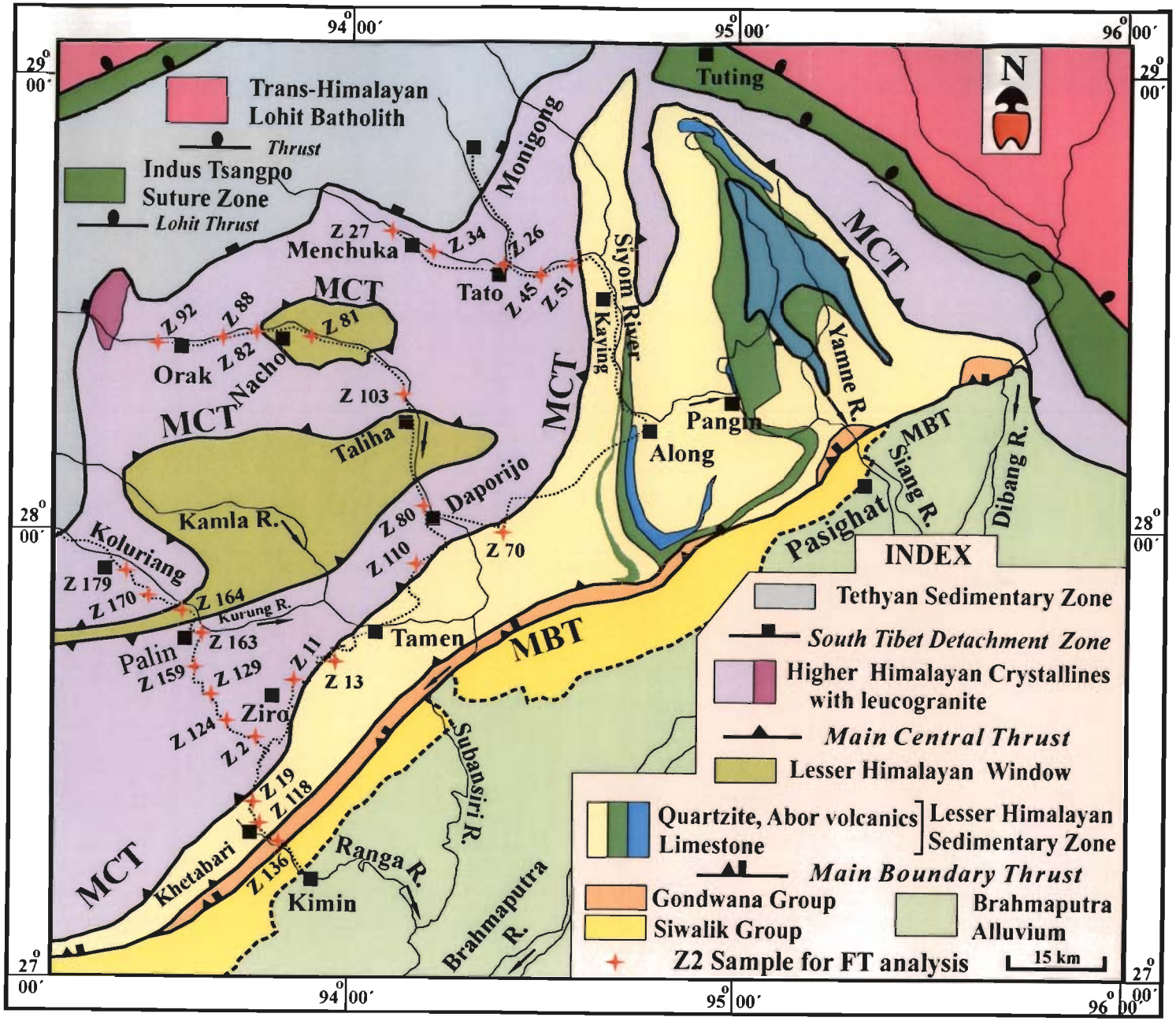

Figure 4.3: Sample location map for fission track mineral ages Subansiri and Siyom Valleys, Arunachal Himalaya.

Table: 4.2: Location, altitude and lithology of FTD samples from Subansiri, Arunachal.

Sr. No.	Sample No.	Altitude (metres)	Latitude	Longitude	Lithology	Tectonic unit
Kimin-Koluriang section						
1.	Z 179	841	27^0 47.442′	93^0 31.689′	Gneiss	HHC
2.	Z 170	892	27^0 54.234′	93^0 22.045′	Mylonite gneiss	HHC
3..	Z 164	1160	27^0 45.254′	93^0 36.824′	Quartzite	LHW
4.	Z 163	1164	27^0 44.186′	93^0 37.234′	Gneiss	DG (LHCB)
5.	Z 159	1101	27^0 40.079′	93^0 37.934′	Migmatite	DG (LHCB)
6.	Z 129	1169	27^0 36.230′	93^0 40.191′	Porphyritic granite gneiss	DG (LHCB)
7.	Z 124	1449	27^0 34.306′	93^0 40.306′	Granite gneiss	DG (LHCB)
8.	Z 2	1213	27^0 32.089′	93^0 45.603′	Porphyritic granite gneiss	DG (LHCB)
9.	Z 11	1694	27^0 37.808′	93^0 50.767′	Porphyritic granite gneiss	DG (LHCB)
10.	Z 13	1406	27^0 40.052′	93^0 53.510′	Phyllite	LHSZ
11.	Z 19	631	27^0 45.338′	94^0 02.481′	Quartzite	LHSZ
12.	Z 118	728	27^0 21.066′	93^0 46.912′	Mylonite gneiss	LHSZ
13..	Z 136	795	27^0 20.038′	93^0 48.768′	Sandstone	LH (Gond. Belt)
Subansiri River section						
14.	Z 92	1245	28^0 21.221′	93^0 31.358′	Grt-Ky-Sil gneiss	HHC
15.	Z 88	1519	28^0 22.338′	93^0 38.872′	Gneiss	HHC
16.	Z 82	795	28^0 24.389′	93^0 46.782′	Porphyritic granite gneiss	HHC
17.	Z 81	775	28^0 24.255′	93^0 49.154′	Phyllite	LHW
18.	Z 103	630	28^0 19.529′	$94^0$03.126′	Granite gneiss	HHC
19.	Z 80	229	28^0 00.344′	94^0 12.153′	Porphyritic granite gneiss	DG (LHCB)
20.	Z 110	882	27^0 51.502′	$94^0$11.966′	Granite gneiss	DG (LHCB)
21.	Z 70	735	27^0 59.409′	94^0 24.329′	Quartzite	LHSZ
Siyom River section						
22.	Z 27	1966	28^0 38.210′	94^0 01.404′	Granite gneiss	HHC
23.	Z 34	2081	28^0 33.278′	94^0 12.269′	Psammatic gneiss	HHC
24.	Z 26	1185	28^0 32.973′	94^0 23.583′	Porphyritic granite gneiss	HHC
25.	Z 45	1212	28^0 30.234′	94^0 24.442′	Granite gneiss	HHC
26.	Z 51	981	28^0 31.060′	94^0 29.465′	Porphyritic granite gneiss	HHC

NOTES: HHC–Higher Himalayan Crystallines. LHW–Lesser Himalayan Window. DG–Daporijo Gneiss (Lesser Himalayan Crystalline Belt). LHSZ–Lesser Himalayan Sedimentary Zone. Gond. Belt–Gondwana Belt.

Table 4.3: AFT and ZFT bedrock ages from Subansiri and Siyom River catchment areas, Arunachal Himalaya

Sr. No	Sample Code	Number of Crystals	Track Densities						P (χ^2) % age	Age (Ma) (±1σ)
			Spontaneous		Induced		Glass Dosimeter			
			ρ_s	N_s	ρ_i	N_i	ρ_d	N_d		
A. Kimin-Koluriang Section										
1.	Z179 A	25	0.334	48	17.16	6920	1.103	2758	34.19	**3.5±0.3**
2.	Z170 A	26	0.085	63	6.453	4723	1.103	2758	57.85	**2.2±0.3**
	Z170 Z	20	0.800	192	23.72	5499	2.21	5544	59.30	**4.3±0.3**
3.	Z164 A	22	0.113	101	9.698	7929	1.103	2758	11.05	**2 ±0.3**
	Z164 Z	19	1.04	134	23.91	3075	2.21	5544	90.65	**5.6±0.5**
4.	Z163 A	36	0.079	89	2.427	2830	1.103	2758	82.06	**5.1±0.6**
	Z163 Z	19	1.26	211	23.65	4011	2.21	5544	6.81	**6.3±0.6**
5.	Z159 A	40	0.115	128	2.522	2886	1.103	2758	73.26	**7.2±0.7**
	Z159 Z	22	2.19	632	26.20	7135	2.21	5544	<1	**9.0±0.8**
6.	Z129 A	34	0.211	127	4.838	2672	1.103	2758	98.71	**7.7±0.7**
	Z129 Z	13	3.52	636	39.54	7248	2.21	5544	<1	**10.4±1.1**
7.	Z124 A	37	0.179	134	2.622	2024	1.233	3038	69.48	**12.1±1.2**
8.	Z2 A	5	0.082	6	2.387	156	1.233	3038	98.11	**7.0±2.9**
9.	Z11 A	23	0.234	94	4.470	1704	1.233	3038	90.75	**10±1.1**
	Z11 Z	20	3.6	1155	34.53	10708	2.21	5544	<1	**13.2±0.7**
10.	Z13 A	6	0.171	30	3.317	574	1.233	3038	96.18	**9.5±1.8**
11.	Z19 Z	16	1.99	288	20.97	2942	2.21	5544	85.98	**12.0±0.8**
12.	Z118 A	22	0.091	34	2.88	1185	1.103	2758	98.01	**4.7±0.8**
13.	Z136 A	36	0.085	65	1.793	1477	1.233	3038	75.20	**8.5±1.1**
B. Subansiri River Section										
14.	Z92 A	31	0.022	26	0.795	947	0.64	1594	85.25	**2.6±0.5**
15.	Z88 A	28	0.043	42	1.448	1375	0.64	1594	97.23	**2.9±0.5**
	Z88 Z	30	0.56	240	20.75	8929	2.21	5544	8.84	**3.3±0.3**

16.	Z82 A	27	0.035	41	1.282	1415	0.64	1594	98.95	**2.7±0.4**
17.	Z81 Z	32	1.06	429	23.13	9422	2.21	5544	20.33	**5.6±0.3**
18.	Z103 A	10	0.032	10	0.566	178	0.64	1594	98.73	**5.3±1.7**
	Z103 Z	9	2.67	225	44.34	3671	2.21	5544	9.73	**7.4±0.6**
19.	Z80 A	31	0.179	129	2.717	1971	0.64	1594	80.04	**6.2±0.6**
	Z80 Z	18	1.3	212	23.41	13920	2.21	5544	6.47	**6.7±0.6**
20.	Z110 A	30	.0.101	134	1.294	1704	0.64	1594	>99	**7.4±0.7**
21.	Z70 Z	27	1.55	570	17.02	6211	2.21	5544	42.36	**11.0±0.6**
C. Siyom River Section										
22.	Z27 A	12	0.043	14	1.455	4530	0.64	1594	70.67	**2.9±0.8**
23.	Z34 Z	26	0.7	186	18.78	4812	2.21	5544	46.93	**4.7±0.4**
24.	Z26 A	26	0.071	66	1.491	1367	0.64	1594	98.61	**4.5±0.6**
	Z26 Z	29	1.11	525	24.03	11228	2.21	5544	37.70	**5.7±0.3**
25.	Z45 A	34	0.066	74	1.496	1731	0.64	1594	95.88	**4.0±0.5**
	Z45 Z	5	1.56	162	27.7	2951	2.21	5544	18.74	**6.7±0.6**
26.	Z51 A	26	0.226	134	3.512	2106	0.64	1594	>99	**6.0±0.6**
	Z51 Z	19	2.1	535	31.85	8461	2.21	5544	9.98	**7.9±0.4**

NOTES: ρ_s=Spontaneous fission track density. N_s=Total number of spontaneous tracks counted. ρ_i=Induced track density. N_i=Total number of induced tracks counted. ρ_d=Induced tracks in dosimeter glass CN5. N_d=Total number of induced tracks measured in dosimeter glass. $P(\chi^2)$=Probability of obtaining the observed χ^2 value for v degrees of freedom, where v=number of crystals-1. Age determined using the equation $T=1/\lambda_d \ln [1+ \zeta\lambda_d(\rho_s\rho_d/\rho_i)]$, where λ_d=Total decay constant of ^{238}U ($1.55125\times10^{-10}a^{-1}$), where G=Geometry factor (0.5 in the present study) and ζ = Zeta Calibration Factor (ζ = Zeta Calibration Factor (CN5 = 295.58±9.20 and CN1 =110±2.6 are used in the present study). Track densities ρ's are measured and are 10^6 tr/cm^{-2}. A–Apatite. Z–Zircon.

4.5.1. Kimin–Koluriang Section

In this traverse, two samples Z179 and Z170 from the extreme northwestern part of the HHC yielded the AFT ages of 3.5±0.3 and 2.2±0.3 Ma, respectively, while the ZFT age of one of the sample Z170 near the MCT had the age of 3.5±0.3 Ma. The Lesser Himalayan Menga Window in this section beneath the crystalline rocks could yield the AFT and ZFT ages from only sample Z164 and are 2.0±0.3 and 5.6±0.5 Ma, respectively. Immediately to the south of the Menga window is the Daporijo Gneiss of the Lesser Himalayan Crystalline Belt, which revealed a string-shaped age pattern. Sample Z163 nearest to the window has an AFT age of 5.1±0.6 Ma and the ZFT age of 6.3±0.6 Ma. Further south, one migmatite sample Z159 yielded the AFT and ZFT ages of 7.2±0.7 and 9.0±0.8 Ma, respectively. Ages get older further south in which the Z129 has the AFT and ZFT ages of 7.7±0.7 and 10.4±1.1 Ma, respectively, while Z124 gave the AFT age of 12.1±1.2 Ma. The apatite FT ages of another two samples Z2 and Z11 near the hangingwall of the Tamen Thrust/MCT are 7.0±2.9 and 10±1.1 Ma, respectively, while the ZFT age from the Z11 sample is 13.2±0.7 Ma, which happens to be the oldest from the whole lot of the Arunachal Himalaya samples under consideration. A granite Z118 has intruded the Lesser Himalaya sedimentary Khetabari Formation and gave an AFT age of 4.7±0.4 Ma and one phyllite sample Z13 gave AFT age of 9.5±1.8. A zircon FT age could be obtained from one Lesser Himalayan quartzite sample Z19, which yielded 12±0.8 Ma. A Permian gritty sandstone sample Z136 from within the Gondwana yielded a reset fission track apatite age of 8.5±1.1 Ma.

4.5.2. Subansiri River Section

In this section, the northernmost sample Z92 from the HHC yielded the AFT age of 2.6±0.5 Ma, while Z88 gave both AFT and ZFT ages of 2.9±0.5 and 3.3±0.3 Ma,

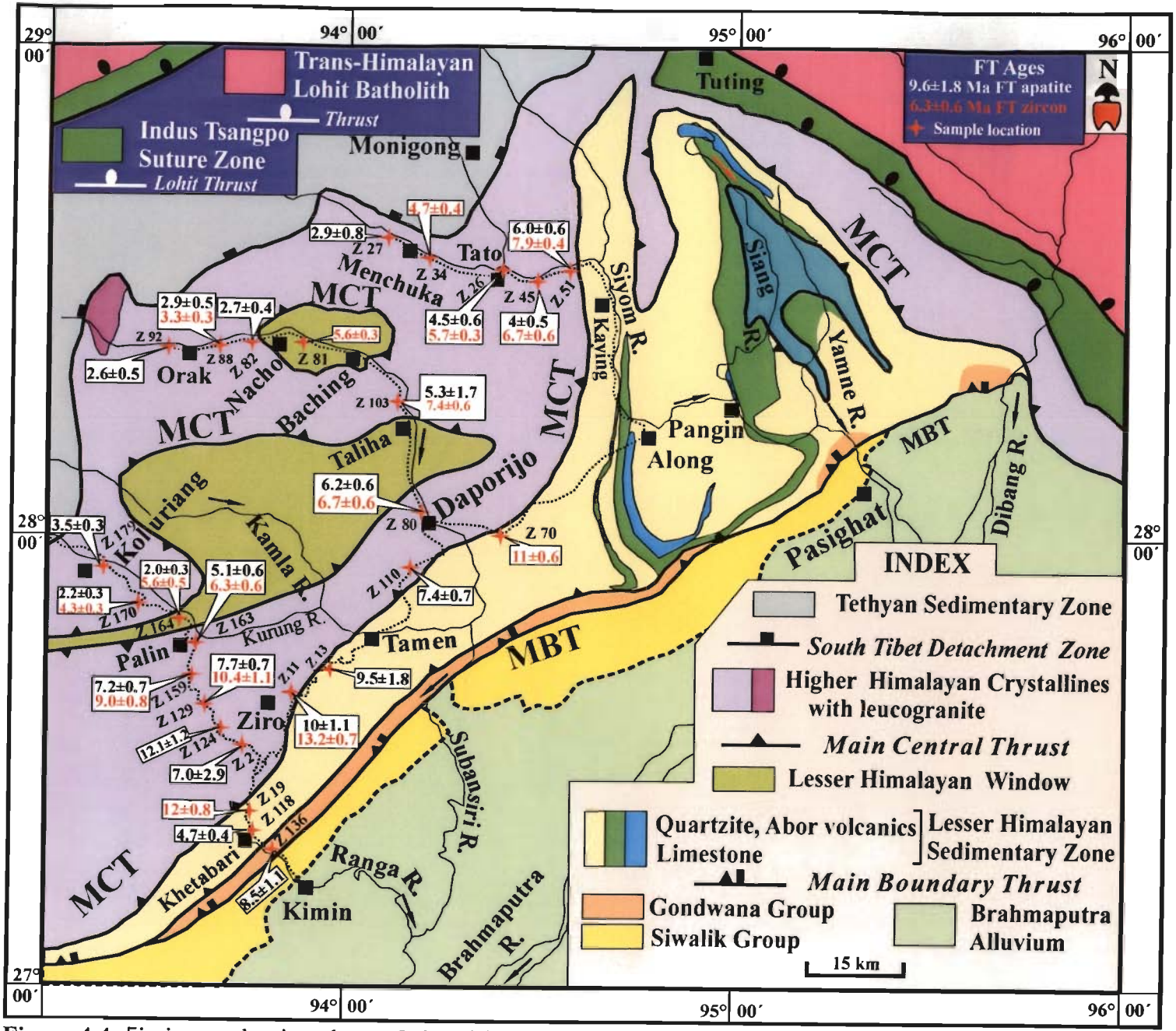

Figure 4.4: Fission track mineral ages,Subansiri and Siyom Valleys, Arunachal Himalaya.

Ages are reduced slightly near the MCT zone in which sample Z82 gave an AFT age of 2.7±0.4 Ma. One sample Z81 from the Lesser Himalayan Nacho Window gave the ZFT age of 5.6±0.3 Ma, but apatite FT age could not be determined from this unit. Further south, the gneissic rock exposed between the two windows yielded the AFT and ZFT ages of 5.3±1.7 and 7.4±0.6 Ma, respectively.

Within the Daporijo Gneiss of this section, the sample Z80 nearest to the Nacho-Menga window gave a fission track ages 6.2±0.6 and 6.7±0.6 Ma for apatite and zircon, respectively. However, sample Z110 of porphyritic granite gneiss yielded an AFT age of 7.4±0.7 Ma. From the outer Lesser Himalayan Sedimentary unit, one sample Z70 yielded the zircon FT age of 11.0±0.6 Ma.

4.5.3. Siyom River Section

Five samples were taken for the fission track study from this traverse. The farthest sample Z27 from the HHC gave an apatite fission track age of 2.9±0.8 Ma, while sample Z34 yielded a ZFT age of 4.7±0.4 Ma. One sample Z26 near the village Tato yielded both the AFT and ZFT ages of 4.5±0.6 and 5.7±0.3 Ma, respectively. Similarly, sample Z45 has ages of 4.0±0.5 and 6.7±0.6 Ma for apatite and zircon, respectively. The sample Z51 near the MCT in this section yielded the AFT and ZFT ages of 6.0±0.6 and 7.9±0.4 Ma, respectively.

4.6. Interpretation

Fission track ages for both the apatite and zircon show more or less same range and pattern reported in the rest of the Himalaya. The AFT age plot against the distance from the southernmost exposure of this folded MCT shows a unique pattern. The AFT

ages are youngest in the Lesser Himalayan Window exposed beneath the crystalline rocks due to erosion of the overthrust crystalline rocks. This is most prominent in the Kimin-Koluriang section (Fig. 4.5 A), where the widow zone rocks show the AFT age of 2 Ma. Immediately to the north of this zone in the HHC, the age slightly increases to 2.2 Ma and further north it increased to 3.5 Ma.

Samples collected from the south of this window within the synformally folded Daporijo Gneiss of the Lesser Himalayan Crystalline Belt shows a bell-shaped age pattern. The sample immediately south of this window has an AFT age of 6.3 Ma. The ages gradually increase as one goes towards the core of this synform with oldest apatite fission track age of 12 Ma. Thus, it seems that the AFT ages are mainly controlled by the kinematics of this folded MCT. The ZFT ages do not mimic the pattern of the present structure (Fig 4.5A). However, the ages gradually decrease as we go away from the southernmost exposure of the MCT with 13.2 Ma in the immediate hanging wall of Tamen Thrust to 4.3 Ma in the core of the HHC. This could be the evidence for the linear cooling along the low-angled MCT till 4.3 Ma. Later this MCT got folded and simultaneous erosion leads to the exposure of Lesser Himalaya. This window controls the late phase cooling pattern in the region. In this traverse, the Tamen Thrust has the least effect in both the AFT and ZFT cooling ages. In other words the thermal signature of the thrusting has been erased off by the doming/window exposure and later is the main factor controlling the age pattern in this area.

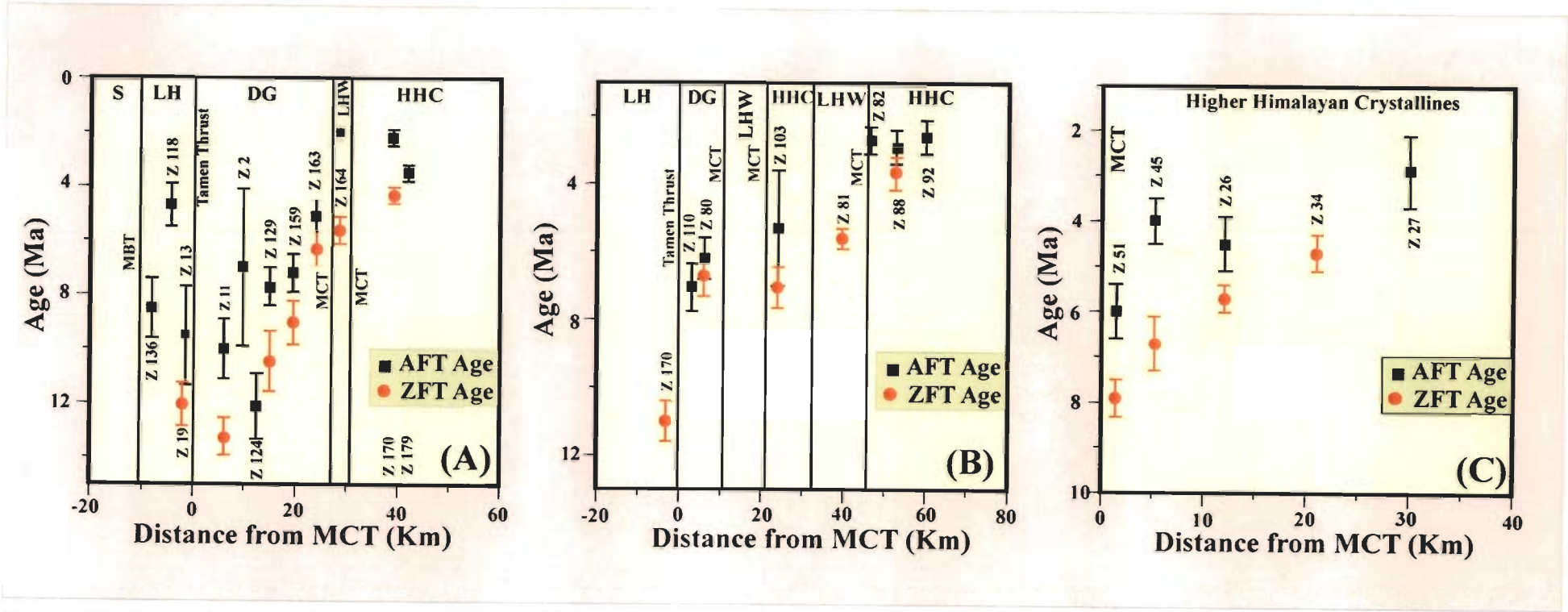

Figure 4.5: Age vs. Distance from MCT (A) Kimin-Koluriang Section. (B) Subansiri River Section. (C) Siyom River Section. **Notes:** S-Siwalik, LH-Lesser Himalaya, DG-Daporijo Gneiss (Lesser Himalayan Crystalline Belt), LHW-Lesser Himalayan Window, HHC- Higher Himalayan Crystallines, MCT-Main Central Thrust, MBT-Main Boundary Thrust.

In Subansiri valley, the pattern is similar to that of Kimin-Koluriang section; the AFT ages in the Daporijo Gneiss drop down from 7.4 Ma near the Tamen Thrust to 6.2 Ma near the Menga window. On the northern side of the window, the AFT age in one of the crystalline rock sample decreases to 5.3 Ma. North of this unit is the Nacho Window, the northern limb shows its thermal signature in the AFT ages. Sample nearest to the window has the AFT age of 2.7 Ma. The age increased to 2.9 as we go away from the window but decreases again to 2.6 Ma in the northernmost sample (Fig. 4.5 B). However, in this traverse, the AFT ages clearly mimic the fold-thrust pattern in the area. However, in case of the zircon FT ages, the ages are reduced gradually from 11 Ma in the Lesser Himalaya to 3.3 Ma within the HHC. Thus, a similar pattern is observed like the Kimin-Koluriang section, where the AFT age pattern is more or less controlled by the window development in the region. In the northern Menchuka section, the window is not exposed so far, however the thermal imprint of an underlying folded structure is clearly indicated in the AFT age pattern. The AFT age near the village Tato is 4.5 Ma and increases to 6 Ma in the basal parts near the MCT, but further upstream of the Siyom River, the AFT ages decrease to 2.9 Ma. This means that the core of an antiform is somewhere between village Tato and sample Z34. The trend for zircon FT ages is almost the same with that of the previous two traverses, where the ZFT ages gradually reduce from the MCT to the interior of the HHC (Fig. 4.5 C). Beside this, a sudden drop in the AFT ages from 6 to 4 Ma from samples Z51 to Z45 may be due to the presence of a thrust between the locations of these two samples. The AFT age pattern in the Arunachal Himalaya strongly mimics the structural layout of the region, thus providing an evidence for the tectonic control on the thermal age pattern of the Himalaya.

Chapter 5: Detrital Thermochronology

5.1. Introduction

Orogenic sediments preserve the signatures of their respective mountainous sources. Of the various techniques applied in deciphering the source characters, detrital thermochronology has become one of the most important methods for understanding the orogenic processes (Cervany et al., 1988; Garver et al., 1999; Sorkhabi, 2000; Bernet et al., 2001, 2004a, 2004b, 2006; Najman et al., 2004; Ruiz et al., 2004; Hodges et al., 2005; Beek et al., 2006; Ruiz and Seward, 2006; Stewart et al., 2008; Jain et al., 2009). Preservation of ages of sedimentary grains, derived by erosion of various source areas, is fragmentary and needs to be re-assembled (Garver et al., 1999), however it offers at least two advantages over bedrock thermochronology (Reiners and Brandon, 2006): (i) ages record much longer history that can be obtained in contrast to the ages of bedrock samples, and (ii) easier sampling over a large area.

Detrital thermochronology is mainly carried out to constrain the provenance of the sediments and unroofing history of the orogenic belt (Reiners and Brandon, 2006; Jain et al., 2009). Other applications include stratigraphic correlation and determining the age of the sedimentary basin and its subsidence history.

Techniques for the detrital thermochronology include Fission track (FT), U-Th/He, Ar/Ar and U/Pb dating. Detrital FT dating of zircon has been used for provenance analysis, starigraphic correlation and dating sediments (Garver et al., 1999 and reference there in; Bernet et al., 2004b; Jain et al., 2009). This alone or in combination with other

thermochronological techniques has been used to quantify the exhumation rate in the source region (Bernet et al., 2004a, b; Rahl et al., 2007).

Although detrital thermochronological approach is very common for the orogenic studies, a very few works on detrital apatite fission track dating in the Himalaya have been done so far (Sorkhabi, 2000; Beek et al., 2006). Such works in the Siwaliks of the Nepalese Himalaya reported both reset as well as un-reset AFT ages. Based on these investigations, the denudational history of the source areas and the post-depositional thermal history of the foreland in the Nepalese Siwaliks have been worked out (Beek et al., 2006). In the Surai Khola section of the Central Nepalese Siwaliks, the AFT ages showed a single population and range between 4.1 to 9.2 Ma. All the samples in this section have central AFT ages older than their depositional ages. These AFT ages increase with the stratigraphic depth, suggesting that they are un-reset. In the Tinau Khola and the Karnali sections, eastward of the Surai Khola in the western Nepal, the Siwalik samples showed both single peak as well as multiple peaks. The peaks range between 1.7 to 25.8 Ma in the Karnali section and between 2.5 and 34.9 Ma in the Tinau section. The stratigraphically-upper samples are un-reset, while deeply-buried samples are partially reset. Based on the un-reset AFT ages of Nepal Siwalik samples, exhumation rate of ~1.8 km/Ma in the central Nepal and between 1.0 and 1.5 km/Ma in the western Nepal in the source area for the last ~7 Ma are reported (Beek et al., 2006). These rates are complemented by detrital ZFT and bedrock AFT thermochronology (Burbank et al., 2003; Bernet et al., 2006). Beside these, based on reset AFT ages, the onset of exhumation of frontal Siwalik along the Himalayan Frontal Thrust has been reported to be at ~2 Ma (Beek et al., 2006).

Apatite fission track dating of a modern sand sediment from a stream at Jhajjar, Jammu and Kashmir, which drains mostly through the Siwaliks before it joins the Tawi River shows an age range between 4.8 and 28.6 Ma and a cluster around 15-20 Ma (Sorkhabi, 2000). The 4-5 Ma grains have been reported to have sourced in the HHC, while the 14-18 Ma old grains were denuded from the Miocene leucogranite in the Higher Himalaya soon after its formation (Sorkhabi, 2000). Similar works from the Trisuli and the Marsyandi Rivers, just before their confluence in the Nepalese Himalaya have reported central ages of 1.9 and 1.7 Ma respectively (Beek et al., 2006). These rivers drain through the Lesser Himalayan Sedimentary belt, the HHC and the Tethyan sediments. These workers also reported a central age of 8.0 Ma in a sediment collected from the Karnali River, just before it enters the Ganga Plains. The old peak could be due to contribution of un-reset apatite grains from the Siwaliks (Beek et al., 2006).

In the present study, detrital FT apatite analysis of the Late Cenozoic Siwaliks of the Himalayan foreland basin and river sands from the Subansiri River and its tributaries, and Siyom River has been carried to decipher the provenance of the sediments and exhumation pattern in the Arunachal Himalaya. In Chapter 4 detailed FT work on bedrock samples in the Arunachal Himalaya has been presented and is compared with detrital thermochronology results in this chapter to analyze the above issues.

5.2. Previous work in the Eastern Himalaya

Recent detrital zircon U/Pb and FT analyses of modern river sediments from the Brahmaputra River showed extremely localized erosion in the Eastern Himalayan Syntaxis (EHS) region (Stewart et al., 2008; Cina et al., 2009), and is supported by the

bedrock thermochronological data set (Booth et al., 2008; Seward and Burg, 2008; Stewart et al., 2008; Cina et al.,2009).

Limited detrital thermochronology research in the Eastern Himalaya has revealed the presence of 'hot spots', which experienced exhumation rate up to 10 mm/yr (Stewart et al., 2008), and also variable source areas for the sediments, including the Gangdese Batholith (Cina et al., 2009). Detrital zircon fission track dating of modern river sand sediments of the Brahmaputra River at Pashighat showed peaks of 0.6, 4.7, 10.0, 18.0 and 37.0 Ma, in which the youngest peak P1 comprises 47% of the total analyzed grains (Stewart et al., 2008). This fraction of zircons has been eroded from the syntaxial bend at Namcha Barwa, where the bedrock thermochronological ages are very young. The $^{40}Ar/^{39}Ar$ mica ages range between 0.9 and 2.5 Ma, while the U-Th/He zircon ages are between 0.3 and 1.0 Ma (Malloy, 2004). The AFT and ZFT ages are the youngest in the whole of the Himalaya, and are as low as 0.5 and 0.2 Ma, respectively at different localities of the EHS (Seward and Burg, 2008). The contribution of the young ages from this region is also supported from the results of detrital ZFT analysis of sediments, collected from different locations in the upstream of the Tsangpo bend. In the upstream region, ZFT peaks of 5.8, 15.0, 25.0 and 56.0 Ma are reported at the mouth of the Parlung River, and ZFT peaks of 7.5, 17.0 and 40.0 Ma are reported at a location 40 km upstream of the bend and lack the very young peak (~ 0.6 Ma) like the one in the Pashighat sample (Stewart et al., 2008).

The detrital U-Pb zircon ages in the upstream of the EHS bend has a younger component coming from the Gangdese Batholith and an older one from the Precambrian Lhasa block (Booth et al., 2008). However, as soon as the river crosses the Namcha Barwa bend it starts eroding the basement gneisses whose crystallization age is about 450

Ma (Burg et al., 1998; Booth et al., 2008) and dilutes the younger component from the Gangdese Batholith. Based on these, Stewart et al. (2008) worked out that 45% of Brahmaputra sand sample at Pashighat are derived from the Namcha Barwa region. This is similar to the detrital U-Pb zircon ages, reported by Cina et al. (2009), in which sand sample collected from the Yalu River has young Gangdese component of <200 Ma comprising up to 65% of the total analyzed grains. This fraction is reduced to 25% in the Siang River at Pashighat, which further decreases to 12% in the sample collected from Brahmaputra River at Tezpur (Cina et al., 2009). The Himalayan component increases downstream. The dilution of the Gangdese component with simultaneous increase of the Himalayan component has been attributed to very fast erosion rate at the syntaxial bend at Namcha Barwa (Stewart et al., 2008; Cina et al., 2009). The Gangdese component is also reported in the Subansiri River, though it does not drain through this batholith. The Subansiri River sediment collected from the north of the Main Boundary Thrust (MBT) has only 3% grains having < 200 Ma U-Pb zircon ages, while south of the Main Frontal thrust (MFT) these increase to 18%. This has been explained by the contributions from the reworked zircon from the Siwaliks (Cina et al., 2009). On the contrary, transverse Teesta and Kameng Rivers do not possess the Gangdese component. In the Lohit River, 36% zircon grains have been reported to have < 200 Ma U-Pb ages (Cina et al., 2009).

The temporal variations of the detritus influx from the Trans-Himalaya have been worked out by investigating the Neogene Foreland Basin sediment (Beek et al., 2006; Cina et al., 2009; Jain et al., 2009). In the Sikkim Himalaya, the Siwaliks lack detrital zircon U-Pb age records of the Gangdese component, while in the Arunachal Himalaya, these show a considerably prominent signature. In Bhalukpong area of the western Arunachal Himalaya, the Subansiri Formation (Upper Miocene) has 31% U-Pb zircon

ages of <200 Ma with a distribution between 20 and 110 Ma and cluster between 40 and 60 Ma. Stratigraphically, older Dafla Formation has just 2% zircons with ages <200 Ma at 125 and 135 Ma (Cina et al., 2009). Similarly, U-Pb zircon ages of less than 200 Ma are 16%, 23% and 15% in samples of the Dafla Formation, Subansiri Formation and Kimin Formation at Itanagar in the Cenozoic Foreland basin, respectively. Majority of the young zircons are between 40 and 110 Ma with a cluster between 40 and 70 Ma (Cina et al., 2009).

5.3. Fundamentals of detrital thermochronology

The principle behind the detrital thermochronology is the lag time, which is the time difference between the thermochronological and depositional ages (Garver et al., 1999). This can be reconstructed by correlating erosion, transport and deposition of sediments. A simplified setting of rocks, exhumed from a depth and simultaneous erosion and deposition in a basin, is given in Figure 5.1. In the basin, there is a mixture of detritus from different sources. If the source has different thermal signatures, it is reflected in these sediments. During the orogenic process, the rock is exhumed and passes through the closure temperature (T_c) of different minerals at different time (t_c) and reached surface where temperature is T_s. The forces behind this exhumation have been explained by tectonics, climatically induced erosion or combination of both (Beek et al., 2006). Once the rock reached the surface, it is being eroded off at a time (t_e), transported through the rivers and finally deposited in an adjacent basin at a time (t_d). This sediment in the basin has contributions from all the sources it has been derived. And, these sediments preserve the signatures of their sources. The time difference (t_d–t_c) is the lag time. For the recent sediments, the transportation and residence time are considered to be almost negligible (Garver et al., 1999). Thus, the cooling ages, derived from the river sediment, is more or

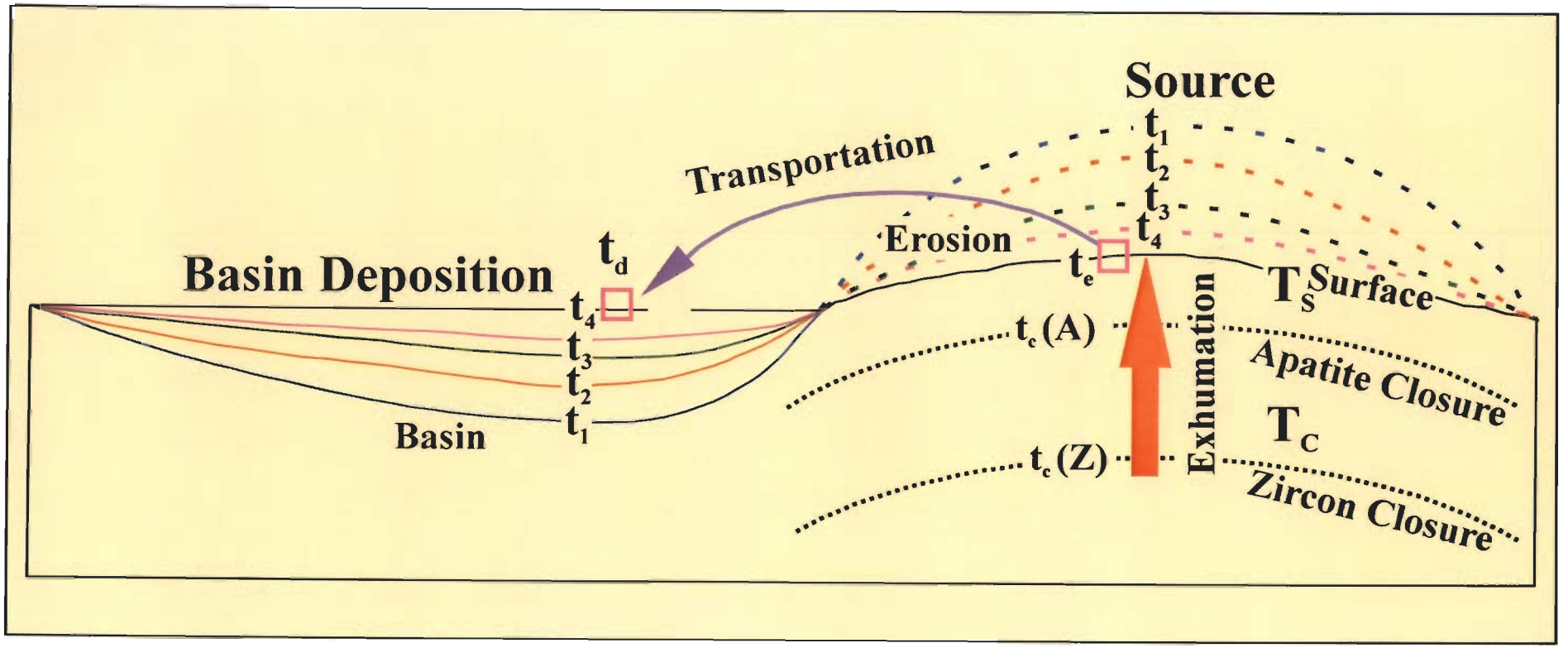

Figure 5.1: Concepts of detrital thermochronology. **Notes:** t_c (Z)-Time for ZFT closure temperatutre. t_c (A)-Time for AFT closure temperature. t_d-Time of deposition. T_e-Time of erosion. T_s-Surface temperature.

less equal to the cooling ages of their respective source areas. In the Himalayan Rivers, the sediments are coming from units of diverse ages (Cerveny et al., 1988; Stewart et al., 2008) and, thus, thermochronological analysis of detrital minerals has different age groups depending on their sources. Generally, different population or peak components from the composite data set are defined by different peak fitting methods for detrital fission track grain analysis (Galbraith and Green, 1990; Brandon, 1992, 1996). In the present work, BINOMFIT software of Brandon (2002) is used for the analysis. These different peaks characterize the different sources, and can be utilized to work out the exhumation rates of the sources (Reiner and Brandon, 2006). Thermal age vs. exhumation rate relationship by 1D thermal modelling (AGE2EDOT) by Brandon et al. (1998) is normally used by defining appropriate thermal parameters of the orogenic belt.

5.4. Sampling and methodology

In the present work, 1 sandstone sample from the Pliocene Kimin Formation of the Siwalik Group and 9 modern river sediments were selected for the detrital apatite fission track thermochronology (Fig. 5.2). Thermochronological analysis of the Siwalik sample is for the source characterization during the Pliocene time (5.0-1.8 Ma), whereas the modern river sediments provide constrains on the present-day sources of the sediments. This kind of study can be utilized to decipher the changes in sources sediments during late Siwalik times to the Present in view of the proposed hypothesis of river capture of the Yule River by the Subansiri during the former period. The Upper Siwalik sample has been collected from the Kimin-Ziro road section, while 7 sand samples are from the main Subansiri River and its tributaries. Two sand samples are from the Siyom River (Fig. 5.2).

Sample Z155 was collected upstream of the Ranga Dam on the Ranga River, which has the catchment area covering parts of the frontal Lesser Himalayan Sedimentary belt (Khetabari Formation) and the Daporijo Gneiss. Downstream from this location along the same river, sample Z145 has additional lithounits of the Gondwana and the Siwalik belts in the catchment.

Sample Z169 from the upper parts of the Kurung River at Koluriang has the catchment covered by the HHC and the Tethyan Sedimentary Zone. This river joins the Kamla River, and the latter joins the main Subansiri River.

Sample Z113 has been collected from Tamen along the Kamla River and covers the catchment, drained by both the Kamla and Kurung Rivers. This sample receives the sediments from (i) the Daporijo Gneiss, (ii) the Lesser Himalayan Window Zone, (iii) the Higher Himalayan Crystalline Belt, and (iv) the Tethyan Sedimentary Zone.

From the main Subansiri River, sample Z93 was collected at Orak in the upper reaches, and has the contributions from the HHC, the Tethyan Sedimentary Zone as well as the Cenozoic Maza Granite. As the Subansiri River originates in Tibet, it drains a very large track of southern Tibet to the north of Bhutan. Sample Z80(S) has contributions from the above mentioned units as well as from the Lesser Himalayan Window Zone and the Daporijo Gneiss. Sample Z185 was collected from Gaurkamukh, where the Subansiri River debouches into the Brahmaputra Plains. It has the catchment across all the above-mentioned units, including the Permian Gondwana and the Siwalik Belts.

Along the upper Siyom River–an important tributary of the Siang River, one sample Z30 was collected from Menchuka with a small catchment in the Tethyan

Sedimentary Zone and the HHC, while other sample Z62 from downstream has inputs from the Lesser Himalaya, also (Fig. 5.2).

Experimental methodology for determining the detrital AFT ages is same, as given in Chapter 4. To summarize, apatite grains were separated by standard methods and hand-picking under binocular microscope. Apatites are arranged in an array of 12x12 and mounted using Araldite epoxy and hardner. The mounts were polished using diamond paste of different grades, as explained in Chapter 4 and etched using 0.6 % HNO_3 at 30°C for 55-70 seconds. Samples were packed with an external detector of low-uranium Brazilian muscovite. Either of the uranium glass standards CN1 or CN5 was placed at the top and bottom of each of the packing tube to measure the neutron fluence. Samples were irradiated at thermal irradiation facility at the CIRUS reactor at Bhabha Atomic Research Centre, Trombay, India. After irradiation, external muscovite detector was etched using HF to reveal the induced tracks. Finally, counting was done using a NIKON Opthiphot Microscope under 100X dry objective. Individual apatite ages were determined by the external detector method (EDM) and the ξ-calibration approach (Naeser, 1979; Hurford and Green, 1983; Jain et al., 2000). ξ-values of 110 ± 2.6 (2σ) for the CN1 glass (Jain et al., 2000) and 295.58 ± 9.20(2σ) for the CN5 glass (calibrated by the author in the present work were used for samples numbered as 1 to 9 and sample number 10, respectively (Table 5.1).

5.5. Data analysis and result

Apatite FT ages of these river sediments and the Upper Siwalik sandstone showed the time elapsed since the grains attained their closure temperature of 135°C (Patel and Carter, 2009; Thiede et al., 2009). These are characterized by mixed population of

different ages, which were reduced to individual peaks (Table 5.1; Fig. 5.2), using binomial peak fitting method by software BINOMFIT (Brandon, 2002). It is a window-based programme, developed by Mark Brandon of Yale University, for estimation of concordant and mixed grain age distributions and reducing to components or peaks from a mixed fission track grain age distribution, using the binomial peak-fitting algorithm of Galbraith and Green (1990) and Galbraith and Laslett (1993). The age distributions are also presented in the form of probability density plots, radial plots and individual grain age plots, covering the full spectrum of ages, peaks and peak ages (Figs. 5.3, 5.4 and 5.5). In the present work, a total of 436 apatite grains were analyzed from 10 samples, which have yielded multiple components/peaks with each peak indicating different sources. Characters of individual samples are given below.

5.5.1. Ranga River Catchment

Two samples from the Ranga River show two peaks each. Upstream of sample Z155, this river drains through the Lesser Himalayan Sedimentary belt and the Daporijo Gneiss. Out of the 50 grains in this sample, AFT ages range between 2.1 to 39 Ma with the youngest P1 Peak showing an age of 6.4 Ma, having 14.2% part of the grains (n=7). The other older P2 Peak has an age of 10.7 Ma containing bulk of the grains (85.8%, n=43). In this sample, one grain has an age of 2.1 Ma, while 10 older grains are between 20.0 to 30.0 Ma with one grain being as old as 39.Ma. Sample Z145, located further downstream, has a much younger peak of 2.1 Ma (13.5%, n=6) and an older peak of 11.3 Ma (86.5%, n=36). In both the samples, bulk of the apatite grains have been dated ~11.0 Ma with 9 older grains between 20.0 to 29.9 Ma and one very young grain of 0.4 Ma.

Table 5.1: Detrital Apatite Fission Track ages of the Upper Siwalik Formation and modern river sediments from the Arunachal Himalaya.

Sr. No.	Sample No.	Sample Location	Latitude and Longitude	Range (Ma)	No. of active grains	Peaks (%), N		
						P1	P2	P3
A. Ranga River Catchment								
1.	Z 155	Ranga Dam, Ranga River	27° 20.536′ 93° 48.720′	2.1 to 39	50	6.4 14.2%, 7	10.7 85.8%,43	———
2.	Z 145	Kimin, Ranga River	27° 21.136′ 93° 57.004′	0.4 to 29.9	42	2.1 13.5%, 6	11.3 86.5%, 36	———
B. Kurung-Kamla Rivers Catchment								
3.	Z 169	Koluriang, Kurung River	27° 53.699′ 93° 20.725′	1.4 to 25.3	48	2.4 63.3%, 30	8.9 36.7%, 18	———
4	Z 113	Tamen, Kamla River	27° 20.536′ 93° 48.720′	1 to 29.9	51	5.0 88.8%, 45	12.0 11.2%, 6	———
C. Subansiri-Kamla-Kurung Rivers Catchment								
5	Z 93	Orak, Subansiri River	27° 45.630′ 94° 00.328′	1.0 to 15.8	47	1.9 81.1%, 38	3.7 18.9%, 9	———
6	Z 80(S)	Daporijo, Subansiri River	28° 00.344′ 94° 12.153′	1.0 to 12.3	58	1.9 7.6%, 4	4.9 92.4%, 54	———
7	Z 185	Gaurkamukh, Subansiri River	27° 26.876′ 94° 15.323′	1.6 to 26.7	52	3.7 53.7%, 28	7.9 37.3%, 19	19.5 9.5%, 5
D. Siyom River Catchment								
8	Z 30	Menchuka, Siyom River	28° 36.283′ 94° 06.600′	1.6 to 24.9	36	4.2 100%, 36	———	———
9	Z 62	Yapuik, Siyom River	27° 13.891′ 94° 41.220′	2.1 to 12.9	15	NO PEAKS	———	———
E. Upper Siwalik sandstone (Kimin Formation)								
10	Z 143	Kimin Formation, (Upper Siwalik)	27° 21.010′ 93° 58.974′	1.8 to 36	37	4.3 82.6 %, 30	13.8 13%, 5	33.1 4.4%, 2

Notes: (P1-P3) - Binomial peak-fit ages determined by BINOMFIT programme (Brandon, 2002). %-Percent of grains. N-Number of grains. Sample (1-9)-CN 1 used as glass standard with zeta value=110±2.6 Sample 10-CN5 used as glass standard with zeta value=295.58± 9.20.

5.5.2. Kurung and Kamla Rivers Catchments

As has been enumerated in Section 5.3, the upper catchment areas of the Kurung River lie within the HHC and partly in the Tethyan Sedimentary Zone. In sample Z169 at Koluriang, two distinct peaks have been obtained from 48 analyzed grains. The P1 Peak of 2.4 Ma contains 63.3% grains (n=30), while the older 8.9 Ma P2 Peak (36.7%, n=18) constitutes an important component as well. Out of these, 2 grains are as young as 1.5 Ma, while an equal amount of grains are more than 20.0 Ma.

Sample Z113, collected from the Kamla River at Tamen has an AFT age range of 1.0-29.9 Ma. 51 analyzed grains yielded two peaks of 5.0 and 12.0 Ma respectively. The youngest P1 Peak contains a huge bulk of 88.8% grains (n=45), while the older P2 Peak of 12.0 Ma has only 11.2% grains (n=6). Two grains are around 1.0 Ma, while 3 grains are between 20.0 and 29.9 Ma. The youngest components must have been contributed by the HHC and Lesser Himalayan window. The later older peak must be from the small area in the Lesser Himalaya, drained by this river up to this location.

5.5.3. Subansiri River Catchment

This is the largest catchment in the region under consideration as far as the southernmost sample Z185 is concerned. From the main Subansiri River, the northernmost river sediment sample Z93, collected from Orak, has 47 apatite grains analyzed, and yielded two main peaks from the BINOMFIT programme. The youngest P1 Peak of 1.9 Ma contains bulk grains having 81.1% population (n=38), with an older subsidiary P2 Peak of 3.7 Ma (18.9%, n=9). Out of this population, 4 grains are around 1.0 Ma, while an equal number of grains are older than 10.0 Ma. From the available geological maps of the southern Tibet, drained by the Subansiri River (Anon, 2004; Cina

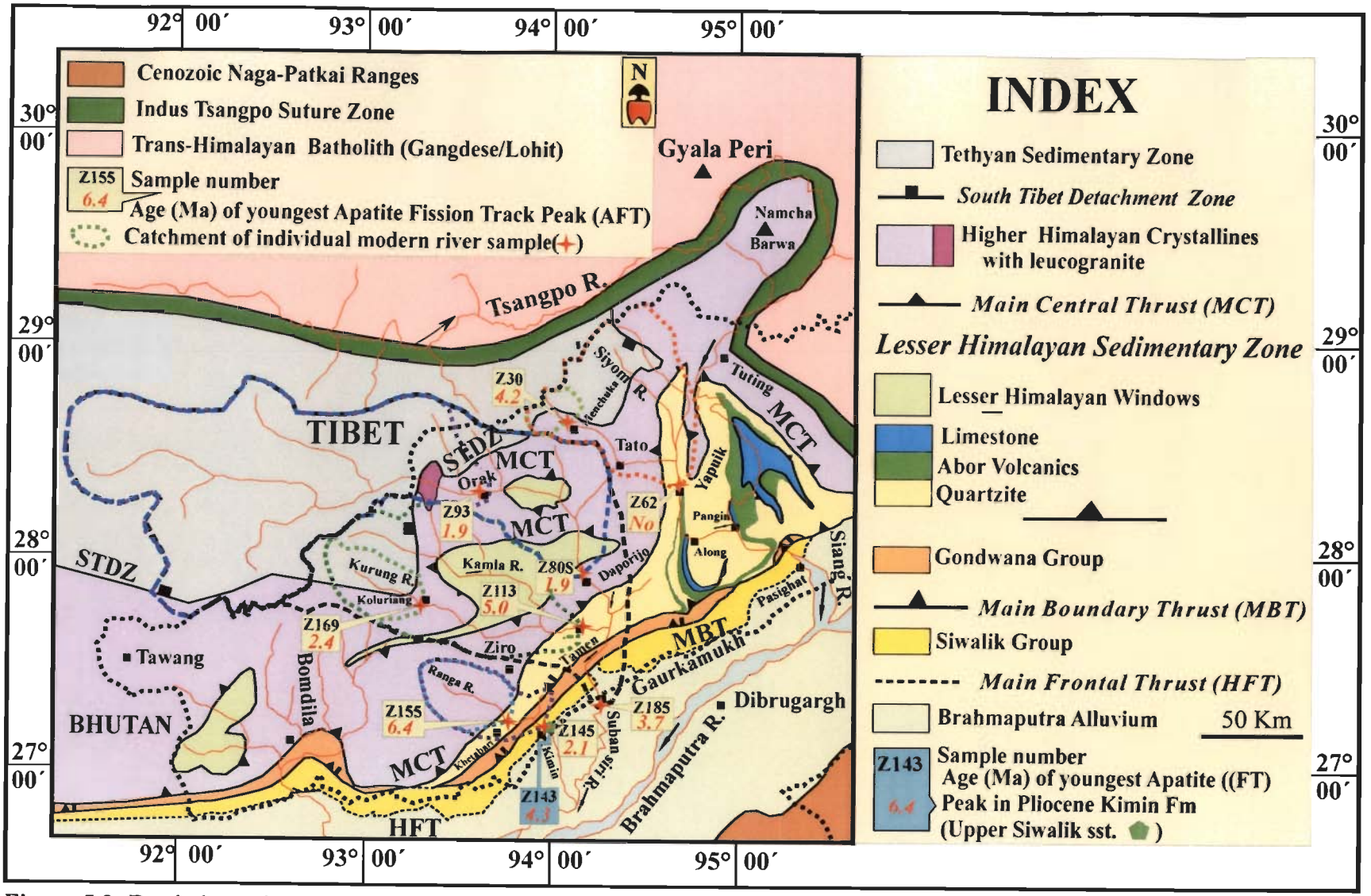

Figure 5.2: Detrital Apatite Fission Track ages of the Upper Siwalik Formation and modern river sediments plotted on the Geological Map of Eastern Himalaya (Map compiled by Prof. A.K Jain, IIT Roorkee).

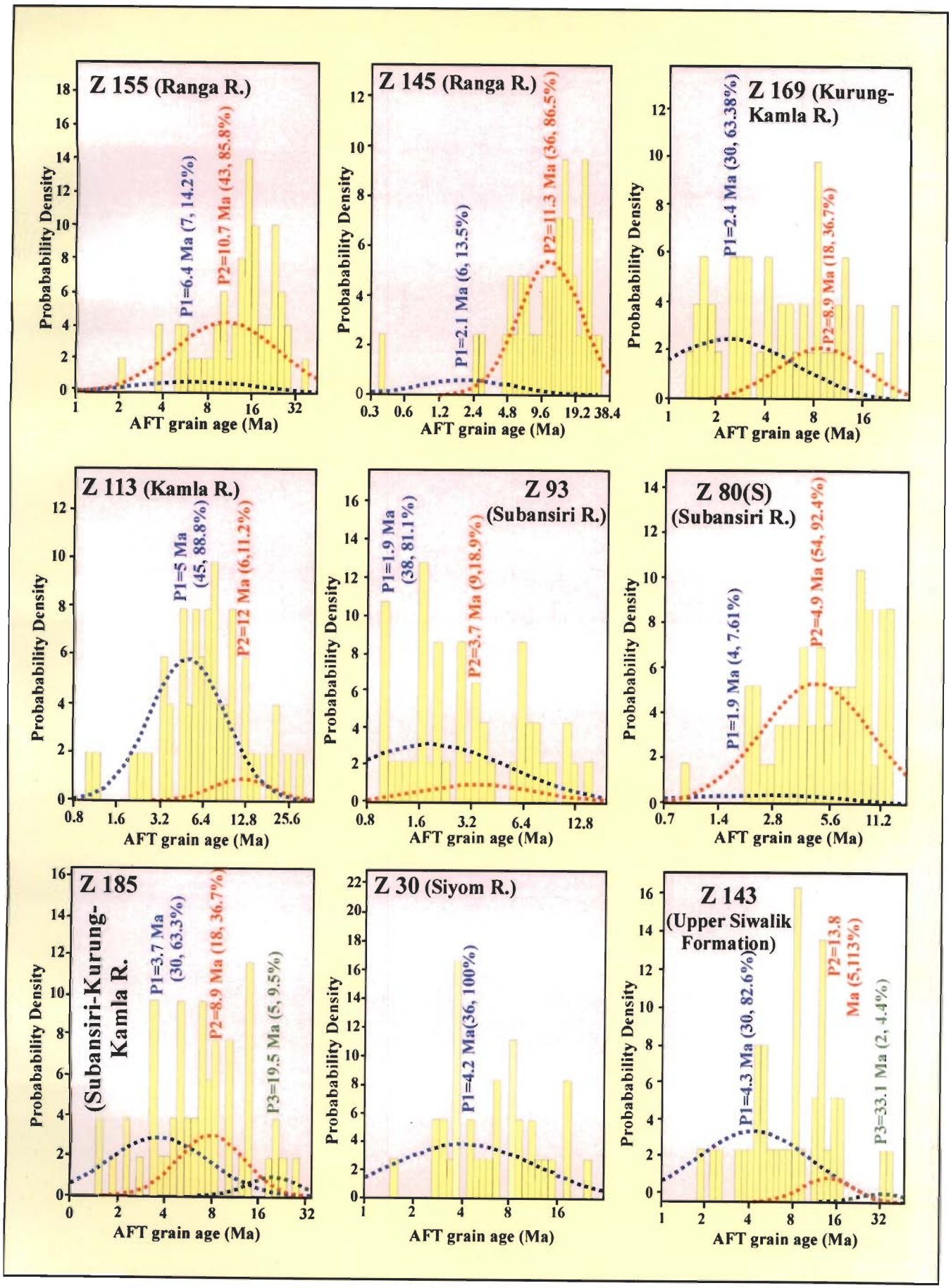

Figure 5.3: Probabilty density plot of AFT ages from the Upper Siwalik Formation and modern river sediments from the Arunachal Himalaya.

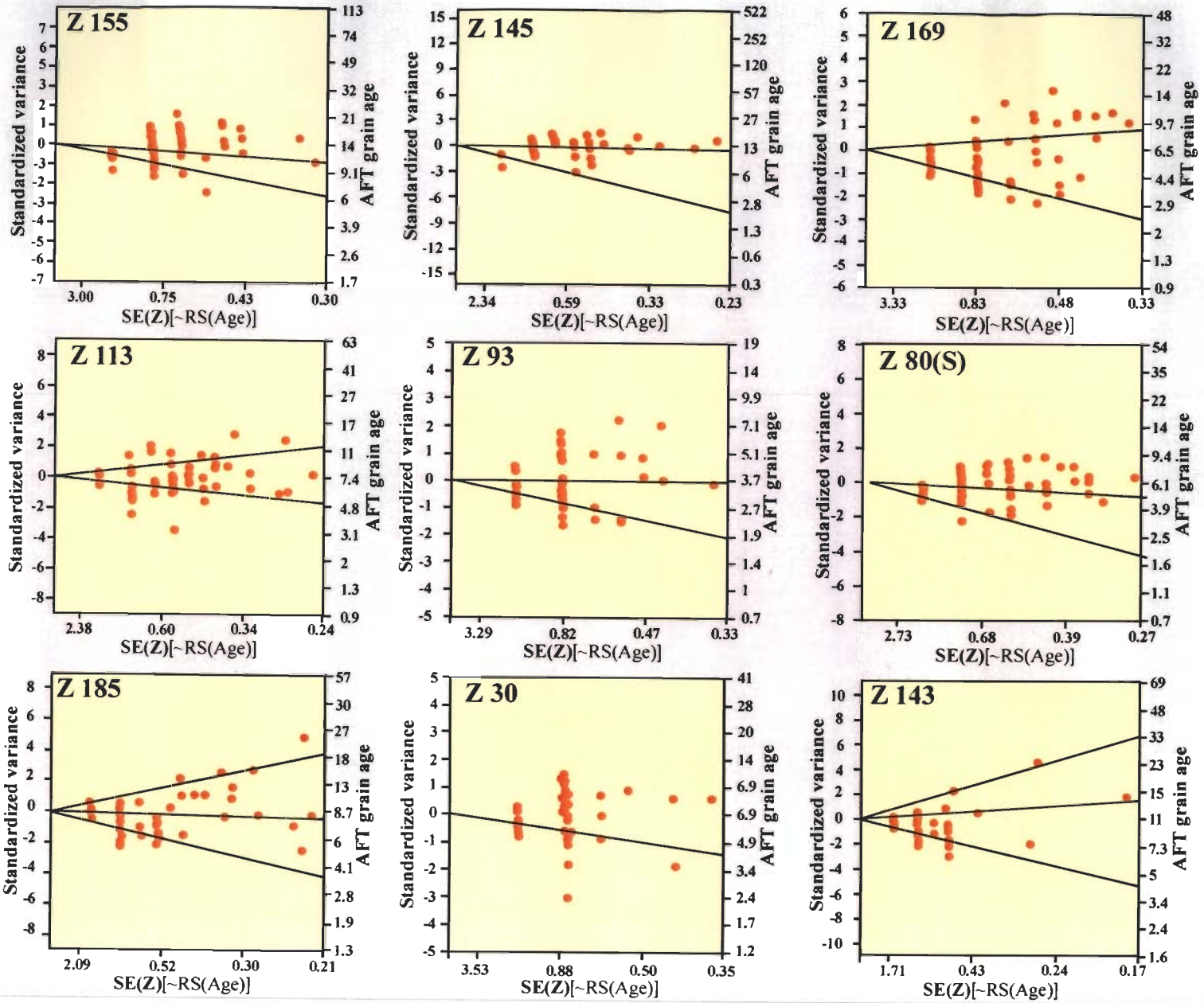

Figure 5.4: Radial plots of the detrital apatite FT data of the Upper Siwalik Formation and modern river sediments from the Arunachal Himalaya.

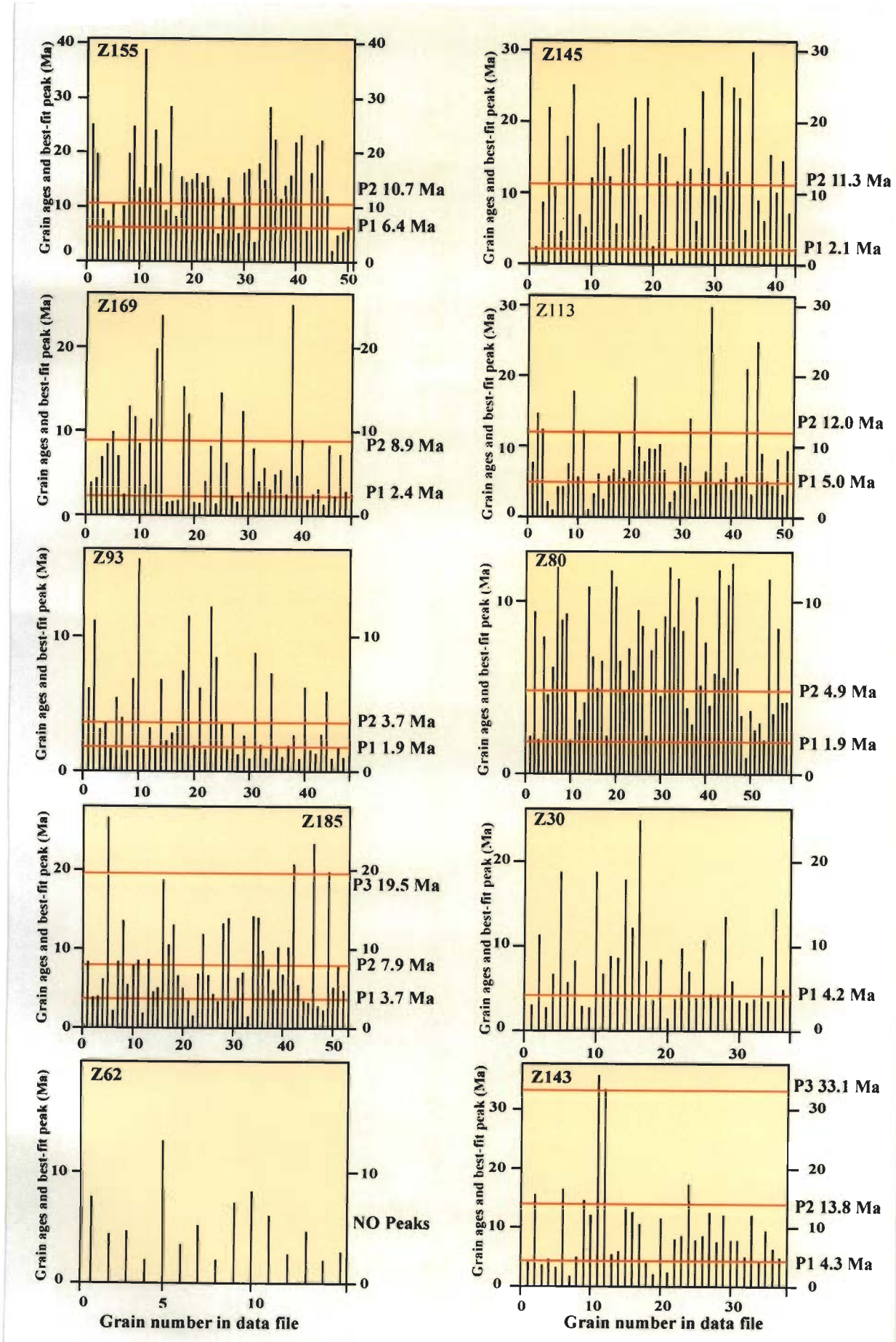

Figure 5.5: AFT grain age plot of modern river sediment of Arunachal Himalaya.

et al., 2009), it appears that a very large part of the catchment lies in the Tethyan Sedimentary Zone with minor components within the HHC.

A sample Z80(S) from further downstream of this river at Daporijo contained 58 of the analyzed apatite grains. The ages fall into two peaks: P1 Peak of 1.9 Ma (7.6%, n=4), while the older P2 Peak of 4.9 Ma contains 92.4% of the grains (n=54) and is the strongest with a possible source within the southern part of the HHC and the Lesser Himalayan Metamorphics. One apatite grain is as young as 1.0 Ma, while 11 grains fall between 10.0 and 12.3 Ma.

The southernmost sample Z185, collected from the Subansiri River at Gaurkamukh, where it debouches into the Brahmaputra alluvial plains, represents the sediments from upstream areas eroded by the main river and its tributaries. 52 grains were analyzed from this sample and produced 3 AFT peaks: (i) P1 of 3.7 Ma (53.7%, n=28), (ii) P2 of 7.9 Ma (37.3 %, n=19) and (iii) P3 of 19.5 Ma (9.5%, n=5). 2 grains have AFT ages of 1.5 and 1.7 Ma, while 4 grains are as old as 20.0 to 26.7 Ma. The youngest P1 Peak might be sourced in the HHC, while the P2 Peak could be coming from a mixed source of the Daporijo Gneiss and the Lesser Himalayan Sedimentary Zone; the oldest P3 Peak is likely to be contributed from the un-reset Siwalik sandstones.

5.5.4 Siyom River Catchment

Along the Siyom Valley, one sediment sample Z30, collected at Menchuka in the upper parts of the catchment, constrains the upstream drainage areas of the Tethyan Sedimentary Zone as well as the HHC. 36 analyzed grains gave range of ages from 1.6 to 24.9 Ma and a single AFT P1 Peak of 4.2 Ma. The second sample Z62, collected further downstream of the Siyom River from Yapuik and draining very large parts of the HHC

and Lesser Himalayan Sedimentary Zone, yielded only 15 AFT ages ranging from 2.1 to 12.9 Ma. However, no BINOMFIT peaks could be obtained due to paucity of grains. The AFT age range reveals mixed source.

5.5.5. Siwalik Sandstone

The sandstone sample Z143, collected from the Kimin-Ziro road section from the upper parts of the Kimin Formation (27° 21.010′: 93° 58.974′) has yielded 37 analyzed grains, whose FT ages fitted into three peaks: (i) P1 of 4.3 Ma (82.6 %, n=30), (ii) P2 of 13.8 Ma (13%, n=5) and (iii) P3 of 33.1 Ma (4.4%, n=2). In addition, 3 grains are younger to its possible stratigraphic age, while another 3 grains are between 30 and 36 Ma. The 4.3 Ma P1 Peak component may have been derived from the HHC, as also have been reported from the Tawi River sediment (Sorkhabi, 2000). The P2 Peaks may be contributed by the Lesser Himalayan Sedimentary Zone during its erosion, while the P3 Peak may have possibly been derived from the Gangdese Batholiths along with older grains, because none of the Himalayan rocks did yield so old bedrock ages.

5.6. Provenance characterization

Source areas generally have distinct thermochronological signatures that are clearly preserved in the eroded detritus. The Himalaya, which is a classical example of continent-continent collision, has four distinct units: the Tethyan Sedimentary Zone, the Higher Himalayan Crystallines, the Lesser Himalayan Sedimentary Sequence and the Siwaliks (Gansser, 1977; Le fort, 1975; Valdiya, 1988; Jain et al., 2002; Yin, 2006a). Thermochronological work across the length and breadth of this orogen along with the Trans-Himalayan domains has so far yielded wealth of mineral ages (Zeitler et al., 1985; Sorkhabi et al., 1996; Burg et al., 1997, 1998; Lal et al., 1999; Jain et al., 2000; Burbank

et al., 2003; Schlup et al., 2003; Vannay et al., 2004; Thiede et al., 2004, 2005, 2006, 2009; Grujic et al., 2006; Kumar et al., 2007; Patel et al., 2007; Whipp et al., 2007; Clift et al., 2008; Seward and Burg. 2008; Patel and Carter, 2009). Apatite Fission Track (AFT) work has consistently shown very young ages of <5 Ma in the HHC part (Jain et al., 2000; Burbank et al., 2003; Patel and Carter, 2009; Thiede et al., 2009) with still younger ages in the windows/domes (Kumar et al., 1995; Seward and Burg, 2008). The Lesser Himalayan metasediments and the Lesser Himalayan Crystallines have older AFT ages up to 15 Ma (Patel et al., 2007). The foreland basin data, however, show both reset as well as un-reset AFT ages (Sorkhabi, 2000; Beek et al., 2006).

Comparisons of the Apatite FT peaks with the AFT ages of the bedrock exposures provide an instructive comparison. Detrital thermochronolgy in the Himalaya has provided long-term insights into the geodynamics of the Himalaya (Zeitler et al., 1986; Cervany et al., 1988; Najman et al., 2004; Beek et al., 2006; Huntington and Hodges, 2006; Foster and Carter, 2007; Stewart et al., 2008; Jain et al., 2009). Another approach for source area characterization is by comparing the isotopic Sm and Nd data of the bedrock samples with that of the foreland basin samples (Robinson et al., 2001). Recent work by Foster and Carter (2007) gave a comparative view of Sm-Nd ratios of apatite taken from river sediments of Bhutan, Nepal, Indus River and Holocene river sediments from West Bengal, in which they observed that most of these sediments are coming from the Higher Himalayan Crystalline rocks of the Himalaya.

In the Arunachal Himalaya, bedrock AFT ages have been worked out in the present work (Chapter 4). These ages are compared with the peak ages derived from the detrital AFT ages. To make the comparison easier, the catchment area of each sample is marked in a simplified geological map (Figure 5.2). In the Kurung River valley, the

bedrock AFT ages range from 2.2 to 3.5 Ma for the HHC. However, the river sand sample Z169, having inputs from the HHC and the Tethyan Sedimentary Zone, has two peaks: P1 and P2 of 2.4 and 8.9 Ma, respectively. The P1 Peak may have its source from the HHC, while the P2 Peak should be from the Tethyan sediments. Bedrock AFT ages from the Daporijo Gneiss of the Lesser Himalayan Metamorphic Belt range from 5.0 to 8.0 Ma, with exception of one sample, having apatite of 12.1 Ma. A single sample from the LH window has AFT age of 2.0 Ma, however these vary from 4.7 to 8.5 Ma in the Lesser Himalaya. Sample Z113 has two peaks with P1 of 5.0 Ma containing 88.8% of the bulk population. This means that majority of the grains are coming from the Daporijo Gneiss but have mixed population. The 12.0 Ma P2 Peak could be assigned to the Lesser Himalaya. In the main Subansiri River valley, the HHC package has AFT ages range from 2.6 to 2.9 Ma, while that of the Daporijo Gneiss is between 6.2 to 7.4 Ma. The 1.9 Ma P1 Peak of sand sample Z93 matches approximately with that of the bedrock AFT ages from the HHC. It is likely that the 3.7 Ma P2 Peak has a source in the leucogranite intrusion within the HHC as well as the Tethyan sediments; a few older AFT ages also sourced within this Phanerozoic sedimentary belt. The picture of sediment source in this river is clearer when we compare with the peak ages of sample Z80(S), where 1.9 Ma P1 Peak is certainly coming from the HHC and the LH windows, while the 4.9 Ma P2 Peak grains are contributed, additionally, from the Daporijo Gneiss and Lesser Himalayan Sedimentary belt. In the sand of sample Z185, the youngest P1 Peak got little diluted to 3.7 Ma, possibly due to admixture of youngest apatite ages from different sources and various tributaries of the Subansiri River. The 7.9 Ma P2 Peak grains might have apatite contributed by the Daporijo Gneiss. Although there is no exposed bedrock with ~20 Ma age, it is likely that 19.5 Ma peak should be from the un-reset Cenozoic foreland basin Siwalik sediments. In this valley most of the sediment carried by the Subansiri River and

its tributaries are eroded of from the Tethyan Sedimentary Zone, the HHC and the LH windows.

The Ranga River drains the Siwaliks, the Lesser Himalayan Sedimentary belt including the Gondwanas and the Daporijo Gneiss. Sample Z155 from the Ranga Dam has sediments coming from the Daporijo Gneiss and the Lesser Himalayan Sedimentary Zone. The 6.4 Ma P1 Peak grains should have come from the LH sedimentary sources, while the 10.7 Ma P2 Peak grains have a mixed source of the Daporijo Gneiss and the Lesser Himalaya. However, the new P1 Peak of 2.2 Ma in the foothill sand sample Z145 is likely to be coming from the youngest Pliocene Kimin Formation of the Siwalik Group or alternatively from the reworked older terraces.

In the Siyom River valley, the 4.4 Ma single P1 Peak of sample Z30 (100%, n=36) should have a mixed source of the HHC as well as the Tethyan sedimentary belt. This argument is based on the bedrock AFT ages from the HHC, which are ~2.9 Ma and getting younger northwest. The Z62 did not yield any peak but individual grain ages range from 2.1 to 12.9 Ma. This means that the sample has a mixed source of different units including the Lesser Himalayan package.

This detrital AFT thermochronological work shows that the major volume of the present-day sediments of the Eastern Himalayan Rivers is contributed from the HHC and the Lesser Himalayan sediments including the windows. This is supported by the detrital ZFT work in the Siang River, where focused erosion of the HHC rocks at the Eastern Himalayan Syntaxis provided bulk of the sediments (Stewart et al., 2008). Sand petrology study from the Bengal data also showed similar results indicating majority of sediments coming from the HHC (Garzanti et al., 2005).

Chapter 6: Discussions and Conclusions

6.1. Introduction

The thermochronological ages are the proxies for cooling and exhumation rates since the closure temperatures of individual minerals and relationship with crustal depths. The closure temperatures, which are the basis for calculating these rates, are estimated on the basis of diffusion kinetics and accumulation in radiometric systems (Dodson, 1973) and numerical modelling (Brandon et al., 1998). The comparison of thermal ages or modelled exhumation rates with probable driving parameters that may cause exhumation like structural layout, precipitation rate etc. in different parts of the Himalaya provide a mechanism to work out the cause for exhumation (Patel and Carter, 2009).

In this chapter, a discussion on the thermal modelling for the estimation of closure temperature and exhumation rate is followed by a detailed account of the cooling and exhumation histories, as calculated from the AFT, ZFT, Rb-Sr (biotite) and Rb-Sr (muscovite) ages.

6.2. Thermal modelling

Thermal modelling has now been extensively followed to deduce the exhumation rate from the thermochronological ages (Patel and Carter, 2009; Thiede et al., 2009). 1D, 2D and 3D models have been developed for understanding the geodynamics of the orogens (Ehlers et al., 2005; Reiners et al., 2005; Whipp and Ehlers, 2007; Whipp et al., 2007). In the present work, 1D modelling has been applied for estimating the exhumation rate from the AFT and ZFT ages. For this we need to define effective closure temperatures for the AFT and ZFT thermochronometers.

6.2.1. Closure temperature for apatite and zircon

The concept of closure temperature, which corresponds to temperature at the time indicated by the cooling age measured by the thermochronometer, was introduced in the landmark paper by Dodson (1973). It provided a clear theoretical basis for understanding the mineral cooling ages due to the interplay between kinetics of diffusion (annealing) and accumulation rates in cooling radiometric systems (Dodson, 1973, 1979; Harrison and Zeitler, 2005; Reiners et al., 2005). Recently, calculations of effective closure temperatures are done by programme CLOSURE, which was first developed by Brandon et al. (1998). The Dodson's estimated closure temperatures for fission track system are within ~1 °C relative to those given by the numerical modelling (Reiners et al., 2005). Numerous workers have estimated the closure temperatures for apatite and zircon by CLOSURE programme (Patel and Carter, 2009; Thiede et al., 2009). In the present work, closure temperature of 135 and 232 °C were used for apatite and zircon respectively, which correspond to the young FT ages (Brandon et al, 1998).

6.2.2. 1D Modelling

In the recent past, the thermal modelling has been applied by various workers to understand the Himalayan orogen (Purdy and Jager, 1976; Laslett et al., 1987; Mancktelow and Grasemann, 1997; Ehlers and Farley, 2003; Whipp et al., 2007; Patel and Carter, 2009; Thiede et al., 2009). In the present study, AGE2EDOT programme by Brandon et al. (1998) was used to translate the cooling age of a thermochronometer into exhumation rate for a rock, which has exhumed under steady-state condition for a layer with a certain thickness L (km), a thermal diffusivity κ (km^2 Ma^{-1}), a uniform internal heat production H_T, a steady surface temperature T_s and an estimate of the near-surface thermal

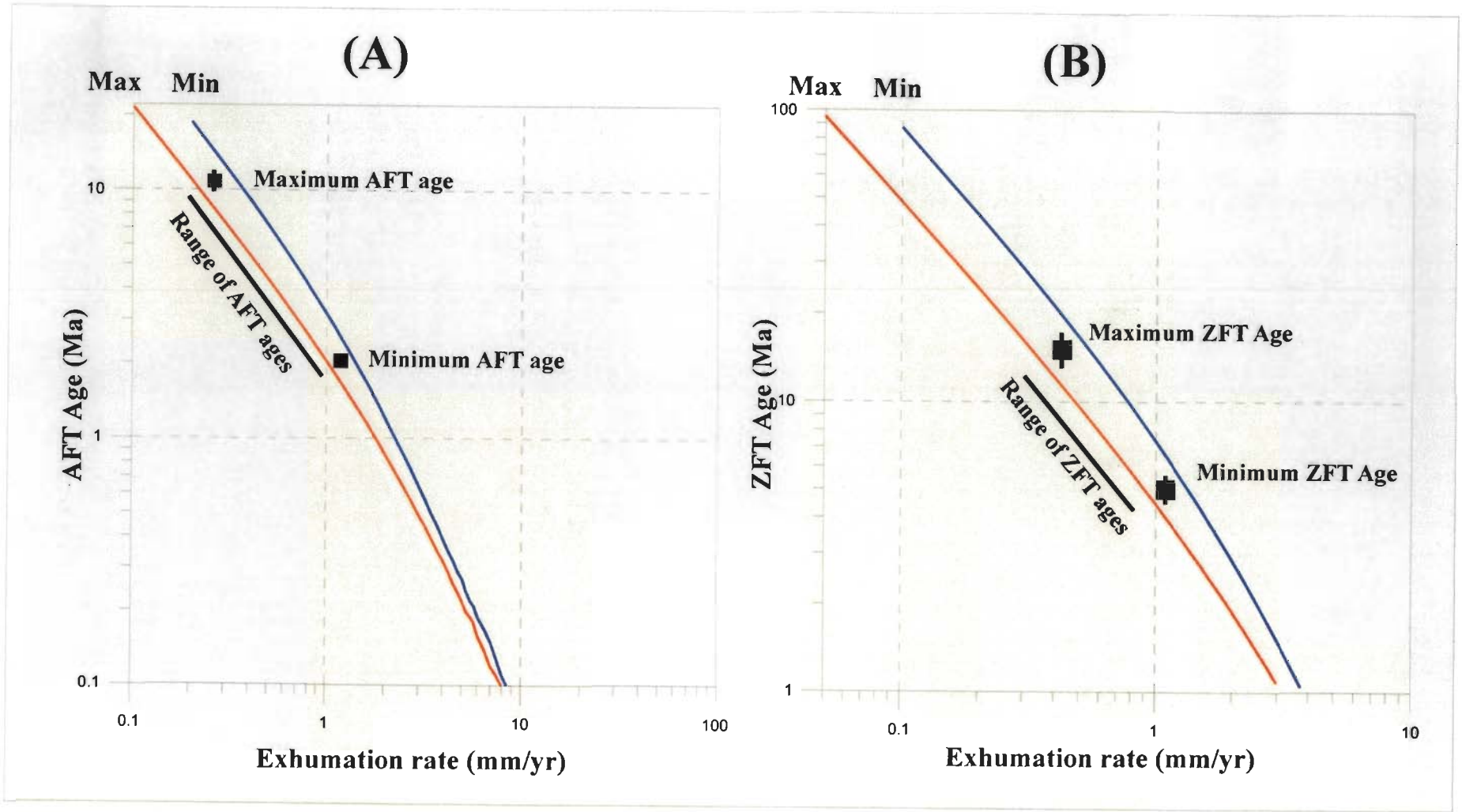

Figure 6.1: Growth curves for exhumation rates, as estimated by 1D modelling. **(A)** From AFT ages. **(B)** From ZFT ages.

gradient for no erosion. This 1D modelling programme has been applied by some workers in the Himalayan studies (Patel and Carter, 2009; Thiede et al., 2009).

The study area has been divided into different tectonomorphic divisions for achieving the steady-state condition. A range of exhumation rate was calculated by taking the set of lower limits of thermal parameters. Similarly, rates were calculated for the upper range of thermal parameters. Finally, the average exhumation rate was obtained for a particular thermal age. This is because of the fact that the thermo-physical values of the Himalayan rocks are limited, and we have to use these inputs, based on certain assumptions or poorly-measured values. The thermal parameters, used in the present study, are given in Table 6.1. Geothermal gradient range of 25-45 °C/km has been considered (Whipp et al., 2007; Patel and Carter, 2009; Thiede et al., 2009). Thermal conductivity values range of 2.1-3.6 $Wm^{-1}M^{-1}$ (Ray et al., 2007; Thiede et al., 2009) and heat production values of between 0.8-3.0 μWm^{-3} (Roy and Rao, 2000; Patel and Carter, 2009; Thiede et al., 2009). Based on the output from the AGE2EDOT programme, 1D modelling growth curve (Fig. 6.1) for exhumation rate against AFT as well as ZFT ages are prepared. From this, a summary of thermal modelling results is given in Table 6.1.

6.3. Cooling and exhumation in the Arunachal Himalaya

As calculated from the AFT, ZFT, Rb-Sr (biotite) and Rb-Sr (muscovite) ages and their respective closure temperatures, the cooling pattern in the Arunachal Himalaya shows variability with time and space. Three representatives regional mean cooling histories for the different tectonomorphic units in the presently-studied traverses of the Arunachal Himalaya are shown in Figure 6.2.

In the Kimin-Koluriang section, there is gradual decrease of the Rb-Sr (muscovite) ages from 24.9 Ma in the LH Sedimentary Belt to 20.36 Ma in the HHC, indicating a linear cooling along the low-angled MCT during the late Oligocene-early Miocene. The mean cooling rate from the muscovite to biotite closure temperatures is 40.5 °C/Ma, 24.6 °C/Ma and 22.7 °C/Ma for the LH, LHCS and HHC, respectively. The rate is reduced to 10.1 °C/Ma, 24.4 °C/Ma and 13.3 °C/Ma in the LH, LHCS and HHC, respectively during the cooling between biotite and ZFT closure temperatures. The sharp increase of cooling rate

Table 6.1: Modelled exhumation rate of the Arunachal Himalaya.

Mineral	Thermal diffusivity (km^2my^{-1})	Internal heat production ($^{\circ}C$ m.y.)	Geothermal gradient ($^{\circ}C\ km^{-1}$)	Exhumation rate range (mm /yr)±2σ			
				LH	DG	LHW	HHC
A. Kimin-Koluriang							
Apatite	29-50	12-35	25-45	0.36±0.1 to 0.59±0.11	0.25±0.07 to 0.52±0.1	1.2±0.2	0.77±0.15 to 1.12±0.16
Zircon	29-50	12-35	25-45	0.54±0.12	0.51±0.13 to 0.84±0.1	1.07±0.2	1.5±0.25
B. Subansiri River section							
Apatite	29-50	12-35	25-45	0.32±0.08	0.39±0.1 to 0.46±0.11	.....	0.89±0.16 to 0.96±0.16
Zircon	29-50	12-35	25-45	0.64±0.2	0.9±0.2	1.07±0.13	1.55 ±0.2
C. Menchuka Section							
Apatite	29-50	12-35	25-45	.....	.....	.....	0.48±0.11 to 0.80±0.17
Zircon	29-50	12-35	25-45	.....	.....	.....	0.78±0.18 to 1.18±0.23

Notes: LH–Lesser Himalaya, **DG**–Daporijo Gneisses, **LHW**–Lesser Himalayan Window. **HHC**–Higher Himalayan Crystallines

to 66.9 °C/Ma in the HHC between the ZFT and AFT closure temperatures is followed by subsequent rate of 43.9 °C/Ma from the AFT closure to the surface temperatures and is

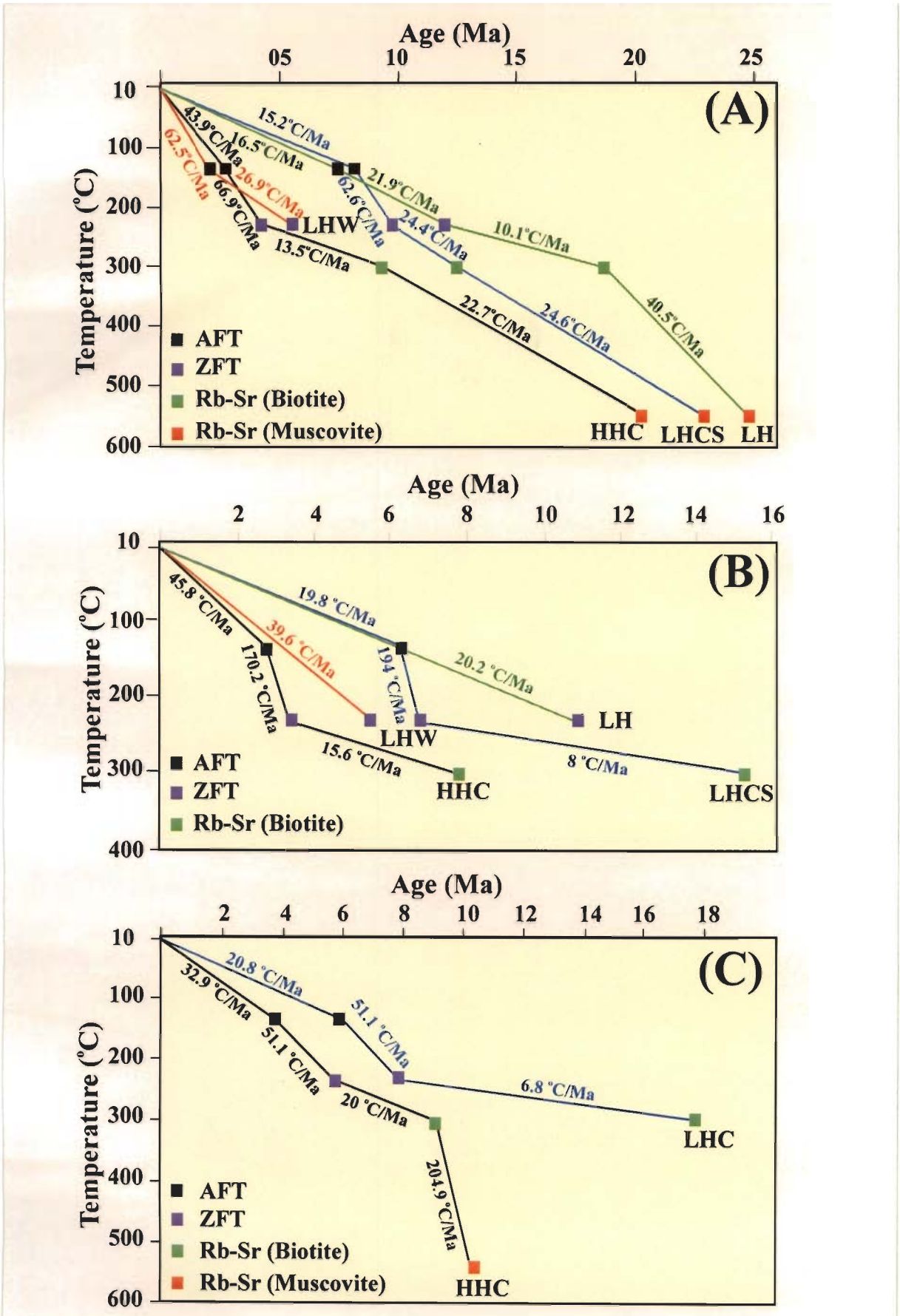

Figure 6.2: Representative mean cooling histories, calculated from closure temperatures, using different thermochronometers of various tectonomorphic packages of the Arunachal Himalaya. **(A)** Kimin-Koluriang section. **(B)** Subansiri River section. **(C)** Siyom River section.

considered as an evidence for the folding of the MCT at ~5 Ma. Later intensification of the doming/folding and subsequent erosion of the HHC has led to the exposure of the LHW within the HMB. This doming/window development has resulted in cooling of the rocks at rates of 26.9 and 62.5 °C/Ma between the ZFT closure depth to the AFT closure depth and from the latter to the surface, respectively. In the LHCS, the cooling rate between the closure temperatures of the ZFT and the AFT is 62.6 °C/Ma, which is further reduced to 15.2 °C/Ma as it approached the surface.

In the Subansiri River valley, the Rb-Sr biotite ages concentrate ~15 Ma in the LH Crystalline Belt and ~7 Ma in the HHC, which means that the rocks of the earlier package cooled earlier than the HHC rocks. The mean cooling rate between the biotite to ZFT closure temperatures is 15.6 °C/Ma for the HHC belt. This rate increased abruptly to 170.2 °C/Ma until the AFT closure, and slowed thereafter at a rate of 45.8 °C/Ma up to the surface. The pattern is the same for the LH Crystalline Belt rocks with a coexisting representative sample exhibiting rates of 8 °C/Ma, 194 °C/Ma and 19.8 °C/Ma for the episodes between the biotite and ZFT closure, ZFT and AFT closure, and AFT closure and surface, respectively. In this traverse, a very fast cooling window between the ZFT closure to AFT closure temperatures may be due to intensification of doming/window development between 3.0 and 6.0 Ma. The LH rocks cooled at a rate of 20.2 °C/Ma from the depth of the ZFT closure temperature, starting at 11.0 Ma. In the LH window zone, the cooling rate since the ZFT closure is 39.6 °C/Ma. The cooling rates, in general, are faster in the HHC and the LH window zone.

In the Siyom River valley, the sudden jump of all the mineral ages between the Z51 and other samples is interpreted due to a tectonic break. This could be due to a concealed thrust, which separates the HHC rocks from the LHCS. Further field correlation

is needed to confirm this postulation. The representative sample from the LHCS gave a cooling rate of 6.8 °C/Ma between the biotite closure and ZFT closure. This is followed by a rate of 51.1 °C/Ma and 20.8 °C/Ma for the episodes between the ZFT and AFT closures, and AFT-surface, respectively. Although, the AFT age pattern indicates an underlying folded structure, the LH part is not exposed within the HMB. The HHC rocks cooled at a faster rate than the LHC rocks. The cooling rates here are 204.9 °C/Ma, 20 °C/Ma, 51.1 °C/Ma and 32.9 °C/Ma for the timing between the muscovite-biotite closure, biotite-ZFT closure, ZFT-AFT closure and AFT closure to surface, respectively.

Calculated exhumation rates, based on 1D modelling, are summarized in Table 6.1. In the Eastern Himalaya, different tectonomorphic provinces experienced variable exhumation pattern spatially and temporally. The exhumation rates, modelled from the AFT ages for the HHC rocks, vary from 0.77 mm/yr to 1.12 mm/yr in the Kimin–Koluriang section, whereas from one ZFT age, the rate is 1.5 mm/yr. In the window zone, the exhumation rate is 1.2 mm/yr and 1.07 mm/yr deduced from the AFT and ZFT, respectively. Modelled exhumation rates for the Daporijo Gneiss vary between 0.25 and 0.52 mm/yr since FT apatite closure and 0.51 to 0.84 mm/yr, as deduced from the zircon FT ages (see Figs. 6.3A, B).

Along the Subansiri River section, the HHC rocks have an exhumation rate range of 0.89-0.96 mm/yr for the AFT ages and 1.55 mm/yr, deduced from a single zircon age. In the window area, the rate is 1.07 mm/yr since the zircon closure for fission track. In the Daporijo Gneiss, the exhumation rate varies from 0.39 to 0.46 mm/yr, as has been calculated from the AFT ages, while the rate since the ZFT closure is 0.9 mm/yr. For the Menchuka section, where there is no exposed Lesser Himalayan window, the exhumation rate, deduced from the AFT ages vary from 0.48 to 0.80 mm/yr, while calculation from

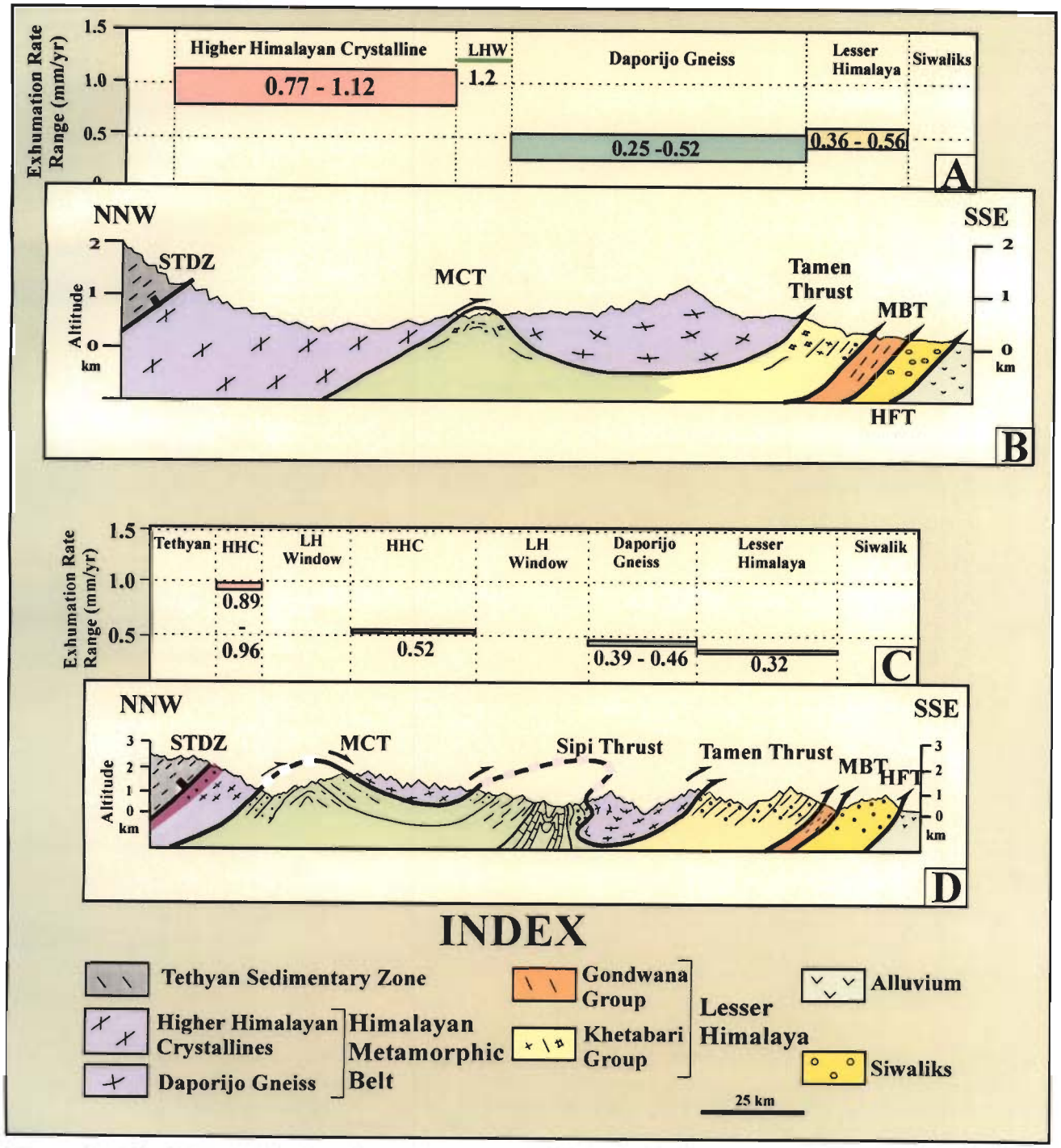

Figure 6.3: Spatial variation in exhumation rates within individual tectonic units of subansiri sector. **(A)** Exhumation rates across Kimin-Koluiang section. **(B)** Geological cross-section of this section. **(C)** Exhumation rates across Subansiri River section. **(D)** Geological cross-section of this section.

the ZFT ages give a range of 0.78 to 1.18 mm/yr. This means that the exhumation rate since the apatite fission track closure is fastest in the window zone and followed by the HHC rocks. However, if we take the overall rate since zircon closure, the highest exhumation rate is in the HHC rocks (Figs. 6.3C, D).

6.4. Comparison with the NW Himalaya

Plots of the exhumation rate range for different tectonic units against the geological cross-sections along the Kimin-Koluriang and Subansiri River sections show a positive correlation with the major structures in the region (Fig. 6.3). Similar pattern is also reported in the Eastern Himalayan Syntaxis in the Namcha Barwa region, where the thermal ages and exhumation behaviour is control by the doming activity (Seward and Burg, 2008). Along the strike, comparison of the Himalayan exhumation shows similar trend for the HHC rocks from the western, central and the eastern region (Jain et al., 2000; Burbank et al., 2003; Blythe et al., 2007; Thiede et al., 2004, 2005, 2009; Patel and Carter, 2009). In the NW Himalaya, breaks in the AFT ages across structural boundaries such as the MCT/Munsiari Thrust/Vaikrita Thrust have been reported by many workers (Jain et al., 2000; Patel and Carter, 2009). These patterns are clear evidences for the control on exhumation by fold and thrust systems in the Himalayan orogen. The Lesser Himalayan package in the Kimin–Koluriang section has exhumed at a rate ranging between 0.36 and 0.59 mm/yr since the apatite closure, whereas the rate deduced from the zircon age is 0.54 mm/yr. In the Subansiri section, the exhumation rate is 0.32 mm/yr and 0.64 mm/yr from the AFT and ZFT ages, respectively.

In order to observe the overall picture of the cooling and exhumation patterns in the Himalaya, it is very important to note the pattern on the regional scale. Earlier

reported thermochronological works have showed rapid exhumation to an extent of >2 mm/yr along the southern front of the Himalaya (Jain et al., 2000; Burbank et al., 2003; Thiede et al., 2004, 2005, 2009; Blythe et al., 2007; Patel and Carter, 2009). Recent compilations of low temperature thermal ages in the NW Himalaya (Patel and Carter, 2009; Thiede et al., 2009) indicate consistently young ages for the package sandwiched between the MCT in the south and the South Tibetan Detachment Zone (STDZ) in the north. However, the thermal ages are older and show variations in the Tethyan Himalaya and Lesser Himalaya including the LHCS rocks (Patel et al., 2007; Thiede et al., 2009). The pattern continues without much variation to the Nepalese Himalaya (Burbank et al., 2003; Blythe et al., 2007) and extends further east to Arunachal Himalaya (Pebam et al., 2008), suggesting fast exhumation in the Higher Himalayan Crystallines for the entire belt, followed by the Tethyan Himalayan and Lesser Himalayan rocks.

An overview of all the available AFT ages in the NW Himalaya provides an interesting clue to the age distribution in this region (Fig. 6.4). The distribution of ages vary from 0.6 Ma to as old as 39.9 Ma, and follows the structural pattern in the region. The ages are youngest in the MCT hanging wall. Similarly, in the Eastern Himalaya, the AFT ages range between 0.4 Ma in the Namcha Barwa region of the Eastern Himalayan Syntaxis to 12.0 Ma in the Arunachal Himalaya (Fig. 6.5). In the Bhutan Himalaya, Grujic et al. (2006) reported the older AFT ages between 3.5 and 8.6 Ma in the eastern region in comparison to the western parts, where the ages range between 1.4 Ma to 6.9 Ma. This was linked to the rainfall distribution in this region, which showed that the eastern region receive less rainfall than the western part, as the later region is geographically situated to lee ward side of the Shillong platue. However, in the other regions of the Eastern Himalaya, variations in the AFT ages occur but they follow the

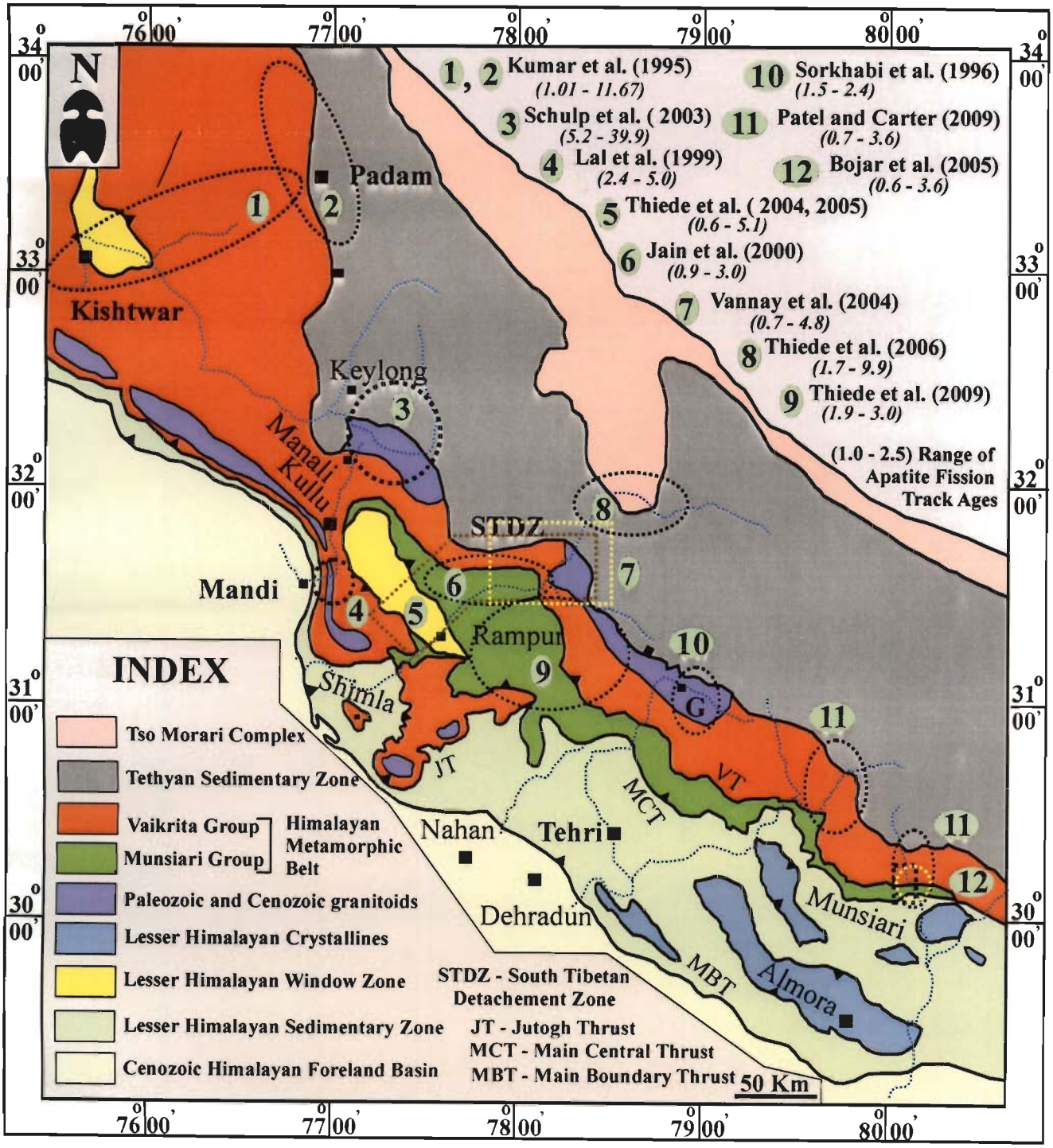

Figure 6.4: Apatite fission track (AFT) ages from the NW Himalaya. Ellipses shows the area of AFT coverage. Numbers indicate source of data (see references for details).

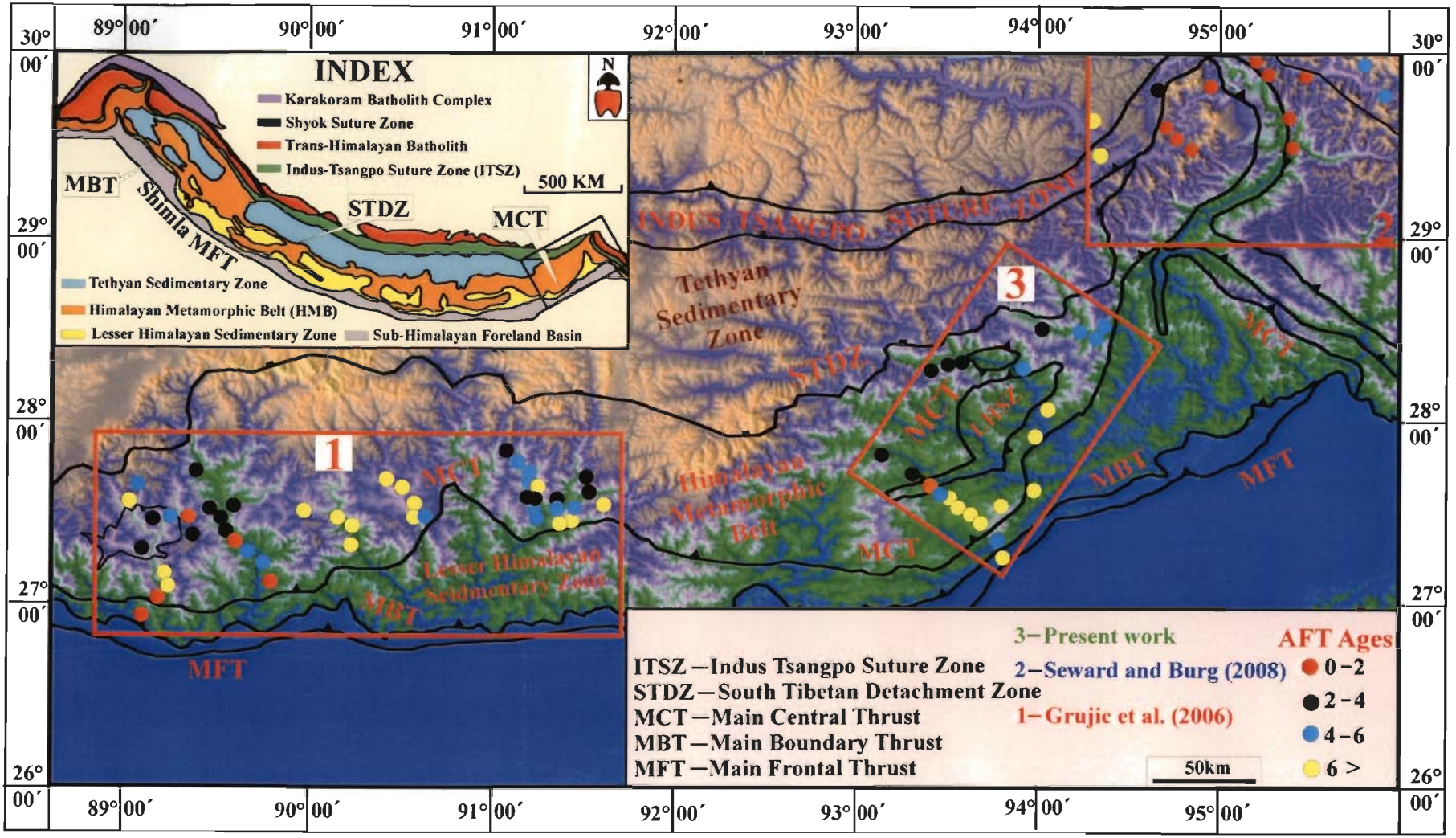

Figure 6.5: Apatite fission track (AFT) ages from the Northeasten Himalaya. Boxes show the areas of the AFT coverage. Numbers indicate sources of data (see references for details). Simplified geological map inserted on SRTM map. Insert shows the overall geology of the Himalaya.

structural pattern. The youngest AFT age of 2 Ma in the Subansiri Valley is found to be from the Lesser Himalayan window, exposed within the HMB. The ages gradually increase as one move away from the window to as high as 12 Ma from the present study. In the whole region, the youngest AFT ages was reported in the Namcha Barwa region (Fig. 6.5). The very young ages has been explained due to the north-trending dome, which began its initiation around 4 Ma (Seward and Burg, 2008). Hence, from the overall analysis of the AFT age distribution in the Himalaya it has been observed that, apart from the hanging wall region of the MCT (the HHC package), other 'hot spot' regions for rapid exhumation are the two syntaxial bends (Nanga Parbat and Namcha Barwa) and domes/windows (Zeitler, 1985; Jain et al., 2000; Seward and Burg, 2008), where the exhumation rates reach up to10 mm/yr.

6.5. What drives exhumation - Tectonics vs. erosion?

The debate over what is driving the exhumation of the Himalayan orogen gave rise to essentially two schools of thoughts for the possible solution. Jain et al. (2000) highlighted the tectonic-driven exhumation in the NW Himalaya. These workers reported accelerated exhumation pulses, where fast exhumation rates are found in the crest of the domes and windows (Suru dome, Chisoti dome, Kisthwar and Kullu-Rampur antiformal windows). These regions experienced exhumation rates ranging from 0.80 to 2.97 mm/yr. The domes and windows were either active independently or in combination with major thrusts as well as extensional normal fault (Jain et al., 2000). Similar works in the Nepalese Himalaya along the Marsyandi River (Burbank et al., 2003) and Kumaon Himalaya along the Goriganga and Dhauli Rivers (Patel and Carter, 2009) indicated totally different trend from the climate-control. In the Marsyandi Valley, the AFT ages

drop abruptly in the HHC rocks with a mean of ~0.5±0.2 Ma from the 3.8 Ma ages in the Lesser Himalaya (Burbank et al., 2003). The ages do not change despite five-fold change in precipitation in the same area. In the Goriganga Valley, there is a step-wise change in ages across the Vaikrita Thrust (VT) that suggests the Quaternary thrust displacements. The VT footwall samples are reported to have a weighted mean apatite FT age of 1.6±0.1 Ma in comparison to 0.7±0.04 Ma in the hanging wall (Patel and Carter, 2009). These patterns indicate that there is no direct correlation between precipitation and exhumation; rather these reveal a strong correlation between tectonics and the AFT age pattern.

Another school supported the climatic controlled-erosion, causing the exhumation of the orogen (Thiede et al., 2004; Grujic et al., 2006; Clift et al., 2008). These workers based their arguments on spatial correlation of zone of high exhumation rates with zones of higher precipitation. More recently, Thiede et al. (2009) gave specific stream power as the proxy for the exhumation to argue for climatic control.

In order to effects of precipitation on the tectonics, a comparison between the precipitation in the NW Himalaya and Eastern Himalaya has been carried out. Rain rate map from the Tropical Rain Measurement Mission (TRMM) data for the Himalayan orogen (Fig. 6.6A) shows that the daily hourly rain rate, based on the rainfall data between May, 1998-May, 2009, varied from 0.02 mm/hr to a maximum of 0.18 mm/hr in the NW Himalaya (Fig 6.6B), whereas, it ranged from 0.06 mm/hr to 0.36 mm/hr in the Eastern Himalaya (Fig 6.6C). Thiede et al. (2004) have shown annual rain rate to a maximum of 2 m/yr in Sutlej the valley, whereas Grujic et al. (2006) observed a maximum rainfall up to 6 m/yr in the western Bhutan. This clearly means that the Eastern Himalaya receives a much higher rainfall than the western part of this orogen. However, comparison of the AFT age distribution in the NW and Eastern Himalayas reveals

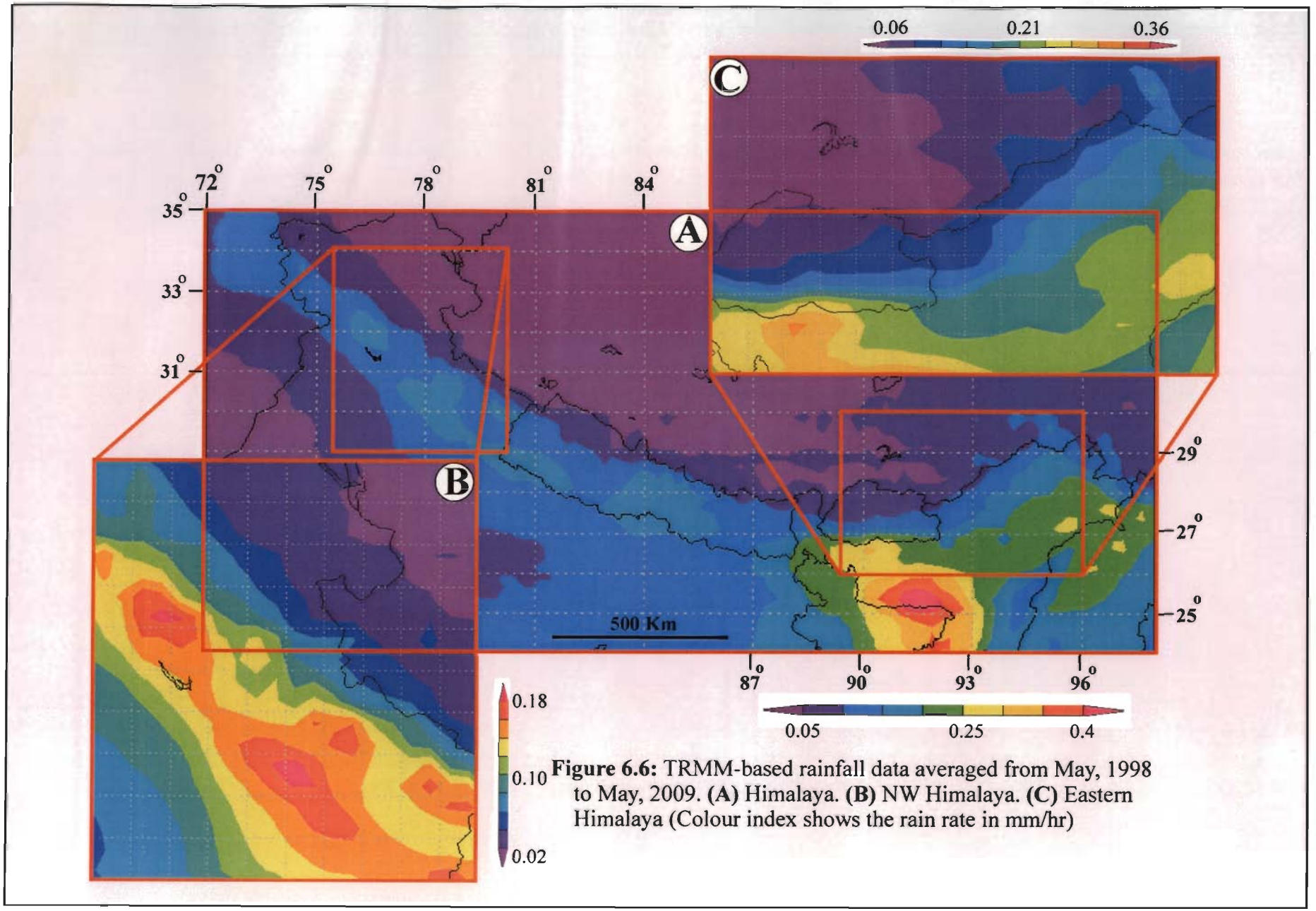

Figure 6.6: TRMM-based rainfall data averaged from May, 1998 to May, 2009. **(A)** Himalaya. **(B)** NW Himalaya. **(C)** Eastern Himalaya (Colour index shows the rain rate in mm/hr)

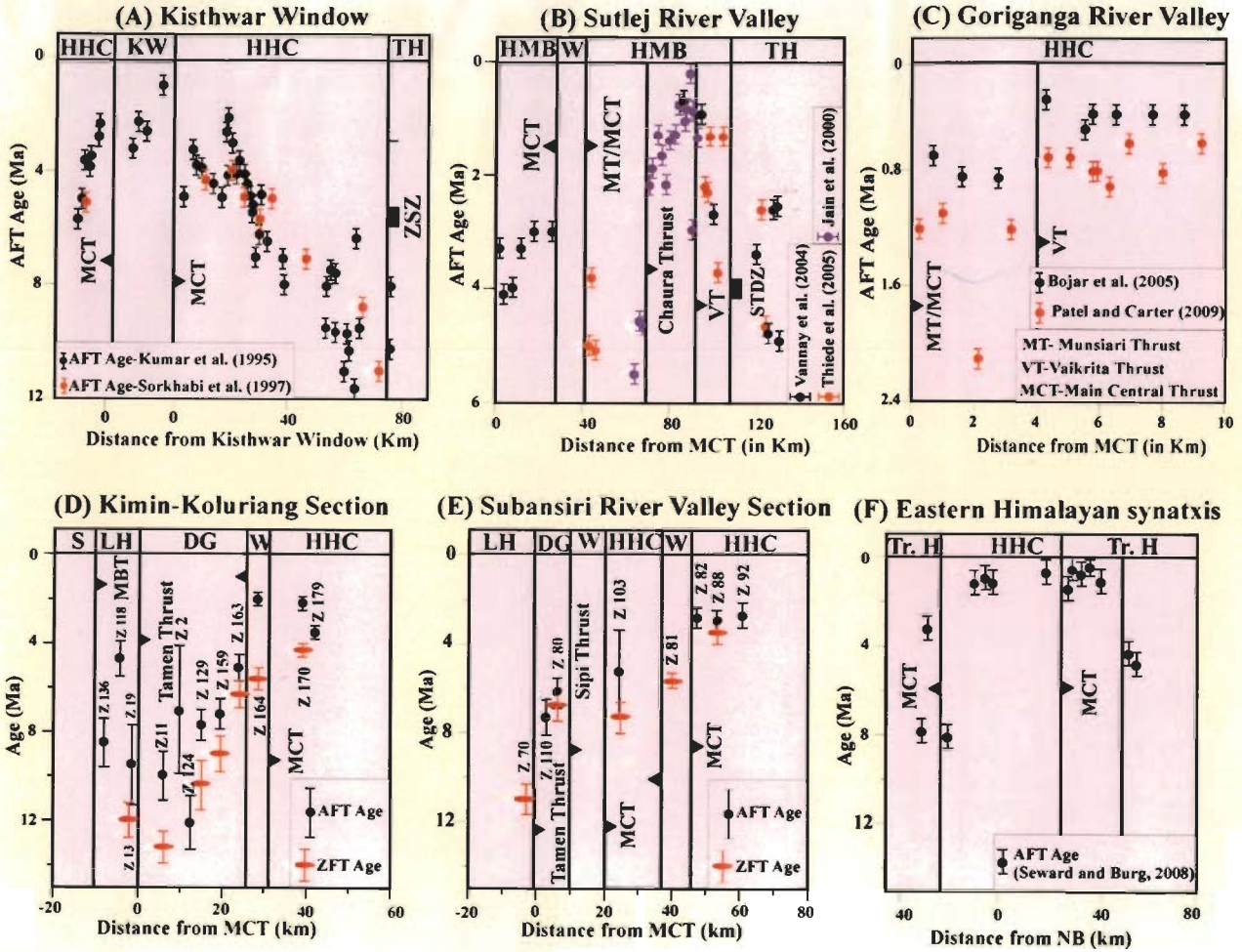

Figure 6.7: Fission track ages from the NW Himalaya and their comparison with those from the Eastern Himalaya. Ages are plotted vs. Distance from the MCT in km across different tectonic units. **(A)** Kishtwar and Zanskar. **(B)** Sutlej Valley, Himachal Pradesh. **(C)** Goriganga Valley, Kumaon. **(D)** Kimin -Koluriang section. **(E)** Subansiri River section. **(F)** Namcha Barwa Dome. **NOTES: S**-Siwalik Belt. **LH**-Lesser Himalayan Sedimentary Belt. **W**- Lesser Himalayan windows. **DG**-Daporijo Gneiss (Lesser Himalayan Metamorphic Belt). **HHC**-Higher Himalayan Crystallines. **TH**-Tethyan Sedimentary Zone. **Tr. H**- Trans-Himalaya. **NB**-Namcha Barwa. **MBT**-Main Boundary Thrust. **MCT**-Main Central Thrust. **STDZ**-South Tibetan Detachment Zone.

insignificant difference in pattern and age range. This clearly means that the precipitation is not the primary driving mechanism for the Himalayan exhumation.

Plots of the FT ages against structural boundaries in six representative areas, three from the NW Himalaya and three from the Eastern Himalaya show distinct correlation between the distribution pattern of these ages with thrusts and domes/windows, and are the proxies for the exhumation rates. Beginning at the westernmost section along the Kishtwar window, previous works (Kumar et al. 1995; Sorkhabi et al. 1997) indicated the AFT ages younging as the sample locations gets closer to the Kishtwar window (Fig 6.7A). The youngest age was obtained within the window region with one sample having AFT age as young as 1.01 Ma. The ages increase gradually as the location shifts towards the Tethyan Sedimentary Zone. In the Sutlej valley, the FT works have been carried out extensively by various workers (Jain et al., 2000; Vannay et al., 2004; Thiede et al., 2004, 2005, 2009). The AFT ages plot against the distance from the southernmost exposure of the MCT shows gradual younging toward the Rampur window, but after crossing the window the ages get older in the rocks of the Munsiari Formation. Within this formation, the AFT ages are reduced abruptly to an extent of 0.74 Ma along the Chaura Thrust (Jain et al., 2000). Other age breaks are seen along the Vaikrita Thrust and the STDZ. North of the STDZ, the AFT ages increase to as old as ~5.0 Ma in the Tethyan sequence (Fig. 6.7B; Vannay et al., 2004). Along the Sutlej Valley, the Chaura Thrust is the most active tectonic feature that controls the exhumation of the region. In the Goriganga Valley, recent AFT dating work revealed a distinct age break along the Vaikrita Thrust (Bojar et al., 2005; Patel and Carter, 2009). In the footwall of this thrust, the AFT age averages around 1.2 Ma, while that of the hanging wall have a mean of about 0.6 Ma (Fig. 6.7C). These representative examples give a strong evidence for the tectonic control on the exhumation in the NW Himalaya.

In the Eastern Himalaya, the AFT age profile along the eastern syntaxial bend at Namcha Barwa shows a strong correlation of the ages with the domal feature, developed due to syntaxial bending. This area records one of the youngest AFT ages in the whole of Himalaya to an extent of 0.4 Ma. The young AFT ages are reported due to doming, which was initiated at around 4.0 Ma (Burg et al., 1997, 1998; Seward and Burg, 2008). The doming also affected the AFT ages in the Trans-Himalayan region along the northern margin of this dome (Fig. 6.7F). From the present study in the Arunachal Himalaya, the youngest AFT ages are found in the antiformal LH window and HHC rocks. As indicated along the Kimin-Koluriang section, the AFT age in the window is 2.0 Ma (Fig. 6.7D), and it gets older as one moves away from it towards the HHC and DG. The youngest AFT age in Subansiri Valley is also found in the HHC package, indicating this as the area of fastest exhumation (Fig. 6.7E). Similar pattern in $^{40}Ar/^{39}Ar$ muscovite age distribution is reported in the western Arunachal Himalaya along Bhalukpong-Zimithang road section, where the ages increase with an increase in structural level. The ages increase from 7.0 to 12.0 Ma in the hanging wall package of the Zimithang thrust. Similarly, in the MCT hanging wall, the $^{40}Ar/^{39}Ar$ muscovite ages shoot up from 8.0 Ma near the MCT to 12.0 Ma at a location ~12 km from MCT (Yin et al., 2009a).

The Himalayan syntaxial bend in the west Himalaya also records very young thermal ages (Zeitler, 1985). In Nanga Parbat region, the $^{40}Ar/^{39}Ar$ biotite ages are as low as 0.9±0.1 Ma (Winslow et al., 1996) and provide evidences that the exhumation was induced by the syntaxial growth due to northerly-plunging anticlinal folds and superposed faulting. Similar evidence for the tectonically-driven exhumation has been reported in Western Alps (Malusa and Vezolli, 2006). Thus, we can trace out fission track ages mimicking the structural pattern in both the eastern and western Himalaya. The pattern is

also observed in other orogenic belt. These observations serve as the most robust evidence for tectonic-driven exhumation of the orogenic belts.

6.6. Detrital thermochronology

Fission track thermochronology in the Eastern Himalaya highlights localized focused erosion in the syntaxial bend (Stewart et al., 2008). Thermal ages distribution in this area provide an indication of long-term erosion rates to an extent up to 3-10 mm/yr (Booth et al., 2004, 2008; Seward and Burg, 2008; Stewart et al., 2008). This rate is supported by estimated present-day erosion rate of ~10 mm/yr (Stewart et al., 2008). Moreover, various other geochemical and mineralogical works support that 50% of the sediment flux in the Brahmaputra and 20% of those reaching the Bay of Bengal are derived from the Eastern Syntaxis (Singh and France-Lanord, 2002; Garzanti et al., 2004; Stewart et al., 2008). Such 'hot spots' of exhumation are absent in other part of this orogen.

In the Arunachal Himalaya, there is temporal variation in the source of sediments. An Upper Siwalik sample highlighted possible inputs from the Gangdese Batholith. Contribution from the Gangdese Batholith in the Neogene foreland sediments of the Arunachal Himalaya have been reported from the detrital zircon U-Pb ages from the Bhalukpong and Itanagar areas (Cina et al., 2009). The detrital component from the Gangdese comprises up to 31% in the Subansiri Formation. These may be explained by the river capture of the Yalu River, which drains through Gangdese Batholith by the Subansiri River at ~10 Ma and later by the Siang River at 3-4 Ma (Cina et al., 2009). The amount of sediments contributed from this batholith varies with time and space. Present-day river sediments in the Yalu River comprise mostly of the Gangdese component,

which gets diluted downstream due to addition of sediments from the extremely fast eroding eastern syntaxial bend at Namcha Barwa (Stewart et al., 2008; Cina et al., 2009). In the present study, the AFT age signatures in the sediments from different rivers of the Arunachal Himalaya indicate detritus coming from all the Himalayan units with majority of the contribution from the Lesser Himalayan windows and the HHC.

6.7. Conclusions

The present work emphasizes mainly on the field investigations, fission track dating of apatite and zircon of bed-rock and of apatite grains from the river sands, and Rb-Sr dating of biotite and muscovite to quantify the various geodynamic processes and to study the interplay between the various surface processes. The main conclusions of this study are as follows:

1. The Arunachal Himalaya occupies the easternmost end of this orogen with the location of the Eastern Himalayan Syntaxis as a major antiform just to its northeast. It has all the classical units of the Himalaya the Siwaliks, the Lesser Himalayan Sedimentary Belt, the Himalayan Metamorphic Belt (HMB), the Tethyan Sedimentary Zone, the Indus Tsangpo Suture Zone and the Trans-Himalayan Batholith. These units are separated by different tectonic boundaries, of which the MCT is the most important one. Folding of the MCT and simultaneous erosion of the overlying package has exposed the LH sedimentary belt into two windows. The movement along the MCT and window development activity is the major controlling factor for the geodynamic activities in Arunachal.

2. The youngest AFT ages are recorded in the Lesser Himalayan window (LHW), followed by the HHC belt in all the three investigated traverses in the Arunachal Himalaya. The youngest AFT age recorded is 2.0 Ma within the LH window in the Kimin-Koluriang section, while the oldest AFT age of 12.1 Ma was recorded from the Lesser Himalayan Crystalline Belt along the same traverse. The ZFT ages vary between 3.3 to 13.2 Ma, with younger ages in the HHC package. In the Kimin-Koluriang section, there is gradual decrease of the Rb-Sr biotite ages from 18.73 Ma in the Lesser Himalaya to a minimum of 9.19 Ma in the HHC. The pattern is similar for the Rb-Sr muscovite ages, indicating linear cooling along the MCT. However, the ages concentrate into two distinct groups in each of the other two traverses. Along the Subansiri Valley, ~7 Ma Rb-Sr biotite age of the HHC rocks is separated from the ~15 Ma-aged biotite of the LHCS by the MCT. The thermochronometry results further enrich the general pattern of thermal age distribution, with younger ages in the HHC and older ages in the LH, as is observed in the whole of the Himalayan orogen.

3. The sharp decline of the AFT age in the Siyom River valley between samples Z45 and Z51 is interpreted for a tectonic break/thrust contact separating the LHCS from the HHC rocks. This is further supported by the Rb-Sr biotite ages, which are reduced from 17.83 Ma in the proposed LHCS to 10.1 Ma in the HHC part. Further field investigation should be done and more thermochronology work should be carried work to confirm this finding.

4. Cooling rates, calculated from closure temperatures of the AFT, ZFT, Rb-Sr biotite and muscovite thermochronometers, indicate variations in the cooling pattern with time and space. The cooling rates vary between 6.8 and 204.9 °C/Ma. The exhumation rates, reduced from the AFT and ZFT ages using the 1D numerical modelling, confirm

the correlation of exhumation rates with the structural layout of the area. The rates vary between 0.25 mm/yr to 1.2 mm/yr. The fastest exhumation rate has been observed in the LH window rocks, followed by the HHC. The LH and LHCS rocks experienced slower exhumation rates. Hence, in the Arunachal Himalaya, the cooling and exhumation of different lithotectonic units are mainly control by the folded MCT and simultaneous doming activity. Thus, these provide evidences for the tectonic forcing on the exhumation of the Arunachal Himalaya.

5. Detrital apatite Fission Track Thermochronology of modern river sediments from the Subansiri River and its tributaries, and Siyom River highlighted different source rocks of the sediments carried by these rivers. Correlation of the different peak ages, reduced from AFT analysis of sediments with the AFT ages of the bedrock samples from this region, showed the contribution from all the lithounits of the Himalaya in the Arunachal region. However, the peak sizes indicated that the majority of the detritus are contributed from the HHC rocks where exhumation rates are very high. One sample from the Upper Siwalik Kimin Formation has yielded AFT peak of 33 Ma, thus indicating a possible source of sediments from the Gangdese Batholith. Further detrital thermochronological investigation using $^{40}Ar/^{39}Ar$ and FTD will be required to confirm this postulate.

6. The bedrock and detrital thermochronology also indicated that, although the LH window and the HHC region in the Arunachal Himalaya experience very high exhumation rates to an extent of 1.2 mm/yr, this area lack exhumation 'hot spots' like the western (Nanga Parbat) and eastern (Namcha Barwa) syntaxial bends, which have rates to a degree up to 10 mm/yr.

7. Taking into consideration all the thermochronological age distribution of different parts of the Himalaya, it is highlighted that young ages are mainly concentrated within the HHC rocks, which are separated from the LH by the MCT. Beside this, another region for young ages is the LH windows, which are exposed due to the folding of the MCT and simultaneous erosion of the overlying HMB cover rocks. These regions experienced consistently high exhumation rates from the westernmost part to easternmost end of this orogen. The east-west similarity is also observed for the LH rocks, except the ages are older and exhumation rates are slower in this package. However, a comparison of the age distribution and exhumation rate patterns with the structural layout shows a positive correlation throughout the Himalaya. Hence, the present work, as also suggested by earlier workers (Jain et al., 2000; Burbank et al., 2003; Bojar et al., 2005; Patel and Carter, 2009), provides a strong thermochronological evidence for tectonic control on the exhumation of the Himalayan orogen, having an obvious erosion of the uplifted rock column.

References

Academica Sinica (1980) A Scientific guidebook to South Xizang (Tibet), June 2-4, *Symposium on Qinhai—Xizang (Tibet) plateau*, 104 pp. and one map 1:1,500,00.

Acharya, S.K. (1976) On the nature of main Boundary Fault in the Darjeeling Sub Himalaya. *Geological Survey Miscellaneous Publication*, v. 24(20), pp. 395-408.

Acharya, S.K., Ghose, S.C., Ghose, S.N. and Shah, S.C. (1975) The continental Gondwana Group and associated marine sediments of Arunachal Pradesh (NEFA), Eastern Himalaya. *Himalayan Geology*, v. 5, pp. 60-82.

Agarwal, R.P., Srivastava, A.K. and Maithani, A. (1991) Geology of eastern Himalayan Foothill Belt of Bhutan and Arunachal Pradesh: an overview. *Journal of Himalayan Geology*, v. 2(2), pp. 197-205.

Ahmad, T., Tanaka, T., Sachan, H.K., Asahara, Y., Islam, R. and Khanna, P.P. (2008) Geochemical and isotopic constrains on the age and origin of the Nidar ophiolitic complex, Indus suture zone, Ladakh, India. *Tectonophysics*, v. 451, pp. 206-224.

Anon (2004) A Guidebook Geological map of the Qunghai-Xizang (Tibet) and Adjacent areas 1:1500 000. *Chendung Institute of Geology and Mineral Resources. China Geological Survey*, 48 pp.

Arita, K. (1983) Origin of inverted metamorphism of the lower Himalaya, Central Himalaya. *Tectonophysics*, v. 95, pp. 43-60.

Auden, J.B. (1934) The Geology of Krol Belt. *Record Geological Survey of India*, v. 67, pp. 357-454.

Auden, J.B. (1935) Traverses in the Himalaya. *Records Geolological Survey of India*, v. 69, pp. 123-167.

Avouac, J.P. and Burov, E.B. (1996) Erosion as a driving mechanism of intracontinental growth. *Journal of Geophysical Research*, v. 101, pp. 13942-13956.

Bakhliwal, P.C., Sangma, L. and Das, A.K. (1979) Geology of Ranga Valley, Subansiri district, Arunachal Pradesh. *Himalayan Geology*, v. 9(1), pp.42-51.

Balasundram, M.S. (1972) Annual general Report. *Record Geological Survey of India*, v. 103(1), pp. 185-187.

Beaumont, C., Fulsack, P. and Hamilton, J. (1992) Erosional control of active compressional orogen. In: McClay, K. (eds.) Thrust tectonics. *Chapman and Hall, New York*, pp. 1-18.

Beek, P.V.D., Robert, X., Mugnier, J.L., Bernet, M., Huyghe, P. and Labrin, E. (2006) Late Miocene–Recent exhumation of the central Himalaya and recycling in the foreland basin assessed by apatite fission-track thermochronology of Siwalik sediments, Nepal. *Basin Research*, v. 18, pp. 413-434.

Bera, M.K., Sarkar , A., Chakraborty, P.P., Loyal, R.S. and Sanyal, P. (2008) Marine to continental transition in Himalayan foreland. *Geological Society of America Bulletin*, v. 120 (9-10), pp. 1214-1232; DOI: 10.1130/B26265.1.

Bernet, M., Beek, P.A.V.D., Pik, R., Huyghe, P., Mugnier, J.L., Labrin, E and Szulc, A.G. (2006) Miocene to recent exhumation of central Himalaya determined from combined detrital fission track and U/Pb analysis of Siwalik sediments, western Nepal. *Basin Research*, v. 18, pp. 393-412.

Bernet, M., Brandon, M.T., Garver, J.I. and Molitor, B.I. (2004a) Fundamentals of detrital zircon fission-track analysis for provenance and exhumation studies with examples from the European Alps. In: Bernet, M. and Spiegel, C. (eds.), Detrital thermochronology-Provenance analysis, exhumation and landscape evolution of mountain belts. *Geological Society of America Special Publication*, v. 378, pp. 25-36.

Bernet, M., Brandon, M.T., Garver, J.I. and Molitor, B.R. (2004b) Downstream changes in Alpine detrital zircon fission-track ages of the Rhone and Rhine Rivers. *Journal Sedimentary Research*, v. 74, pp. 82-94.

Bernet, M., Zattin, M., Garver, J.I., Brandon, M.T. and Vance, J.A. (2001) Steady-state exhumation of the European Alps. *Geology*, v. 29(1), pp. 35-38.

Bhalla, J.K. and Bishui, P.K. (1989) Geochronology and Geochemistry of granite emplacement and metamorphism in northeastern Himalaya. *Record Geological Survey of India*, v. 122(20), pp. 18-20.

Bhalla, J.K., Srimal, N. and Bishui, P.K. (1990) Isotope study of Mishmi Complex, Arunachal Pradesh, Northeastern Himalaya. *Records Geological Survey of India*, v. 123(2), 20 pp.

Bhatia, S.B. (2000) Faunal and floral diversity in the Subathu-Dagshai passage beds: a review. *Himalayan Geology*, v. 21, pp. 87–97.

Bhatia, S.B. and Bhargava, O.N. (2006) Biochronological continuity of the Paleogene sediments of the Himalayan foreland basin: paleontological and other evidences. *Journal of Asian Earth Sciences*, v. 26, pp. 477–487.

Bigazzi, G. (1981) The problem of decay constant of ^{238}U. *Nuclear tracks*, v. 5, pp. 35-44.

Birck (1986) Precision K-Rb-Sr Isotopic analysis: Application to Rb-Sr chronology. *Chemical Geology*, v. 56, pp. 73-83.

Biswas, S.K., Ahuja, A.D., Saproo, M.K. and Basu, B. (1979) Geology of Himalayan Foothill of Bhutan. *Geological Survey of India Miscellaneous Publication*, v. 41(5), pp. 287-307.

Blichert, J. (1993) Manual for Sr and Nd Isotope Geochemistry, Copenhagen. *Unpublished manual*, 122 pp.

Blythe, A.E., Burbank, D.W., Carter, A., Schmidt, K. and Putkonen, J. (2007) Plio-quaternary exhumation history of the central Nepalese Himalaya: 1. Apatite and zircon fission track and apatite (U-Th)/He analysis. *Tectonics*, v. 26, TC3002, doi: 10.1029/2006TC001990.

Bojar, A.V., Fritz, H., Nicolescu, S., Bregar, M. and Gupta, R.P. (2005) Timing and mechanisms of Central Himalayan exhumation: discriminating between tectonic and erosion processes. *Terra Nova*, v. 17, pp. 427–433.

Booth, A.L., Chamberlain, C.P., Kidd, W.S.F. and Zeitler, P.K. (2008) Metamorphic and geochronologic constraints on the tectonic evolution of the eastern Himalayan syntaxis, Namche Barwa. *Geological Society of America Bulletin*, v. 121(3-4), pp. 385-407.

Booth, A.L., Zeitler, P.K., Kidd, W.S.F., Wooden, J., Liu, Y., Idleman, B., Hren, M. and Chamberlain, C.P. (2004) U-Pb zircon constraints on the tectonic evolution of southeastern Tibet, Namche Barwa area. *American Journal of Science*, v. 304(10), pp. 889-929.

Brandon, M.T. (1992) Decomposition of fission-track grain-age distributions. *America. Journal of Science*, v. 292, pp. 535-564.

Brandon, M.T. (1996) Probability density plots for fission-track grain age distributions. *Radiation Measurement*, v. 26, pp. 663-676.

Brandon, M.T. (2002) Decomposition of mixed grain-age distributions using BINOMFIT. *On Track*, v. 24, pp. 13-18.

Brandon, M.T. and Vance, J.A. (1992) Tectonic evolution of the Cenozoic Olympic Subduction Complex, Washington State, as deduced from fission track ages for detrital zircons. *American Journal of Science*, v. 292, pp. 565-636. 26.

Brandon, M.T., Roden-Tice, M.K. and Garver, J.I. (1998) Late Cenozoic exhumation of Cascadia accretionary wedge in the Olympic mountains, northwest Washington state. *Geological Society of America Bulletin*, v. 110, pp. 985-1009.

Brooks, C., Hart, S. R. and Wendt, I. (1972) Realistic use of two-error regression treatments as applied to Rubidium-Strontium data. *Review of Geophysics and Space Physics*, v. 10, pp. 551-577.

Brooks, C., Wendt, I. and Harre, W. (1968) A two-error regression treatment and its application to Rb-Sr and initial Sr^{87}/Sr^{86} ratios of younger Variscan granitic rocks from the Schwarzwald massif, Southwest Germany. *Journal Geophysical Research*, v. 73, pp. 6071-6084.

Brunel, M. (1986) Ductile thrusting in the Himalaya: shear sense criteria and stretching lineation. *Tectonics*, v. 5, pp. 247-265.

Brunel, M., Hodges, K. V., Le Fort, P. and Pêcher, A. (1989) Possible thermal buffering by crustal anatexis in collisional orogens; thermobarometric evidence from the Nepalese Himalaya; comment and reply. *Geology*, v. 17, pp. 575-576.

Burbank, D.W. (2002) Rates of erosion and their implications for exhumation. *Mineralogical Magazine*, v. 66, pp. 25-52.

Burbank, D.W., Blythe, A.E., Putkonen, J., Pratt-Sittaula, B., Gabet, E., Oskin, M., Barros, A. and Ojha, T.P. (2003) Decoupling of erosion and precipitation in the Himalayas. *Nature*, v. 426, pp. 652-655.

Burchfiel, B.C. and Royden, L.H. (1985) North-south extension within the convergent Himalayan region. *Geology*, v. 13, pp. 69-682.

Burg, J.P. and Chen, G.M. (1984) Tectonics and structural zonation of Southern Tibet. *Nature,* v. 311, pp. 219-223.

Burg, J.P., Davy, P., Nievergelt, P., Oberli, F., Seward, D., Diao, Z. and Meier, M. (1997) Exhumation during crustal folding in the Namche-Barwa syntaxis. *Terra Nova*, v. 9(2), pp. 53-56.

Burg, J.P., Nievergelt, P., Oberli, F., Seward, D., Davy, P., Maurin, J.C., Diao, Z. and Meier, M. (1998) Namche Barwa syntaxis; evidence for exhumation related to

compressional crustal folding. *Journal of Asian Earth Sciences*, v. 16(2-3), pp. 239-252.

Caby, R., Pecher, A. and Le Fort, P. (1983) Le M.C.T Himalayan: Nouvelles donnes sur le metamorphisme inverse a la base de la Dalle du Tibet, *Revue de Geographie Physique at de Geologic Dynamigue*, v. 24, pp. 89-100.

Cerveny, P.F., Naeser, N.D., Zeitler, P.K., Naeser, C.W. and Johnson, N.M. (1988) History of uplift and relief of the Himalaya during the past 18 million years: evidence from fission-track ages of detrital zircons from sandstones from the Siwalik Group. In: Kleinspehn, K.L. and Paola, C. (eds.), New Perspectives in Basin Analysis. *Springer-Verlag, New York*, pp. 43-61.

Choudhari, B.K., Gururajan, N.S. and Singh, B. (2009) Geology and structural evolution of eastern Himalayan syntaxis. *Himalayan Geology*, v. 30(1), pp. 17-34.

Choudhary, A.K., Manickavasagam, R.M., Jain, A.K., Singh, S. and Chandra, K. (2004) National Facility on Geochronology and Isotope Geology at IIT Roorkee, Roorkee – New data on Southern Granulite Massif. In: Agarwal, S.K. and Jaison, P.G. (eds.), *Eleventh ISMAS Workshop on Mass Spectrometer*, October, 7-12, Shilon Bagh, Shimla. Indian Society of Mass Spectrometer, pp. 51-58.

Cina, S.E., Yin, A., Grove, M., Dubey, C.S., Shukla, D.P., Lovera, O.M., Kelty, T.K., Gehrels, G.E. and Foster D.A (2009) Gangdese arc detritus within the eastern Himalayan Neogene foreland basin: Implications for the Neogene evolution of the Yalu–Brahmaputra River system. *Earth and Planetary Science Letters*, v. 285, pp. 150–162.

Clift, P.D., Giosan, L., Blusztajn, J., Cambell, I.H., Allen, C., Pringle, M., Tabrez, A.R., Danish, M., Rabbani, M.M., Alizai, A., Carter, A. and Luckje, A. (2008) Holocene erosion of the Lesser Himalaya triggered by intensified summer monsoon. *Geology*, v. 36, pp. 79-82, doi:10.1130/G24315A.1.

Curray, J.R. (1994) Sediment volume and mass beneath the Bay of Bengal. *Earth and Planetary Science Letters*, v. 125, pp. 371-383.

Dadson, S.J., Hovius, N., Chen, H.G., Dade, W.B., Hsieh, M.L., Willet, S.D., Hu, J.C., Horng, M.J., Chen, M.C., Stark, C.P., Lague, D. and Lin, J.C. (2003) Links between erosion, runoff variability and seismicity in Taiwan orogen. *Nature*, v. 426, pp. 648-742.

Dahl, P.S. (1996) The effects of composition on retentivity of Argon and Oxygen in hornblende and related amphiboles: A field tested empirical model. *Geochimica et Cosmochimica Acta*, v. 60, pp. 3687-3700.

Das, D.P. and Ray, S.B. (1982) Report on the Geology of area north east and northwest of Tamen, Lower Subansiri District, Arunachal Pradesh. *Unpublished report of Geological Survey of India northeastern region, Itanagar*, 23 pp.

Das, P.K. (1979) Certain aspects of metamorphic rocks around Yazali-Ziro, Subansiri district. In: Verma P.K. (eds.) Metamorphic rock sequence of the eastern Himalaya. pp. 114-124.

Debon, F., Le Fort, P., Sheppard, S.M.F. and Sonet, J. (1986) The four plutonic belts of the Transhimalaya-Himalaya: A chemical, minerological, isotopic and chronological synthesis along Tibet-Nepal section. *Journal of Petrology*, v.27, pp. 219-250.

Debon, F., Le Fort, P., Sonet, J., Liu, G., Jin, C. and Xu, R. (1981) About the Lower Paleozoic age of Kangmar granite (Lhagoi-Kangri plutonic belt, South Tibet, China) *Tera Cognita special issue*, v. 114, pp. 67-68.

DeCelles, P.G., Robinson, D.M., Quade, J., Ojha, T.P., Garzione, C.N., Copeland, P. and Upreti, B.N. (2001) Stratigraphy, structure and tectonic evolution of the Himalayan fold-thrust belt in Western Nepal. *Tectonics*, v. 20, pp. 487-509.

Desio, A. (1977) On the geology of Deosai plateau, *Kashmir Memoirs Accaddemic Naz. Lincei*, v. 15, pp. 1-19.

Dickin, A.P. (1995) Radiogenic Isotope Geology. *Cambridge University Press*, 452 pp.

Dikshitulu, G.R., Pandey, B.K., Krishna, Veena and Dhana Raju, R. (1995) Rb-Sr systematics of granatoids of the Central Gneissic Complex, Arunachal Himalaya: Implication on tectonics, stratigraphy and source. *Journal Geological Society of India*, v. 45(1), pp. 52-56.

Ding, L., Zhong, D., Yin, A., Kapp, P. and Harrison, T.M. (2001) Cenozoic structural and metamorphic evolution of the Eastern Himalayan Syntaxis (Namche Barwa). *Earth and Planetary Science Letters*, v. 192(3), pp. 423-438.

Dodson, M.H. (1973) Closure temperature in cooling geochronological and petrological systems. *Contribution to Mineralogy and Petrology*, v. 40, pp. 259-264.

Dodson, M.H. (1979) Theory of cooling ages. In: Jager, E. and Hunziker, J.C. (eds.), Lectures in Isotope Geology. *Berlin: Springer-Verlag*, pp. 194-202.

Dodson, M.H. (1981) Thermochronometry. *Nature*, v. 293, pp. 606-607.

Dodson, M.H. and McClellad-Brown, E. (1985) Isotopic and paleomagnectic evidence for rates of cooling, uplift and erosion. In: Snelling, N.J. (eds.), Geochronology and Geologic record. *Memoir Geological Society of London*, pp. 315-325.

Dubey, C.S., Catlos, E.J. and Sharma, B.K., (2005) Modelling P-T-t paths constrained by mineral chemistry and monazite dating of metapelites ion relationship to MCT activity in Sikkim, Eastern Himalayas. In. Thomas, H. (eds.) *Metamorphism and crustal Evolution. Papers in Honor of Prof. R.S. Sharma*, Atlantic Publishers and Distributors, pp. 250-282.

Dumitru, T.A. (2000) Fission Track Geochronology. In: Noller, J.S., Sowers, J.M. and Lettis, W.R. (eds.), Quaternary Geochronology: Methods and applications. *American Geophysical Union Reference Shelf 4, Washington D.C.*, pp. 131-155.

Dutta, A. (1982) Joint scientific survey expedition to Subansiri Valley, Arunachal Pradesh. *Geological Survey Miscellaneous Publication*, v. 41(ii), pp. 102-109.

Dutta, A., Gill, G.K.S. and Srinivasan, J. (1983) Geology of Subansiri and Kamla Rivers. *Geological Survey Miscellaneous Publication*, v. 43, pp. 8-11.

Dutta, S.K., Srivastava, S.C. and Gagoi, B. (1988) Palynolgy of Permian sediments in Kameng District, Arunachal Pradesh. *Geophytology*, v. 18(1), pp. 53-61.

Ehlers, T.A. and Farley, K.A. (2003) Apatite (U-Th)/He thermochronometry: Methods and applications to problems in tectonic and surface processes. *Earth and Planetary Science Letters*, v. 206, pp. 1-14, doi:10.1016/S0012-821X(02)01069-5.

Ehlers, T.A., Chaudhri, T., Kumar, S., Fuller, C.W., Willet, S.D., Ketcham, R.A., Brandon, M.T., Belton, D.X., Kohn, B.P., Gleadow, A.J.W., Dunai, T.J. and Fu, F.Q. (2005) Computational Tools for Low-Temperature Thermochronometer Interpretation. In: Reiners, P.W. and Ehlers, T.A. (eds.), Low-Temperature Thermochronology: Techniques, Interpretations, and Applications. *Reviews in Mineralogy & Geochemistry*, v. 58, pp. 589-622.

England, P. and Molnar, P. (1990) Surface uplift, uplift of rocks and exhumation of rocks. *Geology*, v. 18, pp. 1173-1177.

Farley, K.A. (2000) Helium diffusion from apatite: General behavior as illustrated by Durango flouroapatite. *Journal of Geophysical Research*, v. 105, pp. 2903-2914.

Faure, G. (1989) Principles of Isotope Geology (2nd eds.). *John Wiley, New York*, 589 pp.

Faure, G. and Mensing, T.M. (2005) Isotopes: principles and application (3rd eds.), *John Wiley, New York,* 897 pp.

Fleischer, R.L., Price, P.B. and Walker, R.M. (1965) Ion explosion spike mechanism for formation of charged particles tracks in solids. *Journal of Applied Physics*, v. 36, pp. 3645-3652.

Fleischer, R.L., Price, P.B. and Walker, R.M. (1975) Nuclear Tracks in solids: Principles and applications. *University of California Press, Berkeley*, 605 pp.

Foland, K.A. (1994) Ar diffusion in feldspars. In: Parsons, I. (eds.), Feldspar and their reactions. *Kluwer, Dordrecht*, pp. 415-447.

Foster, G.L. and Carter, A. (2007) Insights into the patterns and locations of erosion in the Himalaya - A combined fission-track and *in situ* Sm-Nd isotopic study of detrital mica. *Earth and Planetary Science Letters*, v. 257, pp. 407-418, doi: 10.1016/j.epsl.2007.02.044.

Frank, W., Thoni, M. and Purtscheller, F. (1977) Geology and Petrography of Kullu-South Lahaul area. *Colloquium of International Centre Natural Res. Science*, v. 33, pp. 147-172.

Freeman, S.R., Inger, S., Butler, R.W.H. and Cliff, R.A. (1997) Dating deformation using Rb-Sr in white micas: greenschist facies deformation ages for the Entrelor Shear Zone, Italian Alps. *Tectonics*, v. 16, pp. 57-76.

Fuchs, G. (1975) Contribution to geology of North-west Himalaya. *Abh. Geology Bundesstalt,* Wein 32, 59 pp.

Galbraith, R.F. and Green, P.F. (1990) Estimating the component ages in a finite mixture. *Nuclear Tracks Radiation Measurement*, v. 17, pp. 197-206.

Galbraith, R.F. and Laslett, G.M. (1993) Statistical models for mixed fission track ages. *Nuclear Tracks Radiation Measurement*, v. 21, pp. 459-470.

Gansser, A. (1977) Geology of the Himalayas. *Willey Interscience London*, 289 pp.

Gansser, A. (1983) Geology of the Bhutan Himalaya. *Birkhäuser Verlag, Boston*, 180 pp.

Garver, J.I., Brandon, M.T., Roden-Tice, M.K. and Kamp, P.J.J. (1999) Exhumation history of orogenic highlands determined by detrital fission track thermochronology. In: Ring, U., Brandon, M. T., Willett, S. D., and Lister, G. S. (eds.), Exhumation processes: Normal faulting, ductile flow and erosion. *Geological Society Special Publications*, v. 154, pp. 283-304.

Garzanti, E. and Van Haver, T. (1988) The Indus clastics fore-arc basin sedimentation in the Ladakh Himalaya (India). *Sedimentary Geology*, v. 59, pp. 237-249.

Garzanti, E., Vezzoli, G., Ando, S., France-Lanord, C., Singh, S.K. and Foster, G. (2004) Sand petrology and focused erosion in collision orogens: the Brahmaputra case. *Earth and Planetary Science. Letters*, v. 220, pp. 157-174.

Garzanti, E., Vezzoli, G., Ando, S., Paparella, P. and Clift, P.D. (2005) Petrology of Indus River sands: a key to interpret erosion history of the western Himalayan Syntaxis. *Earth and Planetary Science Letters*, v. 229, pp. 287-302.

Geng, Q.R., Pan, G.T., Zheng, L.L., Chen, Z.L., Fisher, R.D., Sun, Z.M., Ou, C.S., Dong, H., Wang, X.W., Li, S., Lou, X.Y. and Fu, H. (2005) The Eastern Himalayan Syntaxis: major tectonic domains, ophiolitic melanges and geologic evolution. *Journal of Asian Earth Sciences*, v. 27(3), pp. 265-285.

Gleadow, A.W.J. (1981) Fission Track dating methods: What are the real alternatives? *Nuclear Tracks*, v. 5, pp. 3-14.

Gleadow, A.W.J. and Lovering, J.F. (1975) Fission track dating methods. *Department of Geology, School of Earth Sciences, University of Melbourne*, Publication 3, 93 pp.

Gleadow, A.W.J., Belton, D.X., Kohn, B.P. and Brown, R.W. (2002) Fission track dating of phosphate minerals and thermochronology of apatite. *Reviews Mineralogy and Geochemistry*, v. 94, pp. 405-415.

Gleadow, A.W.J., Duddy, I.R., Green, P.F. and Lovering, J.F. (1986) Confined fission track length an apatite: a diagonostic tool for thermal history analysis. *Contribution to Mineralogy and Petrology*, v. 94, pp. 405-415.

Gleadow, A.W.J., Hurford, A.J. and Quafie, R.D. (1976) Fission Track dating of zircon: improved etching techniques. *Earth and Planetary Science Letters*, v. 33, pp. 273-276.

Group of K-Ar Geochronology Institute of Geology, Chinese Academy of Science, (1979) K-Ar dating and division of the Himalayan movement in southern Xizang. *Scientia Geologica Sinica*, v. 1, pp. 13-21.

Grove, M. and Harrison, T.M. (1996) ^{40}Ar diffusion in Fe-rich biotite. *American Mineralogist*, v. 81, pp. 940-951.

Grujic, D., Countd, I., Bookhagen, B., Bonnet, S., Blythe, A. and Duncan, C. (2006) Climatic forcing of erosion, landscape and tectonics in Bhutan Himalaya. *Geology*, v. 34, pp. 801-804.

Hames, W.E. and Bowring, S.A. (1994) An empirical evaluation of the Argon diffusion geometry in muscovite. *Earth and Planetary Science Letters*, v. 124, pp. 161-167.

Harrison, T.M. (1981) Diffusion of ^{40}Ar in hornblende. *Contribution Mineralogy and Petrology,* v. 78, pp. 324-331.

Harrison, T.M. and McDougal, I. (1981) Excess of ^{40}Ar in metamorphic rocks from Broken Hill, New South Wales: Implication for $^{40}Ar/^{39}Ar$ age spectra and thermal history of the region. *Earth and Planetary Science Letters*, v. 55, pp. 123-149.

Harrison, T.M. and Zeitler, P.K. (2005) Fundamentals of noble gas thermochronometry. *Review of Mineralogy and Geochemistry*, v. 58, pp. 123-149.

Harrison, T.M., Duncan, I. and McDougall, I. (1985) Diffusion of ^{40}Ar in biotite: temperature, pressure and compositional effects. *Geochimica et Cosmochimica Acta*, v. 49, pp. 2461-2468.

Heim, A. and Gansser, A. (1939) Central Himalaya-Geological observations of Swiss Expedition 1936. *Memoirs Societ helve. Science and Nature*, v. 73, 245 pp.

Hodges, K., Ruhl, K., Wobus, C. and Pringle, M. (2005) $^{40}Ar/^{39}Ar$ Ar thermochronology of detrital minerals. *Reviews in Mineralogy and Geochemistry*, v. 58, pp. 239-257.

Hodges, K.V. (2000) Tectonics of the Himalaya and southern Tibet from two decades perspectives. Geological Society of America Bulletin, v. 112, pp. 324-350.

Hodges, K.V., Burchfiel, B.C., Royden, L.H., Chen, Z. and Liu, Y. (1993) The metamorphic signature of contemporaneous extension and shortening in the central Himalayan orogen: Data from Nyalam transect, Southern Tibet. *Journal of Metamorphic Geology*, v. 11, pp. 721-737.

Honegger, K., Dietrich, V., Frank, W., Gansser, A., Thoni, M. and Trommsdorf, V. (1982) Magmatism and metamorphism in the Ladakh Himalayas (the Indus-Tsangpo Suture Zone). *Earth and Planetary Science Letters*, v. 60, pp. 253-292.

Hubbard, M.S. and Harrison, T.M. (1989) $^{40}Ar/^{39}Ar$ age constraints on deformation and metamorphism in the MCT Zone and Tibetan Slab, Eastern Nepal Himalaya. *Tectonics*, v. 8, pp. 865-880.

Huntington, K.W. and Hodges, K. (2006) A comparative study of detrital mineral and bed rock age-elevation methods for estimating erosion rate. *Journal of Geophysical Research-Earth Surface*, v. 111(F3), F03011 10.1029/2005JF00054.

Hurford, A.J. (1990) Standardization of fission track dating calibration: recommendation by fission track working group of IUGS Sub-commission on Geochronology. *Chemical Geology (Isotope Geoscience Section)*, v. 80, pp. 171-178.

Hurford, A.J. and Green, P.F. (1982) A user's guide to fission track dating calibration. *Earth and Planetary Science Letters*, v. 59, pp. 343-354.

Hurford, A.J. and Green, P.F. (1983) The zeta age calibration of fission-track dating, *Chemical Geology*, v. 41, pp. 285-317.

Inger, S. (1988) Timing of extensional detachment during convergent orogeny; new Rb-Sr geochronological data from the Zanskar Shear Zone, northwestern Himalaya. *Geology*, v. 26, pp. 223-226.

Inger, S. and Cliff, R.A. (1994) Timing of metamorphism in the Tauern Window, Eastern Alps. Rb-Sr ages and fabric formation. *Journal Metamorphic Geology*, v. 12, pp. 695-707.

Jager, E., Bhanadari, A.K. and Bhanot, V.B. (1971) Rb-Sr age determinations on Biotites and Whole Rock samples from the Mandi and Chor Granites, Himachal Pradesh, India. *Ecologae Geologica Helvetia*, v. 64(3), pp. 521-527.

Jain, A.K. and Anand, A. (1988) Deformation and strain patterns of an intracontinental ductile shear zone-an example from the Higher Garhwal Himalaya. *Journal Structural Geology*, v. 10(7), pp. 717-734.

Jain, A.K. and Anand, A. (1988) Deformational and strain patterns of an intracontinental collision ductile shear zone-an example from the Higher Garhwal Himalaya. *Journal of Structural Geology*, v. 10(7), pp. 717-734.

Jain, A.K. and Manickavasagam, R.M. (1993) Inverted metamorphism in the intracontinental ductile shear zone during Himalayan collision tectonics. *Geology*, v. 21, pp. 407-410.

Jain, A.K. and Singh, S. (2009) Geology and Tectonics of the Southeastern Ladakh and Karakoram. Geological Society of India. Bangalore. 181 pp.

Jain, A.K., Kumar, D., Singh, S., Kumar, A. and Lal, N. (2000) Timing quantification and tectonic model of Pliocene-Quaternary movements in NW Himalaya: evidences from fission track dating. *Earth Planetary Science Letters*, v. 179 (3-4), pp. 437-451.

Jain, A.K., Lal, N., Sulemani, B., Awasthi, A.K., Singh, S., Kumar, R. and Kumar, D. (2009) Detrital-zircon fission-track ages from the Lower Cenozoic sediments, NW Himalayan foreland basin: Clues for exhumation and denudation of the Himalaya

during the India-Asia collision. *Geological Society of America Bulletin*, v. 21(3-4), pp. 519-535.

Jain, A.K., Singh, S. and Manickavasagam, R.M. (2002) Himalayan Collision Tectonics. *Gondwana Research Group Memoir*, v. 7, 114 pp.

Jain, A.K., Singh, S., Manickavasagam, R.M., Joshi, M. and Verma, P.K. (2003) HIMPROBE Programme: Integrated study on geology, petrology, geochronology and geophysics of the Trans-Himalaya and Karakoram. *Memoir Geological Society of India*, No. 53, pp. 1-56.

Jain, A.K., Thakur, V.C. and Tandon, S.K. (1974) Stratigraphy and structure of the Siang District of Arunachal Pradesh. *Himalayan Geology*, v. 4, pp. 28-60.

Karunakaran, C. and Rao, A.R. (1983) Status for exploration for Hydrocarbon in the Himalayan region - Contribution to stratigraphy and Structures, Himalayan Geology Seminar, New Delhi 1976, *Geological Survey Miscellaneous Publication*, v. 41(III), pp. 1-66.

Ketcham, R.A., Donelick, R.A and Carlson, W.D. (1999) Variability of apatite fission-track annealing kinetics III: Extrapolation to geological time scales. *American Mineralogists*, v. 84, pp. 1235-1255.

Krishnaswami, S., Lal, D., Prabhu, N. and McDougall, D. (1974) Characteristics of fission tracks in zircon: application to geochronology and cosmology. *Earth and Planetary Science Letters*, v. 22, pp. 51-59.

Kumar, A., Lal, N., Jain, A.K. and Sorkhabi, R.B. (1995) Late Cenozoic-Quarternary Thermo-tectonic history of Higher Himalayan Crystalline (HHC) in Kishtwar-Padar-Zanskar region, NW Himalaya: Evidence from fission track ages. *Journal Geological Society of India*, v. 45(4), pp. 375-391.

Kumar, D. (1999) Fission track Zircon-Apatite ages and exhumation of Himalayan Metamorphic Belt (HMB) along Beas-Sutlej Valley, Himachal Pradesh. *Unpublished Ph.D thesis, Kururkshetra University, Kurukshetra, India,* 86 pp.

Kumar, G. (1997) Geology of Arunachal Pradesh. *Geological Society of India*, 217 pp.

Kumar, P., Ashok and Mishra, I.K. (1989) Geology of Lohitpur-Bishamnagar area, Lohit and Dibang valley districts. *Records Geological Survey of India*, v. 124(4), pp. 14-16.

Kumar, R. (2005) Tectonics, geochemistry and geochronology of the Ladakh Batholith, Trans-Himalaya. *Unpublished Ph. D. Thesis, IIT Roorkee*, 195 pp.

Kumar, R., Lal, N., Singh, S. and Jain, A.K. (2007) Cooling and exhumation of the Trans-Himalayan Ladakh Batholith, as constrained by fission track apatite and zircon ages. *Current Science*, v. 92(4), pp. 490-496.

Kumar, S. and Pathak, M. (2008) Geochemistry and petrogenesis of Granitoids from Kameng Corridor of Arunachal Himalaya, Northeast India. *Himalayan Journal of Sciences*, v. 5(7), pp. 132.

Kumar, S. and Rino, V.N. (2006) Mineralogy and geochemistry of microgranular enclaves of Paleoproterozoic Malanjkhand Granitoids, Central India: Evidence of magma mixing, mingling and chemical equilibration. *Contribution to Mineralogy and Petrology*, v. 152, pp. 591-609.

Kumar, S. and Singh, T. (1974) Lithostratigraphy of the southern part of Siang District, Arunachal Pradesh. *Himalayan Geology*, v. 4, pp. 648-56.

Lakshami, K.J.P., Sudheer Kumar, M., Bhalla, M.S. and Rao, G.V.S.P. (2000) Magnetostratigraphy of Himalayan sediments from Himachal Pradesh: *Journal of the Indian Geophysical Union*, v. 4 (2), pp. 147–154.

Lal, N., Mehta, Y.P., Kumar, D., Kumar, A. and Jain, A.K. (1999) Cooling and exhumation history of the Mandi granite and adjoining tectonic units, Himachal Pradesh, and estimation of closure temperature from external surface of zircon. In: Jain, A.K. and Manickavasagam, R.M. (eds.), Geodynamics of the NW Himalaya. *Gondwana Research Group Memoir*, v. 6, pp. 207-216.

Laslett, G.M., Green, P.F., Duddy, I.R. and Gleadow, I.J.R. (1987) Thermal annealing of fission tracks in apatite. 2. A quantitative analysis. *Chemical Geology*, v. 65, pp. 1-13.

Le Fort, P. (1975) Himalayas: The collided range, Present knowledge of the continental arc. *American Journal of Science*, v. 275, pp. 1-44.

Leech, M.L., Singh, S., Jain, A.K., Klemperer, S.L. and Manickavasagam, R.M. (2005) The onset of India-Asia continental collision: early, steep subduction required by the timing of UHP metamorphism in the western Himalaya. *Earth and Planetary Science Letters*, v. 234, pp. 83-97.

Lovera, O.M., Richter, F.M. and Harrison, T.M. (1991) Diffusion domains determined by ^{39}Ar release during step heating. *Journal of Geophysical Research*, v. 96, pp. 2057-2069.

Lovera, O.M., Richter, F.M. and Harrison, T.M. (1997) Systematic analysis of K-feldspar $^{40}Ar/^{39}Ar$ step heating results: I. Significance of activation energy determinations. *Geochimica et Cosmochimica Acta*, v. 61, pp. 3171-3192.

Ludwig, K.R. (2003) User's Manual for Isoplot 3.00: A Geochronological toolkit for Microsoft Excel. *Berkeley Geochronology Centre*, Special Publication No. 4, 70 pp.

Mahe´oa, G., Fayouxa, X., Guillota, S., Garzantib, E., Capieza, P. and Mascle, G. (2005) Relicts of an intra-oceanic arc in the Sapi-Shergol me´lange zone (Ladakh, NW Himalaya, India): implications for the closure of the Neo-Tethys Ocean. *Journal of Asian Earth Sciences*, doi:10.1016/j.jseaes.2005.01.004.

Malloy, M. (2004) Rapid erosion at the Tsangpo knicpoint and exhumation of southeastern Tibet. *M.S thesis, Bethlehem, Pennysylvania, Lehigh University*, 67 pp.

Malusa, G.M. and Vezolli, G. (2006) Interplay between erosion and tectonics in western Alps. *Terra Nova*, v. 18(2), pp. 104-110.

Maluski, H., Matte, P., Brunel, M. and Xiao, X.S. (1988) Ar^{39}/Ar^{40} dating of metamorphic and plutonic events in the north and High Himalaya belts (southern Tibet-China). *Tectonics*, v. 7, pp. 299-326.

Mancktelow, N.S. and Grasemann, B. (1997) Time-dependent effects of heat advection and topography on cooling histories during erosion. *Tectonophysics*, v. 270, pp. 167-195.

Masek, J.G., Isacks, B.L., Fielding, E.J. and Browaeys, J. (1994) Rift flank uplift in Tibet: evidence for a viscous lower crust. *Tectonics*, v. 13, pp. 659-667.

Masoudi, F., Yardley, B.W.D. and Cliff, R.A. (2002) Rb-Sr geochronology of pegmatites, plutonic rocks and a hornfel in the region south west of Arak, Iran. *Journal of Sciences, Islamic Republic of Iran*, v. 13(3), pp. 249-254.

Mattauer, M. (1986) Intracontinental subduction, crust mantle decollement and crustal stacking in the Himalaya and other collision belt. In: Coward, M.P. and Ries, A. (eds.), Collision Tectonics. *Special Publication Geological Society of London*, No. 10, pp. 37-50.

McIntyre, G.A., Brooks, C., Compston, W. and Turek, A. (1966) The statistical assessment of Rb-Sr isochron. *Journal of Geophysical Research*, v. 71, pp. 54-59.

Medlicott, H.B. (1864) On the geological structure and the relationship of the southern portion the Himalayan ranges between Ganges and Ravi. *Memoir Geological Survey of India*, v. 3, 212 pp.

Mehta, P.K. (1977) Rb-Sr geochronology of the Kulu-Mandi belt: its implication for the Himalayan tectonogenesis. *Geologische Rundschau*, v. 66(1), pp. 156-175.

Metcalfe, R.P. (1993) Pressure, temperature and time constraints on metamorphism across the Main Central Thrust zone and High Himalayan slab in the Garhwal Himalaya. In: Treloar, P.J. and Searle, M.P. (eds.), Himalayan Tectonics. *Geological Society Special Publication*, v. 74, pp. 485-509.

Miller, C., Klotzli, U., Frank, W., Thoni, M. and Grasemann, B. (2000) Proterozoic crustal evolution in the NW Himalaya (India) as recorded by circa 1.80 Ga mafic and 1.84 Ga granitic magmatism. *Precambrian Research*, v. 103(3-4), pp. 191-206.

Miyazaki, T., Kagami, H., Shuto, K., Morikiyo, T., Ram Mohan, V. and Rajasekaran, K.C. (2000) Rb-Sr Geochronology, Nd-Sr Isotopes and Whole Rock Geochemistry of Yelagiri and Sevattur Syenites, Tamil Nadu, South India. *Gondwana Research*, v. 3(1), pp. 39-53.

Naeser, C.W. and Faul, H. (1969) Fission track annealing in apatite and sphene. *Journal of Geophysical Research*, v. 74, pp. 705-710.

Naeser, W. (1979) Fission track dating and geologic annealing of fission tracks. In: Jaeger, E. and Hunziker, J.C. (eds.), Lectures in isotope geology. *Heidelberg, Springer Verlag*, pp. 154-169.

Najman, Y. (2006) The sediment record of orogenesis: a review of approaches and techniques used in the Himalaya. *Earth Science Reviews.*, v. 74, pp. 1-72.

Najman, Y. and Garzanti, E. (2000) An integrated approach to provenance studies: reconstructing early Himalayan paleogeography and tectonic evolution from Tertiary foredeep sediments, N. India. *Geological Society of America Bulletin*, v. 112, pp. 435-449.

Najman, Y., Clift, P., Johnson, M.R.W. and Robertson, A.H.F. (1993) Early stages of foreland basin evolution in the Lesser Himalaya, N. India. In: Treloar, P.J. and Searle, M.P. (eds.) *Himalayan Tectonics. Geological Society of London Special Publication*, v. 74, pp. 541-558.

Najman, Y., Johnson, C., White, N.M. and Oliver, G. (2004) Evolution of the Himalayan foreland basin, NW India. *Basin Research.* v. 16, pp. 1-24.

Najman, Y., Johnson, K., White, N. and Oliver, G. (2004) Evolution of the Himalayan foreland basin, NW India. *Basin Research*, v. 16, pp. 1-24, doi: 10.1111/j.13652117.2004.00223.x.

Nandy, D.R. (2002) Geodynamics of northeastern India and the adjoining region. *acp publications*, 209 pp.

Nikunja, B.S.T. (2007) Migmatites of Higher Himalayan Crystallines: Their role in collision Tectonics. *Unpublished Ph. D. Thesis, IIT Roorkee*, 262 pp.

Parrish, R.R. and Hodges, K.V. (1996) Isotopic constraints on the age and provenance of the Lesser and Greater Himalayan sequences, Nepalese Himalaya. *Geological Society of America Bulletin*, v. 108, pp. 904-911.

Patel, R.C. and Carter, A. (2009) Exhumation history of the Higher Himalayan Crystalline along Dhauliganga-Goriganga River Valleys, NW India: New constraints from fission-track analysis. *Tectonics*, Paper in press.

Patel, R.C., Kumar, Y., Lal, N. and Kumar, A. (2007) Thermotectonic history of the Chiplakot Crystalline Belt in the Lesser Himalaya, Kumaon, India: Constraints from apatite fission-track thermochronology. *Journal of Asian Earth Sciences*, v. 29, pp. 430-439.

Paul, Y. (1995) Exhumation history of Mandi-Dalhousie-Bandal regions, NW Himalaya, Himachal Pradesh - a fission track study. *Unpublished Ph. D. Thesis, Kurukshetra University, Kurukshetra (India)*, 134 pp.

Pebam, J., Jain, A.K., Kumar, R., Singh, S. and Lal, N. (2008) Tectonics vs. erosion: evidences from apatite fission track and Rb-Sr (Biotite and Muscovite) thermochronology, Arunachal Himalaya. *Himalayan Journal of Sciences*, v. 5(7), pp. 103-105.

Pêcher, A. (1977) Geology of Nepal Himalaya: deformation and petrography in the main central thrust Zone. In: Himalaya, *Science de la tera, CNRS, Paris*, v. 268, pp. 301-318.

Pêcher, A. (1989) The metamorphism in the central Himalaya. *Journal of Metamorphic Geology*, v. 7, pp. 31-41.

Pilgrim, G.E. and West, W.D. (1928) The structure and correlation of Shimla rocks. *Memoir Geological Survey of India*, v. 53, 140 pp.

Price, P.B. and Walker, R.M. (1963) Fossil tracks of charged particles in mica and the age of minerals. *Journal of Geophysical Research*, v. 68, pp. 4847-4862.

Purdy, J. E., and Jaeger E. (1976) K-Ar ages on rock-forming minerals from the Central Alps. *Memoir Science. Geology*, v. 30, pp. 1-31.

Rahl, J.M., Ehlers, T.A. and van der Pluijm, B.A. (2007) Quantifying transient erosion of orogens with detrital thermochronology from syntectonic basin deposits. *Earth and Planetary Science Letters*, v. 256, pp. 147-161.

Rahn, M.K., Brandon, M.T., Batt, G.E. and Garver, J.I. (2004) A zero-damage model for fission track annealing in zircon. *American Mineralogist*, v. 89, pp. 473-84.

Raiverman. V., Kunte S.V. and Mukherjee. A. (1983) Basin geometry, Cenozoic sedimentation and hydrocarbon prospects in North Western Himalaya and Indo-Gangetic plains. *Petroleum Asia Journal*, November Issue, pp. 67-92.

Ranga Rao, A. (1983) Geology and Hydrocarbon potential of a part of Assam-Arakan and its adjacent region. In: Bhandari, L.L. (eds.), *Petroliferous basin of India*, v. 4, pp. 127-158.

Ratschbacher, L., Frisch, W., Chen, C.S. and Pan, G.T. (1992) Deformation and motion along the southern margin of the Lhasa block (Tibet) prior to and during the India-Asian collision. *Journal of Geodynamics*, v. 16, pp. 21-54.

Ravikant, V. (2006) Utility of Rb-Sr geochronology in constraining the Miocene-Cretaceous events in the Eastern Karakoram, Ladakh, India. *Journal of Asian Earth Sciences*, v. 27(4), pp. 534-543.

Ray, L., Bhattacharya, A. and Roy, S. (2007) Thermal conductivity of Higher Himalayan Crystallines from Garhwal Himalaya, India. *Tectonophysics*, v. 434(1-4), pp. 71-79.

Reddy, D.R.S., Lakshmipathi, N.S. and Das, P.K. (1981) Progress report in geological mapping in parts of Gango-Mari-Shaki area, Upper Subansiri District Arunachal Pradesh. *Unpublished report of Geological Survey of India*, Northeastern region, Itanagar, 17 pp.

Reiner, P.W. and Brandon, M.T. (2006) Using Thermochronology to understand orogenic erosion. *Annual Review Earth and Planetary Science*, v. 34, pp. 419-466.

Reiners, P.W. and Farley, K.A. (1999) He diffusion and (U-Th)/He thermochronometry of titanite. *Geochimica et Cosmochimica Acta*, v. 63, pp. 3845-3859.

Reiners, P.W., Ehlers, T.A. and Zeitler, P.K. (2005) Past, present, and future of thermochronology. In: Reiners, P.W. and Ehlers, T.A. (eds.), Low-Temperature Thermochronology: Techniques, Interpretations and Applications. *Review of Mineralogy and Geochemistry*, v. 58, pp. 1-18.

Reiners, P.W., Spell, T.L., Nicolescu, S. and Zanetti, K.A. (2004) Zircon (U-Th)/He thermochronometry: He diffusion and comparison with $^{40}Ar/^{39}Ar$ dating. *Geochimica et Cosmochimica Acta*, v. 68, pp. 1857-1887.

Robbins, G.A. (1972) Radiogenic argon diffusion in muscovite under hydrothermal condition. *M.S Thesis, Brown University. Providence, Rhode island.*

Robinson, D.M., DeCelles, P.G., Patchett, P.J. and Garzoine, C.N. (2001) The kinematic evolution of the Nepalese Himalaya interpreted from Nd isotopes. *Earth and Planetary Science Letters*, v. 192, pp. 507-521, doi: 10.1016/S0012-821X(01)00451-4.

Rolland, Y., Mahe´oa, G., Guillot, S. and Pecher, A. (2001) Tectonometamorphic evolution of the Karakoram metamorphic complex (Dasau-Askole area, NE Pakistan): exhumation of mid crustal HT.MP gneisses in convergent context. *Journal of Metamorphic Geology*, v. 19, pp. 717-737.

Rolland, Y., Pecher, A. and Picard, C. (2000) Middle Cretaceous back-arc formation and arc evolution along the Asian margin: the Shyok Suture Zone in Northern Ladakh (NW Himalaya). *Tectonophysics*, v. 325, pp. 145-173.

Roy, S. and Rao, R.U.M. (2000) Heat flow in the Indian shield. *Journal of Geophysical Research-Solid Earth*, v. 105(B11), pp. 25587-25604.

Ruiz, G. and Seward, D. (2006) The Punjab foreland basin of Pakistan: a reinterpretation of zircon fission-track data in the light of Miocene hinterland dynamics. *Terra Nova*, v. 18, pp. 248-256.

Ruiz, G.M.H., Seward, D. and Winkler, W. (2004) Detrital thermochronology - a new perspective on hinterland tectonics, an example from the Andean Amazon Basin, Ecuador. *Basin Research*, v. 16, pp. 413-430.

Sangode, S.J., Kumar, R. and Ghosh, S.K. (1996) Magnetic polarity stratigraphy of the Siwalik sequence of Haripur area (H.P.), NW Himalaya. *Journal Geological Society of India*, v. 47, pp. 683–704.

Sangode, S.J., Kumar, R. and Siddaiah, N.S. (2005) Magnetic polarity and rock magnetic studies across marine to continental transition (Subathu-Dagshai sequence) in the Himalayan foreland. *Asia Oceania Geosciences Society Second Annual Meeting*, SE30/3A-01-3/206.

Satouru, K., Ahmed, T., Tsuyoshi, T., Bagati, T. N., Mishra, M., Kumar, R., Islam, R. and Khanna, P. P. (2001) Early cretaceous radiolarians from the Indus suture zone,

Ladakh, North India. *News of Osaka Micropaleontologists*, Special Volume. No. 12, pp. 257-270.

Scharer, U., Hamet, J., and Allegre, C. J. (1984) The Transhimalaya (Gangdese) plutonism in the Ladakh region: a U-Pb and Rb-Sr study. *Earth and Planetary Science Letters*, v. 67, pp. 327-339.

Schulp, M., Carter, A., Cosca, M. and Steck, A. (2003) Exhumation history of eastern ladakh revealed by $^{40}Ar/^{39}Ar$ and fission track ages: the Indus river-Tso Morari transect, NW Himalaya. *Journal of the Geological Society, London*, v.160, pp. 385-399.

Searle, M.P., Rex, A.J., Tirrul, R., Windley, B.F., St. Onge, M. and Hoffman, P. (1986) A geological profile across the Baltoro Karakoram Range, N. Pakistan. *University of Peshawar, Geological Bulletin*, v. 19, pp. 1-12.

Searle, M.P., Simpson, R.L., Law, R.D., Parrish, R.R. and Waters, D.J. (2003) The structural geometry, metamorphic and magmatic evolution of the Everest massif, High Himalaya of Nepal-South Tibet. *Journal of the Geological Society, London*, v. 160, pp. 345-366.

Seward, D. and Burg, J.P. (2008) Growth of the Namche-Barwa Syntaxis and associated evolution of the Tsangpo Gorge: Constraints from structural and thermochronological data. *Tectonophysics*, v. 451, pp. 282-289.

Sharma, K.K. (1982) Ladakh-Deosai batholith and its surrounding rocks. *Contribution to Himalayan Geology*, v. 2, pp. 180-187.

Sharma, K.K. and Choubey, V.M. (1983) Petrology, geochemistry geochronology of the southern margin of the Ladakh Batholith between Upshi and Chumthang. In: Sharma, K.K. (eds.) Geology of Indus Suture Zone of Ladakh. *Wadia Institute of Himalayan Geology, Dehradun*, pp. 41-60.

Sharma, K.K., Choubey, V.M. and Chatti, H.R. (1991) Geological setting of the ophiolites and magmatic arc of Lohit Himalaya (Arunachal Pradesh) India with special reference to their petrochemistry In: Sharma, K.K. (eds.) Geology and Geodynamic Evolution of the Himalayan Collision Zone. Part-2. *Physics and Chemistry of Earth*, v. 18, pp. 221-236.

Singh, I.B. (1978) On some sedimentological and palaeoecological aspects of Subathu-Dagshai- Kasauli succession of Simla Hills: *Journal of the Paleontological Society of India*, v. 21-22, pp. 19–28.

Singh, S and Jain, A.K. (1993) Deformation and strain pattern in parts of the Jutogh Nappe along the Sutlej Valley in Jeori Wangtu region, Himachal Pradesh. *Journal of Himalayan Geology*, v. 4(1), pp. 41-45.

Singh, S. (1989) A note on the stratigraphic status of quartzite of Siang Valley, Arunachal Himalaya. *Indian Minerals*, v. 43(2), pp. 162-166.

Singh, S. (1992) Lithotectonic units in parts of Arunachal Pradesh (India) and Bhutan, Eastern Himalaya: an appraisal. *Journal of Himalayan Geology*, v. 3(2), pp. 171-177.

Singh, S. (1993) Geology and Tectonics of the Eastern Syntaxial Bend, Arunachal Himalaya. *Journal of Himalayan Geology*, v. 4(2), pp. 149-162.

Singh, S. and De, A.K. (1989) Geology and structure of Siyom Valley. In: Saklani, P.S. (eds.), Current trends in Geology: Metamorphics, Ophiolites and Orogenic Belts. *Todays and Tomorrows printer and publishers, New Delhi*, pp. 191-206.

Singh, S. and France-Lanord, C. (2002) Tracing the distribution of erosion in Brahmaputra watershed from isotopic composition of stream sediments. *Earth and Planetary Science Letters*, v. 252, pp. 645-662.

Singh, S. and Jain A. K. (2003) Himalayan Granitoids. In: Singh, S. (eds.) Granitoids of the Himalayan Collisional Belt. *Journal of the Virtual Explorer*, v. 11, pp.1-20.

Singh, S. and Jain, A.K. (2007) Geology and tectonics of the Subansiri Corridor, Arunachal Himalaya. *DCS-DST News (January issue)*, pp. 21-24.

Singh, S. and Sharma, R. (1990) Geology of part of Lower Subansiri East Kameng district, Arunachal Pradesh. *Records Geological Survey of India*, v. 41(4), pp. 3-5.

Singh, S., Patra, B.A., Vijan, A.R. and Jain, A.K. (2006) Biotite Rb-Sr Ages: Constraints on Exhumation of Karakoram Metamorphic Complex, Eastern Ladakh. *Journal Geological Society of India*, v. 67, pp. 27-31.

Singh, S., Reddy, K.V.S., Bindal, C.M. and Ganesh, B.V. (1997) Geology of the upper parts of the Subansiri Valley, Upper Subansiri District, Arunachal Pradesh. *Records Geological Survey of India*, v. 118, pp. 3-8.

Sorkhabi, R.B. (2000) Fission-Track Analysis of Apatites from the Tawi River Sands, NW India (Jammu and Kashmir). *Himalayan Geology*, v. 21(1-2), pp. 201-207.

Sorkhabi, R.B., Jain, A.K., Itaya, T., Fukui, S., Lal, N. and Kumar, A. (1997) Cooling age record of domal uplift in the core of the Higher Himalayan Crystallines (HHC), southwest Zanskar, India. *Proceeding of Indian Academy of Science (Earth and Planetary Science)*, v. 106(3), pp. 169-179.

Sorkhabi, R.B., Stump, E., Foland, K.A. and Jain, A.K. (1996) Fission-track and $^{40}Ar/^{39}Ar$ evidence for episodic denudation of the Gangotri granites in the Garhwal Himalaya, India. *Tectonophysics*, v. 260, pp. 187-199, doi: 10.1016/0040-1951(96)00083-2.

Srikantaia, S.V. and Bhargava, O.N. (1988) The Jutogh Group of Metasdiments of the Himachal Himalaya. *Journal Geological Society of India*, v. 32, pp. 279-294.

Srikantia, S.V., Ganesan, T.M. and Wangdus, C. (1982) A note on the tectonic framework and geological set-up of Pangong-Chusul sector, Ladakh Himalaya. *Journal Geological Society of India*, v. 23, pp. 354-357.

Steiger, R.H. and Jager, E. (1977) Sub-commission on geochronology: convention on the use of decay constants in geo and cosmochronology. *Earth and Planetary Science Letters*, v. 36, pp. 359-362.

Stewart, R.J., Hallet, B., Zeitler, P.K., Malloy, M.A., Allen, C.M. and Trippett, D. (2008) Brahmaputra sediment flux dominated by highly localized rapid erosion from the easternmost Himalaya. *Geology*, v. 36(90), pp. 711-714.

Stüwe, K. and Foster, D. (2001) Ar^{40}/Ar^{39}, pressure, temperature and fission-track constraints on the age and nature of metamorphism around the Main Central Thrust in the Eastern Bhutan Himalaya. *Journal of Asian Earth Sciences*, v. 19, pp. 85-95.

Tagami, T. and O'Sullivan, P.B. (2005) Fundamentals of Fission Track Thermochronology. *Reviews in Mineralogy and Geochemistry*, v. 58, pp. 19-47.

Tagami, T., Galbraith, R.F., Yamada, R. and Laslett, G.M. (1998) Revised annealing kinetics of fission tracks in zircon and geological implications. In: Van den Haute, P. and De Corte, F. (eds.), Advances in fission track geochronology. *Kluwer academic publishers, Dordretch, The Netherlands*, pp. 99-112.

Tewari, V.C. (2001) Discoveries and sedimentology of microstromatolites from Menga Limestone (Neoprotrozoic/Vendian, Upper Subansiri District, Arunachal Pradesh, Northeast Himalaya, India. *Current Science*, v. 80(1), pp. 1440-1444.

Tewari, V.C. (2003) Sedimentology, Paleobiology and stable isotopes chemostratigraphy of the terminal Proterozoic Buxa Dolomite, Arunachal Pradesh, NE Lesser Himalaya. *Himalayan Geology*, v. 24(2), pp. 1-18.

Thakur, A.K. and Lal, N. (1993) Determination for Zeta calibration factor for fission track dating of apatite, sphene and zircon. *Indian Journal of Pure and Applied Physics*, v. 31, pp. 241-250.

Thakur, V. C. and Jain, A. K. (1975) Some Observations on deformation, metamorphism and tectonic significance of the rocks of some parts of the Mishmi Hills, Lohit district (NEFA), Arunachal Pradesh. *Himalayan Geology*, V. 5, pp. 339-363.

Thakur, V.C. (1993) Geology of the western Himalaya. *Oxford and New York, Pergamon Press*, 355 pp.

Thakur, V.C. and Jain, A.K. (1974) Tectonics of the region of Eastern Himalayan syntaxis. *Current Science*, v. 43, pp. 783-785.

Thiede, R.C., Arrowsmith, J.R., Bookhagen, B., McWilliams, M.O., Sobel, E.R. and Strecker, M. R. (2005) From tectonically to erosionally controlled development of the Himalayan orogen. *Geology*, v. 33, pp. 689-692, doi:10.1130/G21483.1.

Thiede, R.C., Arrowsmith, J.R., Bookhagen, B., McWilliams, M.O., Sobel, E.R. and Strecker, M.R. (2006) Dome formation and extension in the Tethyan Himalaya, Leo Pargil, NW-India. *Geological Society of America Bulletin*, v. 118, pp. 635-650, doi:610.1130/B25872.25871.

Thiede, R.C., Bookhagen, B., Arrowsmith, J.R., Sobel, E.R. and Strecker, M.R. (2004) Climatic control on rapid exhumation along the Southern Himalayan Front. *Earth and Planetary Science letters*, v. 222, pp. 791-806.

Thiede, R.C., Ehler, T., Bookhagen, B. and Strecker, M.R. (2009) Erosional variability along the northwest Himalaya. *Journal of Geophysical Research*, v. 114, F01015, doi:10.1029/2008JF001010.

Thiel, K. and Herr, W. (1976) The ^{238}U spontaneous fission decay constant re-determined by fission tracks. *Earth and Planetary Science Letters*, v. 30, pp. 50-56.

Tripathi, C., Gaur, R.K., Tewari, M., Shankar, J. and Dungrakoti, B.D. (1982) On the geology of Sipi-Mara window, Arunachal Pradesh. *Himalayan Geology*, v. 10, pp. 366-373.

Tripathi, C., Reddy, D.R.S., Gupta, P.D., Roy Choudhary, J. and Lakshminarayana, G. (1983) On the investigation of Limestone in Menga area, Upper Subansiri District, Arunachal Pradesh. *Indian Mineralogists*, v. 37(1), pp. 33-38.

Valdiya, K.S. (1979) Outline of the structures of the Kumaon Himalaya. *Journal Geological Society of India*, v. 20, pp. 145-157.

Valdiya, K.S. (1980) Geology of the Kumaon Lesser Himalaya. *Wadia Institute of Himalayan Geology*, Dehradun, 299 pp.

Valdiya, K.S. (1981) Tectonics of the central sector of the Himalaya. In: Gupta, H.K. and Dalaney, F.M. (eds.), Zagros-Hindukush-Himalaya: Geodynamic evolution. *American Geophysical Union Series 3*, Washington, pp. 87-111.

Valdiya, K.S. (1988) Dynamic Himalaya.*Universities Press, Hyderabad*, 178 pp.

Valdiya, K.S., Paul, S.K., Chandra, T., Bhakuni, S.S. and Upadhay, R.C. (1999) Tectonics and Lithological characterization of Himadri (Great Himalaya) between Kali and Yamuna Rivers, Central Himalaya. *Himalayan Geology*, v. 20(2), pp. 1-17.

Vannay, J.C., Grasemann, B., Rahn, M., Frank, W., Carter, A., Baudraz, V. and Cosca, M. (2004) Miocene to Holocene exhumation of metamorphic crustal wedges in the NW Himalaya: Evidence for tectonic extrusion coupled to fluvial erosion. *Tectonics*, v. 23, TC1014, doi:10.1029/2002TC001429.

Verma, P.K. and Tandon, S.K. (1976) Geological observations in part of Kameng District, Arunachal Pradesh (NEFA). *Himalayan Geology*, v. 6, pp. 259-286.

Verma, P.K. (Ed.) (1999) Geological studies in the Eastern Himalayas. Pilgrim Book (Pvt.) Ltd., New Delhi,264 pp.

Wadia, D. N. (1937) The Cretaceous volcanic series of Astor-Deosai, Kashmir and its intrusion. *Records Geolological Survey of India*, v. 72, pp. 151-161.

Wadia, D.N. (1931) The syntaxis of Northwest Himalaya: its rocks, tectonics and orogeny. *Records Geological Survey of India*, v. 65(2), pp. 189-220.

Wagner, G.A. and Van den haute, P. (1992) Fission Track Dating. *Kluwer academic publisher, Derdrecht Solid Earth Science Library*, v. 6.

Watt, S. and Durani, S.A. (1985) Thermal stability of fission tracks in apatite and sphene: using confined track length measurements. *Nuclear Tracks*, v. 10, pp. 349-357.

Weinberg, R.F. and Dunlop, W.J. (2000) Growth and deformation of Ladakh Batholith, Northwest Himalaya: implications for the timing of continental collision and origin of calc alkaline batholiths. *Journal of Geology*, v. 108, pp. 303-320.

Whipp, D.M. and Ehlers, T.A. (2007) Influence of groundwater flow on thermochronometer-derived exhumation rates in the central Nepalese Himalaya. *Geology*, v. 35, pp. 851-854, doi:10.1130/G23788A.1.

Whipp, D.M., Ehlers, T.A., Blythe, A.E., Huntington, K.W., Hodges, K.V. and Burbank, D.W. (2007) Plio-Quaternary exhumation history of the central Nepalese Himalaya: 2. Thermokinematic and thermochronometer age prediction model. *Tectonics*, v. 26, TC3003, doi:10.1029/2006TC001991.

White, N. M., Pringle, M., Garzanti, E., Bickle, M., Najman, Y., Chapman, H. and Friend, P. (2002) Constraints on the exhumation and erosion of the High Himalayan Slab, NW India, from foreland basin deposits. *Earth and Planetary Science Letters*, v. 195, pp. 29–44.

White, N.M., Parrish, R.R., Bickle, M.J., Najman, Y.M.R., Burbank, D. and Maithani, A. (2001) Metamorphism and exhumation of the NW Himalaya constrained by U–Th–Pb analyses of detrital monazite grains from early foreland basin sediments. *Journal of the Geological Society,* v. 158, pp. 625–635.

Winslow, D.M., Zeitler, P.K., Chamberlain, C.P. and Williams, I.S. (1996) Geochronologic constraints on syntaxial development in the Nanga Parbat region, Pakistan. *Tectonics* v. 15, pp. 1292-1308.

Yin, A. (2006) Cenozoic tectonic evolution of the Himalayan orogen as constrained by along-strike variation of structural geometry, exhumation history and foreland sedimentation. *Earth Science Reviews*, v. 76(1-2), pp. 1-131.

Yin, A., Dubey, C.S., Kelty, T.K., Gehrel, G.E., Chou, C.Y., Grove, M. and Lovera, O. (2006) Structural evolution of Arunachal Himalaya and implication for asymmetric evolution of the Himalayan orogen. *Current Science*, v. 90, pp. 195-206.

Yin, A., Dubey, C.S., Kelty, T.K., Webb, A.A.G., Harrison, T.M., Chou, C.Y. and Célérier, J. (2009a) Geologic correlation of the Himalayan orogen and Indian Craton: Part 2. Structural geology, geochronology and tectonic evolution of the eastern Himalaya. *Geological Society of America Bulletin*, In press.

Yin, A., Dubey, C.S., Webb, A.A.G., Kelty, T.K., Grove, M., Gehrels, G.E. and Burgess, W.P. (2009b) Geologic correlation of the Himalayan orogen and Indian Craton: Part 1. Structural geology, U-Pb zircon geochronology and tectonic evolution of the Shillong plateau and its neighbouring regions in NE India. *Geological Society of America Bulletin*, In press.

York, D. (1966) Least square fitting of straight line. *Canadian Journal of Physics*, v. 44, pp. 1079-1086.

York, D. (1969) Least square fitting of straight line with correlated errors. *Earth and Planetary Science Letters*, v. 5, pp. 320-324.

Zeitler, P.K. (1985) Cooling history of the NW Himalaya, Pakistan. *Tectonics*, v. 4, pp. 127-151.

Zeitler, P.K., Johnson, N.M., Briggs, N.D. and Naeser, C.W. (1986) Uplift history of the NW Himalaya as recorded by fission-track ages on detrital Siwalik zircons. In: Jiqing, H. (eds.), Proceedings of the Symposium on Mesozoic and Cenozoic Geology in Connection of the 60th Anniversary of the Geological Society of China. *Geological Publishing House, Beijing, China,* pp. 48-496.

Zhang, Y.Q., Dai, T.M. and Hong, A.S. (1981) Isotopic geochronology of granitoid rocks in Southern Xiang Plateau. *Proceedings of Symposium on Qinghai-Xizang (Tibet) Plateau, (Beijing, 1980)*, Science Press, Beijing, v. 1, pp. 483-495.

Zhang, Z.G., Zhao, J.S. and Cheng, C.L. (1987) Isotopic dating of the metamorphic rocks in the Namjag Barwa region. *Science Bulletin*, v. 2, pp. 133-137.

Zheng, X. and Chang, C. (1979) A preliminary note on the tectonic features of the lower Yalu-Tsangpo River region. *Scientia Geologica Sinica*, v. 2, pp. 116-126.